Mode Localization in a Nearly Cyclic Symmetric System

Ya-Fang Chen

A dissertation
submitted in partial fulfillment of the
requirements for the degree of

Doctor of Philosophy

University of Washington

2016

Reading Committee:

I-Yeu (Steve) Shen, Chair

Per G Reinhall

Duane W Storti

Brian C. Fabien

Program Authorized to Offer Degree:
Mechanical Engineering

University of Washington

Abstract

Mode Localization in a Nearly Cyclic Symmetric System

Ya-Fang Chen

Chair of the Supervisory Committee:
Professor I-Yeu (Steve) Shen
Mechanical Engineering

Cyclic symmetric systems have been widely used in industry, such as turbines, propellers, and compressors. An ideal, tuned, cyclic symmetric system consists of multiple substructures with same geometry and material properties. In a real system, however, there are always slight differences among the substructures (known as mistuning) as a result of imperfections from manufacturing, wear, and damage. The presence of the mistuning could cause mode shapes to localize on a few substructures leading to a phenomenon called "mode localization." As the system spins at high speed, force excitations from the spin together with the mode localization will expedite fatigue failure and jeopardize the safety of the system.

Due to the mistuning, the system is not perfectly cyclic symmetric and cannot be predicted by a single substructure. To reduce computational costs, researchers have dedicated for years to developing reduced-order models to accurately predict mode localization. Nevertheless, fundamental understanding, such as when and where mode localization will occur, remains open. Many researchers believe that curve veering of eigenvalue loci is the main contributor of mode localization, but mode localization is also found in a frequency range without any curve veering.

Moreover, most studies for mode localization only considered rotors as independent components, so fixed boundary condition was typically applied to the inner rim of

the rotors. In a real system, a rotor is always connected with other mechanical components. Recently, researchers started to analyzed turbinemachinery in greater detail by modeling multi-stage rotors or a rotor connected to a shaft. Nevertheless, effects of flexible bearings and housing on mode localization remain unknown. In a broader context, implications of the boundary effects and how boundary conditions affect mode localization are still open.

The objective of this thesis is to develop a rigorous mathematical formulation to deduce concrete conditions under which mode localization will occur. The mathematical formulation also provides an effective means to significantly reduce computational costs in predicting mode localization. With the understanding of the conditions for mode localization to occur, the effects of flexible bearings and housing are investigated numerically and interpreted with deductive reasonings.

When slight mistuning is introduced into a tuned, cyclic symmetric system, occurrence of mode localization requires the localized mode shapes deviate dramatically from tuned mode shapes. Enlightened by perturbation theory and Fourier analysis, this behavior will occur only when the following two conditions are met: (1) there is a group of tuned modes that have nearly identical natural frequencies, and (2) this group of modes contains a wide range of wave numbers. Mode localization (i.e. localized modes) will be formed as linear combinations of this group of tuned modes. Without these two conditions, researchers traditionally would predict localized modes using Rayleigh-Ritz methods by including many tuned modes in a frequency range as trial vectors. If the prediction of mode localization fails, more tuned modes would be included for a wider frequency range and the calculation is repeated. To improve computational efficiency, a visual method is developed in this thesis to pinpoint those tuned modes that will contribute significantly to the linear combinations. With the visual method, the tuned modes are screened carefully so that mode localization can

be predicted without iterations and redundant tuned modes. Numerical examples verify that the computational cost for mode localization can be reduced 36%.

In this thesis, the effects of flexible bearings and housing are studied through use of finite element analyses. Three models are studied: (1) a reference rotor system in the form of bladed disk with a fixed inner rim, (2) a rotor-bearing system with the fixed boundary condition at the inner rim replaced by flexible bearings, and (3) a rotor-bearing-housing system that connects the reference rotor with a stationary housing via the bearings. All the systems are studied with a tuned version and a mistuned version. Mode localization is compared among the three mistuned systems. The simulated results show that not only the number of localized modes changes but also the natural frequencies and mode shapes of existing localized modes. Consequently, forced response of the localized modes will also change. When bearings and housing are present, vibration of the housing may excite localized modes of the rotor to resonance. These simulation results can all be deduced theoretically from the two mode localization conditions and existing knowledge on vibration of cyclic symmetric structures.

This thesis not only identifies the criteria governing occurrence of mode localization, but also provides an effective method to significantly reduce the computational costs for predicting mode localization. This thesis provides physical insights and qualitative predictions regarding how bearings and housing may affect mode localization. The results discussed in this thesis are general and are valid for any cyclic symmetric system.

TABLE OF CONTENTS

LIST OF FIGURES

LIST OF TABLES

ACKNOWLEDGMENTS

I would like to thank Prof. Shen, my advisor, for his experience, knowledge, patience and guidance. He has provided me with very valuable advice and direction. I would also like to thank Prof. Per G Reinhall, Prof. Brian C. Fabien, Prof. Duane W Storti, and Prof. Gregory Miller (GSR) for serving on my doctoral committee and providing me with helpful suggestions.

A special acknowledgment should be given to my first manager, Kevin Tzou. Without his job offer and support, I might not be able to keep my graduate study.

I am very grateful for my friends in my lab, especially Wei-Che Tai, Hsien-Lin (Stacey) Huang, Weiwei Xu, Chuan Luo, Bobby Manson, Mark Janikowski. Your support and camaraderie have helped me conquer frustrations and difficulties.

I am very thankful for my friends from Seattle, especially Tsrong-Yi Wen, Chi Hou Lei, Kebin Gu, Chi-Jung Lee, Hong-Ren Lin, Yih-Yan Lin, James Sung, Mimi Nguyen, Poshen Lee, Morris Chuang, Chieh-Lun Li, Hsiao-Hsin (Doris) Chien, Chia-Hsuan Chen, Hsin-Hsuan Huang, Yi-Chia (Chloe) Huang, Hsiang-Yuan Wu, Isaac Chang, Sally Che, Cathy Yang, Yu-Rong Liu, Wen-Pei Tsai, Angel Yang, Harley Pan. Your kindness and encouragement supported me to move forward on my project.

I also greatly appreciate my friends from San Jose, especially Hsin-Ying Chiu, Doris Ho, Adam Brzezinski, Yu Chen, Daphne Ho, Hao-Chien Hsu, Terrence Chen, Anderson Yeh, Joanne Wang. You have shown me the value of dedication and helped me to broaden my problem-solving perspective.

Finally, I would like to thank my family, especially my parents, Juen-Man Chang, Jung-Huang Cheng, my sisters, Kuan-Ting Chen, Ching-Jen Chen, and all my true

friends who unselfishly share their life experience and happiness with me, especially Yuan-Chieh Tsai. Words cannot express my gratitude for you. I hope I can someday support others as well as you have supported me.

DEDICATION

This Ph.D. dissertation is dedicated to my beloved parents and my respected gradnparents. All what I have today is because of their deep love and cultivation.

Chapter 1

INTRODUCTION

Mode localization is a well-known phenomenon in nearly cyclic symmetric structures. It occurs when mistuning is introduced into a perfectly cyclic symmetric structure that consists of multiple identical substructures. When mode localization occurs, a couple of substructures vibrate significantly while others barely do. Since mode localization does not appear in the tuned, cyclic symmetric structure, mode shapes must undergo significant changes as tiny mistuning is introduced in order to realize the mode localization.

One important application of mode localization is turbine disks with multiple blades that are evenly spaced in the circumferential direction [1, 2]. Ideally, the blades are identical thus forming a cyclic symmetric rotor with the disk. Due to manufacturing tolerance, wear, or damage, the blades will in general vary slightly from one another, and the blade variation is known as mistuning. With the presence of the mistuning, the disk-blade systems may undergo highly localized vibration under some circumstances, thus forming mode localization. The phenomenon of mode localization could premature high cycle fatigue and accelerate damage to the bladed disks [3]. Moreover, when mode localization occurs, amplitude of a few blades is largely amplified under engine order excitation of pressure [4].

Mode localization can also appear in a nonlinear periodic structure consisting of multiple identical substructures without mistune. The nonlinearity may arise from fluid-structure interaction or dry friction damping [5]. Since the substructures are identical, the periodic structure is *tuned*. Therefore, the linear and nonlinear mode localization phenomena are totally different. The former occurs in a linear mistuned

structure but the latter in a tuned nonlinear structure. Here, I only focus on linear mode localization in this thesis.

1.1 Literature Review

1.1.1 Reduced-order Model for Cyclic Symmetric Rotor Systems

Due to its potential impact, mode localization has been studied via various approaches. Historically, the phenomenon of mode localization was first studied via lumped-parameter mass-spring systems [6, 7, 8]. Such approach potentially simplifies the systems, reduces calculation costs, and facilitates Monte-Carlo simulations. The lumped-parameter approach, however, is not effective for industrial rotors that bear complex geometry. To address this issue, two major approaches have been developed in the last several decades for mistuned bladed disks. A major effort is to obtain reduced-order models (ROMs) that are capable of predicting mode localization and forced response.

The first approach is component mode synthesis (e.g., [9, 10] and many others). In this approach, the disk and each blade are treated as individual components. Natural frequencies and mode shapes of these components are obtained numerically and subsequently synthesized to obtain the ROMs of the entire bladed disk. During the mode synthesis, mistuning is introduced and incorporated into the ROMs.

The second approach is to use the tuned, cyclic symmetric, bladed disk as a nominal system and consider the mistuning as an *add-on* component [11, 12, 13, 14]. Natural frequencies and mode shapes of the nominal system are retained to predict mode localization when the mistuning is added. The prediction method can be Rayleigh-Ritz [11, 12], Taylor expansion [15], or component-mode synthesis [16].

In both approaches, the phenomenon of mode localization is explored numerically through the following procedure. First, natural frequencies of all vibration modes are plotted with respect to the number of nodal diameters of the disk. These natural

frequencies are grouped into families, ranging from low to high frequencies, to generate a set of eigenvalue loci of the bladed disk. A common belief is that mode localization occurs at places where eigenvalue loci veer [17, 18]. Therefore, families of modes involved in the veering are retained to predict the localization [9]. Alternatively, all modes whose natural frequencies are close to the veering frequency (e.g., 5% frequency band around the veering frequency) are retained to predict the mode localization phenomenon [11, 16]. If the prediction is not successful, the frequency band will be increased and the calculation resumes.

The common belief that curve veering is a critical contributor of mode localization stems from prior research on periodic systems that have simple geometry [17, 18]. Chan and Liu [18] shows that vibration mode localization and frequency loci veering occur simultaneously when small disorders exist in aircraft structures. Pierre [17] shows that mode localization occurs when eigenvalue loci of a tuned periodic system (e.g., a coupled pendulum oscillators or a multi-span beam) veer away with respect to its parameters (e.g., the distance between two coupled pendulums or the length of beam span). Also, mode localization occurs when the mistuning and coupling of neighboring substructures are on the same order [19, 20].

When applying this common belief to mistuned bladed disks, however, there are some issues that are not quite worked out. First, eigenvalue loci are not continuous. In [17, 18], the system parameters vary continuously and eigenvalue loci are continuous. Therefore, one can easily identify when eigenvalue loci veer away from each other. In bladed disks, eigenvalue loci are plotted with respect to the number of nodal diameters, which is discrete. Therefore, eigenvalue loci are not continuous, and it is not clear whether eigenvalue loci actually veer or cross.

The second issue is that not every veering in eigenvalue loci leads to mode localization for bladed disk systems. It becomes very challenging to find out exactly when mode localization will occur. Moreover, this observation implies that there are other important contributors causing mode localization than veering of eigenvalue loci. If

so, what are those unknown contributors? For example, Feiner and Griffin [12] use a family of modes with no curve veering to demonstrate mode localization. Although many ROMs have been developed thus far to predict localized modes of mistuned bladed disks, it remains open why and when mode localization occurs.

Finally, there lacks an effective and precise method to retain modes in predicting mode localization. When a frequency band or several families of modes are retained to predict mode localization, many of the retained modes do not significantly contribute to the mode localization. There is a need for a more precise way to pinpoint the modes that should be retained. This could significantly reduce the order of ROMs and reduce the iteration of calculation.

1.1.2 Effects of Mechanical System Interaction on Mode Localization

In many studies of mode localization, a simplified bladed-disk model is used as a benchmark to facilitate prediction of mode localization. The benchmark model often has a single disk with multiple blades simulating a single-stage rotor. In addition, the inner rim of the bladed-disk is fixed to simplify the analysis. Although the simplified model has successfully demonstrated the phenomenon of mode localization, the model does not account for effects of other machine components, such as the shaft supporting the bladed disk, bearings, and housing. Therefore, how these machine components would affect mode localization remains unknown. Moreover, if these components did affect mode localization, what would be the underlying mechanisms and physics? If the mode localization were affected, what would be its implication to the performance of the entire rotor assembly?

Recently, researchers started to analyze vibration of turbomachinery rotors more accurately by modeling multi-stage bladed disks [21, 22, 23, 24]. A key observation is that the presence of interconnecting boundary conditions between stages affects mode localization. Specifically, some extremely localized modes present in a single-stage system are mitigated after the stages are connected together. Root causes behind the

mitigation or evolution of the localized modes are not well understood. The recent studies on multi-stage rotor vibration echo the three questions raised above: how would mode localization be affected, what would be the underlying mechanisms, and what would be its implications?

1.2 Objectives

In fact, the issues and questions raised above do not only occur to mistuned bladed disks. They occur to all nearly cyclic symmetric systems with mistuning. Objectives of this thesis are (a) to find out the key insights of mode localization in nearly cyclic symmetric systems, (b) to develop general criteria governing where and when mode localization would occur, and (c) to investigate how boundary conditions affect mode localization. To achieve these research objectives, the following tasks must be performed.

1. To find out the key factors of mode localization, the circumstance of when mode shape may change significantly and what are necessary to form a localized mode shape are investigated theoretically. Hence, a hypothesis is developed to provide the criteria of occurrence of mode localization.

2. To develop a precise method to select significant modes for mode localization, the equation of motion of a mistuned system is derived. With lights of the perturbation theory and Fourier analysis, the equations can be interpreted with mathematical insights. Therefore, a critical matrix is found to reveal the relationship between mistuning and coupling among substructures of the rotor system. By plotting the magnitude of the matrix, called as the visual method, the important modes for the linear combination can be pinpointed and the efficiency of prediction of mode localization can be improved significantly.

3. To verify the hypothesis and the effectiveness of the visual method on numeri-

cal examples, four representative mistuning configurations are considered that cover different mistuning patterns, mistuning amounts and mistuning sources. The results are compared with finite element analysis. The effects of mistung configuration on mode localization is also studied among the numerical examples.

4. To study how the supporting shaft, bearings and housing affect mode localization of a mistuned bladed disk, the following three systems are analyzed: (1) the reference system which is a rotor with fixed boundary condition at the inner rim, (2) the rotor-bearing system which is the rotor connecting to flexible bearings at the inner rim, and (3) the rotor-bearing-housing system which is the rotor connecting to a stationary housing via flexible bearings. Mode localization is compared among the three systems.

5. The mechanism of how boundary conditions affect mode localization is investigated from the perspective of how the participating modes will be changed by the change of boundary conditions. Deductive reasoning is based on previous theoretical analysis and existing literature.

6. Two direct implications of the change of boundary condition are forced response and bearing force. Differences of frequency response function of a blade imply how forced response will be affected and show the significance of effects of boundary condition on mode localization. Bearing force is compared between the tuned and the mistuned rotor-bearing system.

1.3 Outline

This section is to describe the organization of this thesis corresponding to the objectives above. The thesis contains five chapters. Chapter 1 gives the introduction of mode localization firstly. Literature reviews briefly summarize the background and

current studies about mode localization and explain the motivations of this research. Objectives and outline of the thesis are also given in Chapter 1.

In chapter 2, the hypothesis of when and where mode localization occurs in a cyclic symmetric system is elucidated. The hypothesis is developed from the theoretical analysis in the following sections. Since mistuning warrants itself to be treated as perturbation of the tuned system, the perturbation theory is studied on a discrete, mistuned system and cases of a singular natural frequency and repeated natural frequencies are considered. The derivation shows that only when a group of tuned modes has nearly identical natural frequencies, mode shapes will change significantly when mistuning is present. Secondly, the Dirac delta function in the circumferential direction is considered as an extremely localized mode shape. Fourier analysis on the delta function reveals that mode localization has to be formed with a group of tuned modes containing a wide range of wave numbers. Thus, two conditions for the occurrence of mode localization are proposed as mentioned in the hypothesis. Also, some intrinsic questions about mode localization are answered in this section.

In previous literature, researchers use the Rayleigh-Ritz method to predict mode localization with a group of tuned modes around veering of eigenvalue loci. If the prediction is not successful, the calculation will be resumed with more modes included as the trial vectors. To pinpoint the important modes for forming of mode localization, the visual method is developed in this section. The visual method is to plot the magnitude of entries in a critical matrix $\hat{\mathbf{L}}$ which depicts the relationship between mistuning and coupling among substructures of the system. The coupling is corresponding to the diagonal entries of $\hat{\mathbf{L}}$ while the mistuning is corresponding to the off-diagonal terms. If diagonal and off-diagonal terms of a mode have about the same order of magnitudes, the mode will actively contribute to form mode localization. With the visual method, the trial vectors can be selected effectively and mode localization can be predicted efficiently with significant reduction in the dimension of the eigenvalue problem.

In chapter 3, a rotor system that consists of a circular disk with 24 identical blades is used to verify the hypothesis and the effectiveness of the visual method. Also, effects of different mistuning is studied by comparing mode localization with four different mistuning configurations. The four configurations cover different mistuning amounts, mistuning patterns, and mistuning sources. First, a bladed disk with fixed boundary condition at its inner rim is described in detail. Convergence test for different meshes is studied to be used in finite element analysis to establish the baseline. Natural frequency distribution of the tuned system is plotted with respect to the number of nodal diameter. Curve veering sites are found in four frequency ranges and the corresponding modes are listed. Also, there are two frequency ranges that satisfy the two conditions in the hypothesis. Mistuning sets are introduced into the system individually and mode localization is examined in each frequency range. Also, the effectiveness of Rayleigh-Ritz method with the visual method is evaluated in the mistuned systems by comparing with the results of finite element analysis. Effect of mistuning configuration is demonstrated by comparing mode localization among the mistuned systems.

In Chapter 4, the effects of flexible bearings and housing are investigated. The effect of bearings is studied via two different approaches. The first approach is to observe how mode localization evolves by conducting a finite element analysis on a reference system. Specifically, the reference system is a mistuned, bladed disk with a fixed inner rim. To simulate the presence of bearing supports, the fixed inner rim is replaced with an elastic boundary condition. Finally, a housing is coupled with the reference system through the flexible bearings. The second approach is via a deductive reasoning from existing literature to obtain qualitative theoretical predictions to justify the finite element results. For example, Chen and Shen [25] have identified two conditions for mode localization to occur in a cyclic symmetric system with mistune. Kim et al. [26] show that vibration modes of a rotor will evolve in a certain manner when bearings are introduced to support the rotor. Predictions

of the finite element analysis should be consistent with conclusions drawn from these prior publications.

Therefore, Chapter 4 is organized as follow. First, finite element analyses (FEA) is conducted on the reference system to establish baseline mode localization behavior. Then the FEA are extended to a bladed disk with bearings (modeled as elastic boundary conditions at the inner rim) and a bladed disk connected to a flexible housing via elastic bearings. With the FEA results, we observe how mode localization evolves as the bearings and housing are introduced into the reference model and how differently the frequency response function of a blade may change. The effect of mode localization on bearing force is also studied. To conclude, we conduct a simple theoretical analysis to reveal root causes that change mode localization behavior via bearings and housing.

In chapter 5, conclusions of all previous chapters are summarized and future work is proposed based on the current findings in this thesis. Even though a bladed disk is used in this thesis, the hypothesis and findings are well applied for any cyclic symmetric system since the approaches and studies are supported by mathematical and theoretical investigations.

Chapter 2

HYPOTHESIS AND THEORETICAL ANALYSIS

2.1 The Hypothesis

I hypothesize that mode localization will occur when the following two conditions are met: (a) there is a group of vibration modes of the tuned cyclic symmetric rotor whose natural frequencies are nearly identical, and (b) this group of modes contains a wide range of wave numbers.

The first condition can be interpreted using perturbation theory. The small mistuning warrants itself to be treated as perturbation to the tuned cyclic symmetric rotor (i.e., the nominal or unperturbed system). Occurrence of localization implies that mode shapes of the unperturbed system have experienced significant changes at the zeroth order when the perturbation is introduced. For spectral perturbation theories, this only occurs when the unperturbed system processes a group of vibration modes that has the same natural frequency. The presence of small perturbation will then linearly combine these tuned vibration modes to seek a stationary energy state.

Since a cyclic symmetric rotor consists of many identical substructures, each substructure will have identical vibration modes. Nevertheless, elastic coupling between two neighboring substructures causes these vibration modes to deviate from their common natural frequency. When the deviation is small, the vibration modes are still similar enough to enable the linear combination. When the deviation is too large, the vibration modes become so distinct in frequency that they cannot be linearly combined. That is why mode localization requires a group of vibration modes whose natural frequencies are nearly identical.

The second condition makes sense in the context of Fourier analysis. If mode

localization is approximated as Dirac delta function in the circumferential direction, its spatial Fourier spectrum must contain a wide range of wave numbers; hence, the vibration modes with nearly identical frequencies must form a complete set in the circumferential direction. Otherwise, these vibration modes will not have enough wave numbers to linearly combine themselves to realize mode localization. Also, changing the mistuning will change the mode localization pattern. Mode localization present in cyclic symmetric systems is only possible when the vibration modes involved contain a wide range of wave numbers in the circumferential direction.

2.2 Theoretical Analyses

This section is to provide some theoretical analyses to support the hypothesis. These theoretical analyses include a Fourier analysis, mode shapes of cyclic symmetric rotors, a Rayleigh-Ritz approximation, and a mode selection criterion. These analyses provide mathematical insights of why mode localization occurs and how it can be better predicted.

2.2.1 Perturbation Theory applying on cyclic symmetric system

To understand how mistuning perturbs a tuned cyclic symmetric system, I first derive perturbation on a N-degree-of-freedom system. The tuned system has a stiffness matrix $\mathbf{K}$ and a mass matrix $\mathbf{M}$, and the corresponding natural frequencies and mode shapes, ω_n and $\mathbf{u}_n$, with $n = 1, 2, ..., N$, will satisfy the following eigenvalue problem.

$$(\mathbf{K} + \lambda_n \mathbf{M})\,\mathbf{u}_n = \mathbf{0} \tag{2.1}$$

The mistuning warrants itself to be treated as the perturbation which is considered as $\varepsilon\overline{\mathbf{K}}$, where ε represents the order of perturbation. The equation of motion for the mistuned system is considered as below.

$$\left(\mathbf{K} - \varepsilon\overline{\mathbf{K}} - \overline{\lambda_n}\mathbf{M}\right)\overline{\mathbf{u}_n} = \mathbf{0} \tag{2.2}$$

, where $\overline{\lambda_n}$ and $\overline{\mathbf{u}_n}$ are the new eigenvalue and eigenvector of the mistuned system. According to the perturbation theory, the new eigenvalue and eigenvector will change slightly from the original eigenvalue and eigenvector and can be represented in the following forms.

$$\overline{\lambda_n} = \lambda_n + \varepsilon\lambda_n^{(1)} + \varepsilon^2\lambda_n^{(2)} + \dots \tag{2.3}$$

, where $\lambda_n^{(i)}$ is the i-th order perturbation term of the n-th eigenvalue.

$$\overline{\mathbf{u}_n} = \mathbf{u}_n + \varepsilon\mathbf{u}_n^{(1)} + \varepsilon^2\mathbf{u}_n^{(2)} + \dots \tag{2.4}$$

, $\mathbf{u}_n^{(i)}$ is the i-th order perturbation term of eigenvector. (2.3) and (2.4) are valid when eigenvalues are distinguish with each other ($\lambda_n \neq \lambda_m$, for $n \neq m$ and $n, m \subset [1, N]$). By substituting (2.3) and (2.4) into (2.2), the zeroth order perturbation terms will be exactly the same as the left side of (2.1) which equals $\mathbf{0}$. Therefore, for the other terms of perturbation, the parameters of each order must to be $\mathbf{0}$ to satisfy (2.2). Hence, bounch or equations are generated to solve the eigenvalue and the eigenvector for each perturbation order sequentially.

By making the parameters of the first order of perturbation equal zero, the following equation is obtained.

$$\mathbf{u}_m^T\mathbf{K}\mathbf{u}_n^{(1)} - \mathbf{u}_m^T\overline{\mathbf{K}}\mathbf{u}_n + \lambda_n\mathbf{u}_m^T\mathbf{M}\mathbf{u}_n^{(1)} + \lambda_n^{(1)}\mathbf{u}_m^T\mathbf{M}\mathbf{u}_n = \mathbf{0} \tag{2.5}$$

Since both $\mathbf{K}$ and $\mathbf{M}$ are symmetric, (2.5) can be simplified as

$$(\lambda_n - \lambda_m)\,\mathbf{u}_m^T\mathbf{M}\mathbf{u}_n^{(1)} = \mathbf{u}_m^T\overline{\mathbf{K}}\mathbf{u}_n - \lambda_n^{(1)}\delta_{mn} \tag{2.6}$$

, where δ_{mn} is the Kronecker delta. For $n = m$, $\lambda_n^{(1)}$ can be solved from

$$\mathbf{u}_m^T\overline{\mathbf{K}}\mathbf{u}_n - \lambda_n^{(1)}\delta_{mn} = \mathbf{0} \tag{2.7}$$

For $n \neq m$, $\mathbf{u}_n^{(1)}$ can be solved from

$$\mathbf{u}_m^T\mathbf{M}\mathbf{u}_n^{(1)} = \frac{\mathbf{u}_m^T\overline{\mathbf{K}}\mathbf{u}_n}{\lambda_n - \lambda_m} \tag{2.8}$$

If there are repeated tuned eigenvalues such that $\lambda_j = \lambda$ with $j = 1, 2, \ldots, \alpha$ and $\alpha \leq N$. Then the zeroth order of perturbation in (2.4) will change.

$$\overline{\mathbf{u}_n} = \mathbf{u}_n^* + \varepsilon \mathbf{u}_n^{(1)} + \varepsilon^2 \mathbf{u}_n^{(2)} + \ldots \tag{2.9}$$

, where the zeroth order of the eigenvector will be the linear combination of the tuned eigenvectors.

$$\mathbf{u}_n^* = \gamma_{nk} \mathbf{u}_k \tag{2.10}$$

with $n, k \leq \alpha$. And the first order perturbation terms of (2.2) will become

$$\left(\lambda_n - \lambda_m\right) \mathbf{u}_m^T \mathbf{M} \mathbf{u}_n^{(1)} = \gamma_{mk} \left(\mathbf{u}_k^T \overline{\mathbf{K}} \mathbf{u}_n - \lambda_m^{(1)} \delta_{mk} \right) \tag{2.11}$$

Since $\lambda_n = \lambda_m$, (2.11) can be written as an eigenvalue problem.

$$\left(\mathbf{U}^T \overline{\mathbf{K}} \mathbf{U} - \lambda_j^{(1)} \mathbf{I} \right) \mathbf{v}_j = \mathbf{0} \tag{2.12}$$

, where

$$\mathbf{U} = [\mathbf{u}_1, \mathbf{u}_2, \ldots, \mathbf{u}_\alpha] \tag{2.13}$$

,

$$\mathbf{v}_j = [\gamma_{j1}, \gamma_{j2}, \ldots, \gamma_{j\alpha}]^T \tag{2.14}$$

(2.12) is valid only if $\mathbf{U}^T \overline{\mathbf{K}} \mathbf{U}$ is a Hermitian or a real matrix.

To apply the perturbation on a cyclic symmetric system, let us consider a cyclic symmetric rotor consisting of N identical substructures, each spanning an angle of $2\pi/N$ in the circumferential direction. For each vibration mode, let $\mathbf{W}^{(i)}(\mathbf{r})$ and $\mathbf{W}^{(i+1)}(\mathbf{r})$ denote the mode shape at the i-th and $(i+1)$-th substructures, respectively. According to [27], the mode shape at these two neighboring substructures differs by a constant phase angle; that is,

$$\mathbf{W}(\mathbf{r})^{(i+1)} = \mathbf{W}(\mathbf{r})^{(i)} e^{j 2\pi n/N}; \quad n \in (1, 2, 3, ..., N) \tag{2.15}$$

where j denotes an imaginary number and n is the phase index which characterize a vibration mode of a cyclic symmetric rotor.

Moreover, each mode shape of a perfectly cyclic symmetric rotor can be represented as a Fourier series in the circumferential direction as [27]

$$\mathbf{W}(\mathbf{r}) = \sum_{k=n+\mathbf{M}(N)} \mathbf{A}_k(r,z)e^{jk\theta} \tag{2.16}$$

where (r,θ,z) is the cylindrical system, $\mathbf{M}(N)$ denotes integer multiples of N and $\mathbf{A}_k(r,z)$ are the Fourier coefficients.

In a cyclic symmetric system, most of modes are a pair of complex conjugate with repeated eigenvalues. The discretized mode shape will be

$$\mathbf{u}_1 = [\sum_{k=n+\mathbf{M}(N)} \mathbf{A}_k(r,z)e^{jk\theta}, \sum_{k=n+\mathbf{M}(N)} \mathbf{A}_k(r,z)e^{j2k\theta}, \ldots, \sum_{k=n+\mathbf{M}(N)} \mathbf{A}_k(r,z)e^{jNk\theta}]^T \tag{2.17}$$

Then

$$\mathbf{u}_2 = [\sum_{k=n+\mathbf{M}(N)} \bar{\mathbf{A}}_k(r,z)e^{-jk\theta}, \sum_{k=n+\mathbf{M}(N)} \bar{\mathbf{A}}_k(r,z)e^{-j2k\theta}, \ldots, \sum_{k=n+\mathbf{M}(N)} \bar{\mathbf{A}}_k(r,z)e^{-jNk\theta}]^T \tag{2.18}$$

Assume $\overline{\mathbf{K}}$ has entries k_{nm}, where

$$k_{nm} = \begin{cases} 1, & \text{if } n = m = 2 \\ 0, & \text{otherwise.} \end{cases} \tag{2.19}$$

The first term in (2.20) becomes

$$\bar{\mathbf{U}}^T\overline{\mathbf{K}}\mathbf{U} = \begin{bmatrix} Z_0\bar{Z}_0, & \bar{Z}_0\bar{Z}_0 \\ Z_0Z_0, & Z_0\bar{Z}_0 \end{bmatrix} \tag{2.20}$$

, where $Z_0 = \sum_{k=n+\mathbf{M}(N)} \mathbf{A}_k(r,z)e^{j2k\theta}$ and $\bar{Z}_0 = \sum_{k=n+\mathbf{M}(N)} \bar{\mathbf{A}}_k(r,z)e^{-j2k\theta}$. Thus, the corresponding eigenvalues and eigenvectors for (2.20) will be

$$\lambda_1^{(1)} = 0, \text{and} \mathbf{v}_1 = \begin{bmatrix} 1 \\ -\frac{Z_0}{\bar{Z}_0} \end{bmatrix} \tag{2.21}$$

and

$$\lambda_2^{(1)} = 2Z_0\bar{Z}_0, \text{and} \mathbf{v}_2 = \begin{bmatrix} 1 \\ \frac{Z_0}{\bar{Z}_0} \end{bmatrix} \tag{2.22}$$

Then, the zeroth order of eigenvector in (2.10) will be

$$\mathbf{u}_1^* = 1\mathbf{u}_1 - \frac{Z_0}{\bar{Z}_0}\mathbf{u}_2 = \frac{\bar{Z}_0\mathbf{u}_1 - Z_0\bar{\mathbf{u}}_1}{\bar{Z}_0} = j\frac{2}{\bar{Z}_0}\mathrm{Im}(\bar{Z}_0\mathbf{u}_1) \tag{2.23}$$

, and

$$\mathbf{u}_2^* = 1\mathbf{u}_1 + \frac{Z_0}{\bar{Z}_0}\mathbf{u}_2 = \frac{\bar{Z}_0\mathbf{u}_1 + Z_0\bar{\mathbf{u}}_1}{\bar{Z}_0} = \frac{2}{\bar{Z}_0}\mathrm{Re}(\bar{Z}_0\mathbf{u}_1) \tag{2.24}$$

This simple derivation shows that when mistuning is present, mode shapes will only change at the first or higher orders of perturbation for the case of a signle mode or a pair of repeated modes. Although the zeroth order of mistuned mode shapes for the repeated mode is recalculated as the linear combination of the original mode shapes, the linear combination of repeated modes will not form different mode shapes but only change the phase angles. To make mistuned mode shape change dramatically from the tuned mode shapes, the change must occur at the zeroth order. Hence, a group of tuned modes must contain different mode shapes with nearly identical natural frequencies. When mistuning is present, this group of tuned modes can linear combine with each other to form the zeroth order of mistuned mode shapes.

2.2.2 Fourier Analysis of Model Localization

As an extreme case, mode localization is modeled as a Fourier series approximation of the Delta function centered at $\theta = a$, where θ is the parameter in circumferential direction. Hence,

$$\delta(\theta - a) = \frac{1}{2\pi} + \frac{1}{\pi}\left[\sum_{n=1}^{\infty}\cos(na)\cos(n\theta) + \sin(na)\sin(n\theta)\right] \tag{2.25}$$

As reasoned in the hypothesis, a localized mode shape results from linearly combining the tuned vibration modes whose natural frequencies are nearly identical. Equation (2.25) further imposes another condition on these tuned modes. Basically, (2.25) implies that mode localization requires participation of many tuned mode shapes with a wide range of wave numbers n in the circumferential directions. In other words, the tuned mode shapes must form some sort of a complete set in order to form

a Delta function through linear combinations. Moreover, the coefficients in (2.25) do not diminish as n increases. This implies that the contribution of each tuned mode shape in the complete set must be large enough for a wide range of n.

This simple Fourier analysis in (2.25) helps answer several questions regarding why mode localization occurs. The first question is, "*why is mode localization phenomenon only present in nearly cyclic symmetric rotors but not in axisymmetric systems*?"

The answer lies in mode shape structures of the tuned cyclic symmetric rotor. Equation (2.16) shows that the mode shape in a cyclic symmetric system with phase index n has not only wave number n but also higher harmonics $n\pm N$, $n\pm 2N$, $n\pm 3N$, and so on. So if a group of vibration modes contains every phase index n from 1 to N, this group of vibration modes will have all the wave numbers needed in (2.25) to form the Delta function. If the vibration modes in the group happen to have nearly identical natural frequencies, small mistuning will linearly combine these modes to realize localization.

In contrast, each mode shape of axisymmetric systems only contains one harmonic in the circumferential direction. It is now obvious why axisymmetric rotors cannot present the phenomenon of mode localization. The axisymmetry mandates that such rotors will only have $\cos n\theta$ and $\sin n\theta$ modes with repeated frequencies but not higher harmonics. Therefore, axisymmetric rotors do not possess a large group of vibration modes that have nearly identical natural frequencies and simultaneously cover a wide range of wave number n.

The second question is, "*why does mode localization tend to occur when the number of substructures N of the cyclic symmetric rotor is large*?"

The answer lies in the fact that Fourier coefficient $\mathbf{A}_k(r,z)$ in (2.16) decreases as k increases to cover higher and higher wave numbers from the cyclic symmetry. Let us consider a case when N is small, say $N = 3$. Also, there is a group of 3 modes with nearly identical natural frequencies. Moreover, these 3 modes have phase indices $n = 1, 2, 3$. The first mode with $n = 1$ has mode shape with Fourier coefficients

$\mathbf{A}_p(r,z)$ with circumferential wave numbers $p \in 1,4,7,\ldots$. Since $p > 1$ corresponds to a higher harmonic, the magnitude of $\mathbf{A}_4(r,z)$, $\mathbf{A}_7(r,z)$, ... is significantly smaller than $\mathbf{A}_1(r,z)$. Similarly, the second mode with $n = 2$ will have Fourier coefficients $\mathbf{A}_q(r,z)$, where $q \in 2,5,8,\ldots$, with circumferential wave numbers $q > 2$ being the higher harmonics. The third mode with $n = 3$ will have Fourier coefficients $\mathbf{A}_l(r,z)$, where $l \in 3,6,9,\ldots$ with circumferential wave numbers $l > 3$ being the higher harmonics.

When small mistuning is present, these 3 modes will be linearly combined in some manners to form new mode shapes. Linear combinations of these 3 modes, of course, will give all the wave numbers needed in (2.25), i.e., $k = 1,2,3,\ldots$. Nevertheless, the Fourier coefficients from the linear combinations will start to diminish beyond the third term, because $\mathbf{A}_k(r,z)$ with $k = 4,5,6,\ldots$ result from the higher harmonics. This contradicts with the observation in (2.25), where the Fourier coefficients of a Delta function remain on the same order as the wave number k increases. Therefore, the linear combinations will not be able to mimic a Delta function when number of substructure N is small.

In contrast, if N is large (say $N = 36$), linear combinations of this group of N modes will have a large number of Fourier coefficients on the same order, thus approximating a Delta function (or an impulse-like function) with much higher fidelity. Therefore, one will need large N to observe the phenomenon of mode localization.

The third question is, "*how does veering of eigenvalue loci contribute to mode localization*?"

The answer is that vibration modes near a veering of eigenvalue loci may or may not contribute to mode localization depending on their mode shapes. Now let us consider the case of a group of N modes, where N is large enough, with phase indices $n = 1,2,...,N$ and nearly identical natural frequencies. Let us call this group G. Although linear combinations of group G modes may create a Fourier series that contain all wave numbers with Fourier coefficients of roughly the same order, convergence of the Fourier series to an impulse-like distribution will only occur in the circumferential

direction. In other words, the Fourier coefficients $\mathbf{A}_k(r, z)$ of group G modes will determine the localized mode shape in the radial and axial directions.

If eigenvalue loci diverge, additional modes appear at the divergence location. The natural frequencies of the additional modes are similar to those of the group G modes. Let us call these additional modes at the divergence as group V. If group V modes and group G modes have similar $\mathbf{A}_k(r, z)$—for example, group G modes have torsional vibration and group V modes have half torsional and half out-of-plane vibration—their modes can interfere and yield adjusted resulting mode shapes. Hence, group V modes contribute to mode localization.

On the contrary, if group V modes and group G modes have very different $\mathbf{A}_k(r, z)$—for example, group G modes have in-plane vibration and group V modes have out-of-plane vibration—the presence of group V modes tends to drastically change the localized mode shape formed by the group G modes in the r and z directions. However, the number of group V modes is too small to result in a Delta function of their own. In this case, group V modes do not contribute to the mode localization.

Throughout the entire Fourier analysis above, a subtle mathematical condition was implicitly assumed, that is, $\mathbf{A}_1(r, z)$, $\mathbf{A}_2(r, z)$, ..., $\mathbf{A}_N(r, z)$ are about the same order, where N is the number of substructures. This condition must be satisfied for a region R inside the domain of the cyclic symmetric rotor. (For example, R could be the region consisting of all the blades in a disk-blade system.) Then these N modes will have enough wave numbers to mimic the Delta function and realize mode localization inside the region R of the cyclic symmetric rotor. Since $\mathbf{A}_k(r, z)$, $k = 1, 2, \ldots, N$, are functions of r and z, there may not exist a region R in which $\mathbf{A}_1(r, z)$, $\mathbf{A}_2(r, z)$, ..., $\mathbf{A}_N(r, z)$ are about the same order. If so, what happens?

Let us consider the following scenario for instance: a bladed disk system with 24 blades (i.e., $N = 24$). In addition, the bladed disk system has 24 vibration modes that have nearly identical natural frequencies and span all phase indices from 1 to 24. Moreover, 10 of the 24 modes have mode shapes dominated by blade deformation and

the rest 14 modes have mode shapes dominated by disk deformation. Let R be the region consisting of all 24 blades. For $(r, z) \in R$, the corresponding $\mathbf{A}_k(r, z)$ of the 10 blade-dominated modes will be much larger than that of the 14 disk-dominated modes. Since $\mathbf{A}_k(r, z)$, $k = 1, 2, \ldots, N$, are not on the same order, linear combinations of these 24 modes will not lead to a genuine localized mode in R to mimic the Delta function in (2.25).

From the Fourier analysis, curve veering is not a key factor contributing to mode localization in the following ways. First, mode localization will not occur at a point where eigenvalue loci veer, if the conditions in the hypothesis are not met. Second, when mode localization does occur, not every vibration mode involved in eigenvalue veering contributes significantly to the mode localization. Note that the statements above are valid for free vibration only. Curve veering may have significant influence on mode localization for forced vibration [28].

2.2.3 Rayleigh-Ritz Method

The Fourier analysis in the previous section supports the second condition of the hypothesis while a Rayleigh-Ritz approximation to be discussed in this section will support the first condition of the hypothesis. The Rayleigh-Ritz approximation also facilitates an efficient and effective reduced-order model to predict mode localization.

First of all, I use the tuned cyclic symmetric rotor as a nominal system like [11]. The tuned system has a stiffness matrix $\mathbf{K}$ and a mass matrix $\mathbf{M}$. I can then solve for natural frequencies and mode shapes, for example, using finite element methods. Unlike [11], I will not start from veering of eigenvalue loci when predicting mode localization. Instead, I look for a group of modes that have nearly identical natural frequencies [12]. Let us call this group T and denote its natural frequencies and mode shapes as ω_n and $\mathbf{u}_n$, with $n = 1, 2, ..., n_t$, where n_t is the number of modes in group

T. Moreover, the group T modes will satisfy the following eigenvalue problem.

$$\left(\mathbf{K} - \omega_n^2 \mathbf{M}\right) \mathbf{u}_n = \mathbf{0} \tag{2.26}$$

Also, the mode shapes $\mathbf{u}_n$ are orthonormal with respect to the mass matrix, i.e., $\mathbf{u}_m^T \mathbf{M} \mathbf{u}_n = \delta_{mn}$, where δ_{mn} is the Kronecker delta. Note that the group T modes may potentially include the group G modes and group V modes.

Now consider a nearly cyclic symmetric system with stiffness mistuning $\Delta\mathbf{K}$ and mass mistuning $\Delta\mathbf{M}$. Therefore, a localized mode shape $\mathbf{v}$ with a natural frequency λ should satisfy the eigenvalue problem

$$\left[\mathbf{K} + \Delta\mathbf{K} - \lambda^2 \left(\mathbf{M} + \Delta\mathbf{M}\right)\right] \mathbf{v} = \mathbf{0} \tag{2.27}$$

The group T modes will now serve as trial vectors for the Rayleigh-Ritz approximation. When mistuning is introduced, the group T modes will combine linearly to form the localized mode $\mathbf{v}$, i.e.,

$$\mathbf{v} = \sum_{k=1}^{n_t} a_k \mathbf{u}_k \tag{2.28}$$

where a_k is the contribution of each trial vector. Substitution of (2.28) into (2.27) and use of (2.26) result in

$$\left\{\text{diag}\left[\omega_1^2, \omega_2^2, \ldots, \omega_{n_t}^2\right] + \Delta\hat{\mathbf{K}} - \lambda^2 \left(\mathbf{I} + \Delta\hat{\mathbf{M}}\right)\right\} \mathbf{a} = \mathbf{0} \tag{2.29}$$

In equation (2.29), $\mathbf{a} \equiv (a_1, a_2, \ldots, a_{n_t})^T$ and $\Delta\hat{\mathbf{K}}$ and $\Delta\hat{\mathbf{M}}$ are defined as

$$\Delta\hat{\mathbf{K}} \equiv \mathbf{U}^T \Delta\mathbf{K}\mathbf{U}, \quad \Delta\hat{\mathbf{M}} \equiv \mathbf{U}^T \Delta\mathbf{M}\mathbf{U} \tag{2.30}$$

where

$$\mathbf{U} \equiv [\mathbf{u}_1, \mathbf{u}_2, \ldots, \mathbf{u}_{n_t}] \tag{2.31}$$

Now let us define a mean square frequency $\bar{\omega}^2$

$$\bar{\omega}^2 \equiv \frac{1}{n_t} \left(\omega_1^2 + \omega_2^2 + \cdots + \omega_{n_t}^2\right) \tag{2.32}$$

and a deviatoric matrix

$$\hat{\mathbf{D}} \equiv \text{diag}\left[\omega_1^2 - \bar{\omega}^2, \omega_2^2 - \bar{\omega}^2, \ldots, \omega_{n_t}^2 - \bar{\omega}^2\right] \tag{2.33}$$

Substitution of (2.32) and (2.33) into (2.29) results in

$$\left(\bar{\omega}^2\mathbf{I} + \hat{\mathbf{D}} + \Delta\hat{\mathbf{K}}\right)\mathbf{a} = \lambda^2\left(\mathbf{I} + \Delta\hat{\mathbf{M}}\right)\mathbf{a} \tag{2.34}$$

When $\Delta\hat{\mathbf{M}}$ is small,

$$\left(\mathbf{I} + \Delta\hat{\mathbf{M}}\right)^{-1} \approx \left(\mathbf{I} - \Delta\hat{\mathbf{M}}\right) \tag{2.35}$$

So the eigenvalue problem can be approximated as

$$\left\{\left(\bar{\omega}^2 - \lambda^2\right)\mathbf{I} + \hat{\mathbf{L}}\right\}\mathbf{a} = \mathbf{0} \tag{2.36}$$

where

$$\hat{\mathbf{L}} \approx \hat{\mathbf{D}} + \Delta\hat{\mathbf{K}} - \Delta\hat{\mathbf{M}}\left(\bar{\omega}^2\mathbf{I} + \hat{\mathbf{D}} + \Delta\hat{\mathbf{K}}\right) \tag{2.37}$$

Although Rayleigh-Ritz method has been used in FFM [12], the formulation in (2.36) and (2.37) is new and reveals several important mathematical insights.

First, the term $(\bar{\omega}^2 - \lambda^2)\,\mathbf{I}$ represent a group of n_t vibration modes of identical natural frequency $\bar{\omega}$. This directly support condition 1 of the hypothesis. Therefore, any perturbation will linearly combine the unperturbed mode shapes, which correspond to $\mathbf{u}_1$, $\mathbf{u}_2$, …, $\mathbf{u}_{n_t}$. And the combinations of this group of modes will contain lots of phase indices. This supports condition 2 of the hypothesis.

Second, $\hat{\mathbf{L}}$ represents an equivalent perturbation to the n_t modes of the identical natural frequency $\bar{\omega}$. According to (2.37), the perturbation consists of two sources. One is $\hat{\mathbf{D}}$, which represents coupling among substructures. The other is $\Delta\hat{\mathbf{K}}$ and $\Delta\hat{\mathbf{M}}$, which represents the mistuning in stiffness and mass. When the coupling is too strong, $\hat{\mathbf{D}}$ becomes very big causing the n_t modes to become distinct. Since these n_t modes are no longer repeated, their mode shapes will not be linearly combined when the mistuning is introduced. (This happens only because $\hat{\mathbf{D}}$ is diagonal.) When

the coupling is about as strong as the mistuning, $\hat{\mathbf{D}}$, $\Delta\hat{\mathbf{K}}$ and the term associated with $\Delta\hat{\mathbf{M}}$ will have the same order; therefore, the repeated n_t mode shapes are linearly combined to form localized modes. This agrees with current observation in the literature, e.g., [14].

It is also very easy to find out whether or not $\hat{\mathbf{D}}$ is dominant. $\hat{\mathbf{D}}$ is a diagonal matrix. In contrast, $\Delta\hat{\mathbf{K}}$ and the term associated with $\Delta\hat{\mathbf{M}}$ are full matrices. Therefore, comparison of the diagonal and off-diagonal elements of $\hat{\mathbf{L}}$ can lead to a quick evaluation whether or not $\hat{\mathbf{D}}$, $\Delta\hat{\mathbf{K}}$ and the term associated with $\Delta\hat{\mathbf{M}}$ are of the same order. Since the number of trial vectors n_t is small, the calculation of $\hat{\mathbf{L}}$ is easy and straightforward.

Finally, spectral perturbation theories indicate that eigenvalues and eigenvectors of matrix $\hat{\mathbf{L}}$ will determine natural frequencies and mode shapes of the localized mode. Therefore, the matrix $\hat{\mathbf{L}}$ can be used to identify which modes will actively participate in mode localization. For example, if all entries of $\hat{\mathbf{L}}$ are uniformly small for $\mathbf{u}_3$, it implies that $\mathbf{u}_3$ does not contribute to $\hat{\mathbf{L}}$ that perturbs the n_t modes with repeated natural frequency $\bar{\omega}$. Therefore, $\mathbf{u}_3$ will have no significant role in mode localization. Inspection of $\hat{\mathbf{L}}$ then provides an effective and efficient way to formulate a reduce-order model for mode localization.

Chapter 3
NUMERICAL EXAMPLES

In this section, I use a bladed disk model in Fig. 3.1 to verify our hypothesis and demonstrate the mathematical insights conceived in Chapter 2. Our numerical model consists of 24 identical sectors; therefore, the tuned system has 24 phase indices ranging from 1 to 24. The circular disk has an outer diameter of 1200 mm, an inner diameter of 200 mm, and a thickness of 50 mm. The blades have a length of 200 mm, a width of 80 mm, and a thickness of 20 mm. A fixed boundary condition is imposed at the inner rim while the 24 blades are evenly attached to the outer rim and are subjected to a free boundary condition. Finite element methods are used to calculate all natural frequencies and mode shapes. [1]

3.1 Convergence Test for The Finite Element Model

The finite element model in Fig. 3.1 is established after convergence test. The convergence test considers different mesh patterns on blade and disk with many combinations. To save some space, Figure 3.2 shows five representative examples of mesh pattern on a blade and on disk of a half substructure. The disk mesh becomes finer from Fig. 3.2(a) to (e) and the finest mesh in Fig. 3.2(e) is considered to be the baseline which contains 84048 nodes for the complete bladed disk. Convergence tests are considered for disk-dominant modes and blade-dominant modes separately. For disk-dominant modes, the natural frequencies of the first out-of-plane mode and in-plane mode are used to calibrate and normalized to the natural frequencies of the finest model. As shown in Figure 3.3, normalized natural frequencies of both modes con-

[1] Please refer to Appendix A for building and solving finite element model in ANSYS.

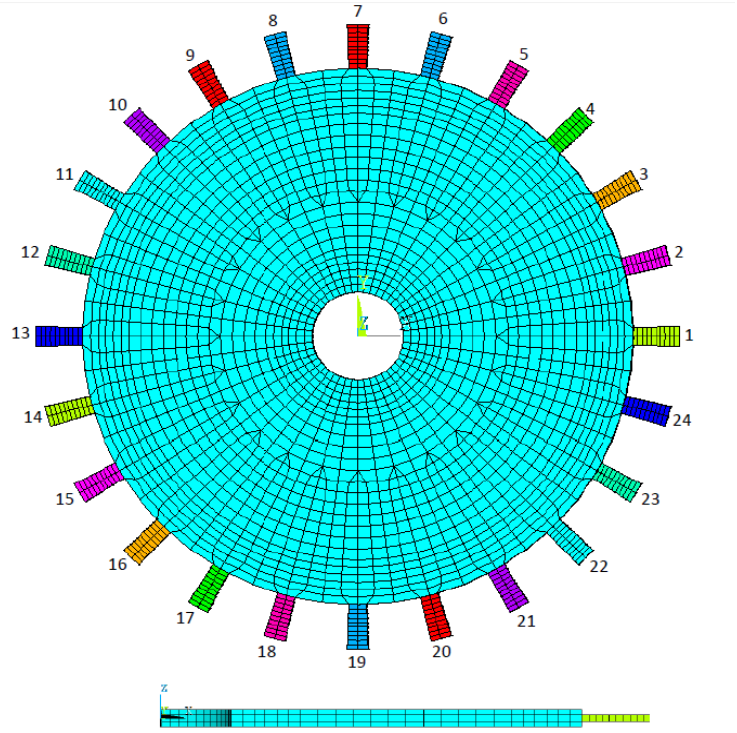

Figure 3.1: Finite element model of a cyclic symmetric rotor

verge to less than 1.1, which means 1ess than 10% error, at mesh pattern (c). Fig. 3.3 also indicates that the natural frequency of the out-of-plane mode changes more than the in-plane mode and the mesh does affect solved natural frequencies significantly.

For blade-dominant modes, the natural frequencies of the first in-plane mode and the first torsional mode are used to calibrate for different blade meshes. In Fig. 3.2, the coarsest mesh to the finest mesh on blade are corresponding to plots (a), (d), (b), (c), and (e), respectively, so as the label of x-axis in Fig. 3.4. Fig. 3.4 also shows the natural frequencies normalized to the natural frequency of the finest model, and the natural frequencies of both in-plane mode and torsional mode change obviously. For blade-dominant modes, natural frequencies converge to less than 1.1 at mesh pattern (b). For the sake of computation cost, I do not choose the finest mesh in our

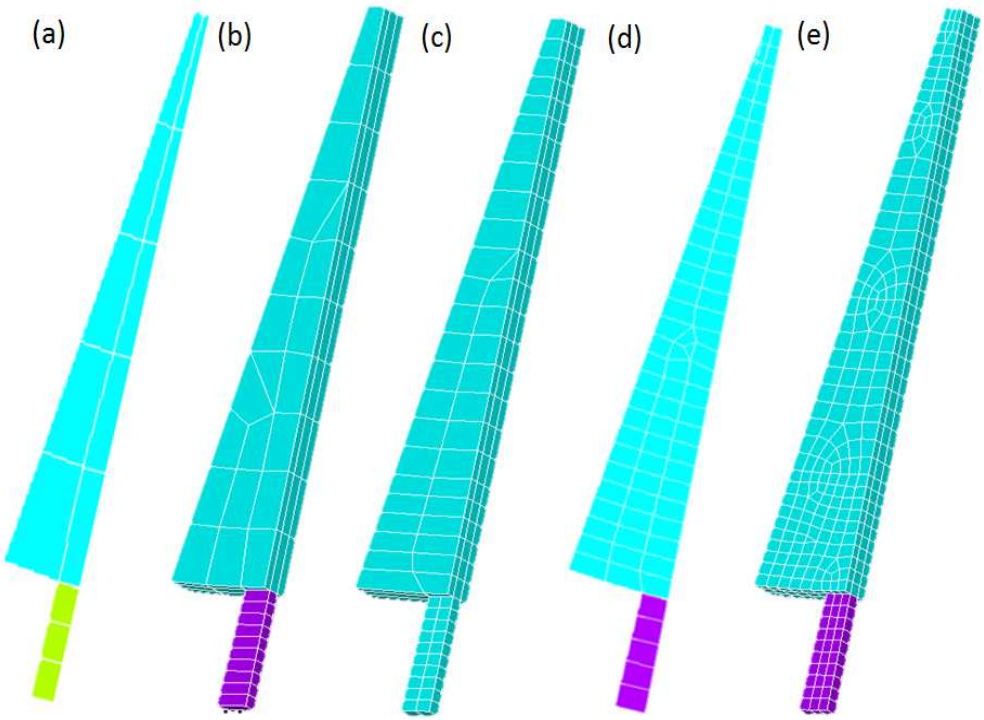

Figure 3.2: Examples of different mesh on blade and disk of a half substructure

convergence test. I choose the mesh pattern (c) for disk and mesh pattern (b) for blade instead. The error of natural frequency of all modes of interest in this thesis is less than 10% compared to the natural frequencies solved by the finest model.

3.2 Tuned System

The material of the bladed disk is Nickel Alloy with density of 855 kg/m^3 and Young's modulus of 85 GPa. Figure 3.5 shows the natural frequencies of the tuned system with respect to the number of nodal diameters. [2] A simple way to construct eigenvalue loci is to connect the natural frequencies from low to high frequencies through all

[2]Please refer to Appendix B for obtaining phase index for each mode from model blade displacements.

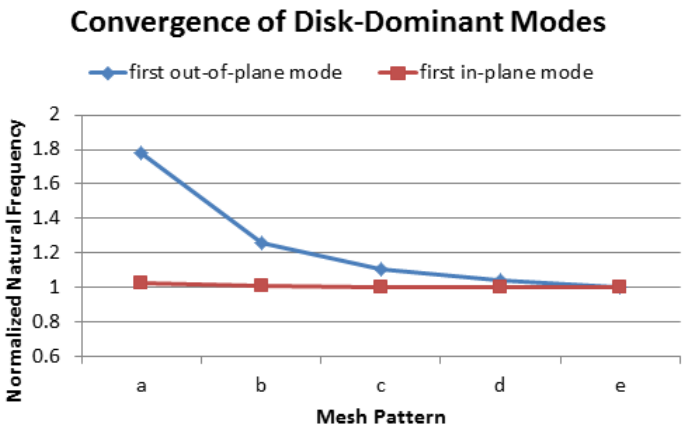

Figure 3.3: Examples of different mesh on blade and disk of a half substructure

numbers of nodal diameters as shown in Fig. 3.5.

Although the eigenvalue loci in Fig. 3.5 are easy to construct, they do not bear any physical insights. Another way to construct eigenvalue loci is to inspect mode shape associated with each natural frequency and connect modes that have similar mode shape characteristics (i.e. $A_k(r, z)$ in (2.16)). Figure 3.6 shows such an eigenvalue plot. In Fig. 3.6, the legend of each line shows the characteristics of the family of modes. The legend is coded in three words. The first word indicates the dominating part of the mode shapes. For example, D represents that the disk deformation dominates the mode shapes while B represents that blade deformation dominates the mode shapes. The second word indicates whether the mode shapes have out-of-plane displacement (out) or in-plane displacement (in) over the disk-blade system. The third word shows the number of nodal circles or if the modes have torsional, radial (r) or circumferential (theta) vibration. The advantage of this approach to construct eigenvalue loci is its clear physical meaning of each eigenvalue locus, thus allowing us to understand what types of modes are participating in a localized mode.

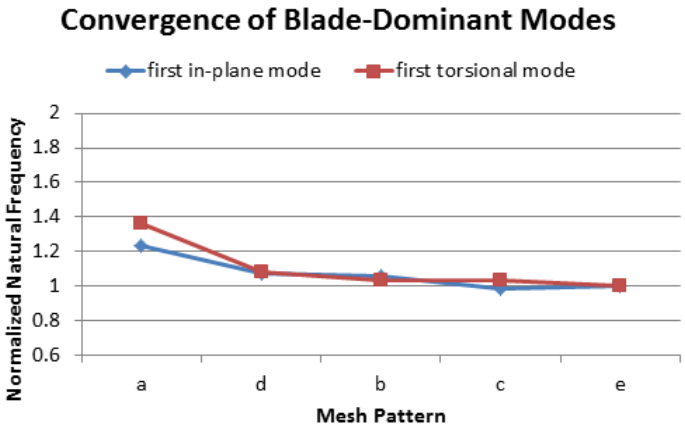

Figure 3.4: Examples of different mesh on blade and disk of a half substructure

In addition, there are several things worth noting in Fig. 3.5 and Fig. 3.6. First, the cyclic symmetry guarantees that two modes of phase indices n and $N-n$ will have the same eigenvalue. Therefore, these two modes cannot be distinguished in Fig. 3.5, but they are marked in Fig. 3.6 for distinction. Black numbers around each point represent the mode numbers of each point in Fig. 3.6 which is sorted by ascending natural frequencies. Also, as a result of the geometry of this bladed disk model, it turns out that modes with phase indices n and $N-n$ both have n nodal diameters. Therefore, the eigenvalue plot in Fig. 3.5 and Fig. 3.6 only needs to include up to 12 nodal diameters.

Second, there are two eigenvalue loci that are nearly horizontal and cover all number of nodal diameters in Fig. 3.5. One is around 800 Hz and the other around 1100 Hz. According to Fig. 3.6, these two groups of modes are B-in-0 family and B-out-torsion family, respectively. Within each group of vibration modes, natural frequencies are nearly identical and the modes contain all 24 phase indices. According to our hypothesis, these two groups of modes are likely candidates to present mode

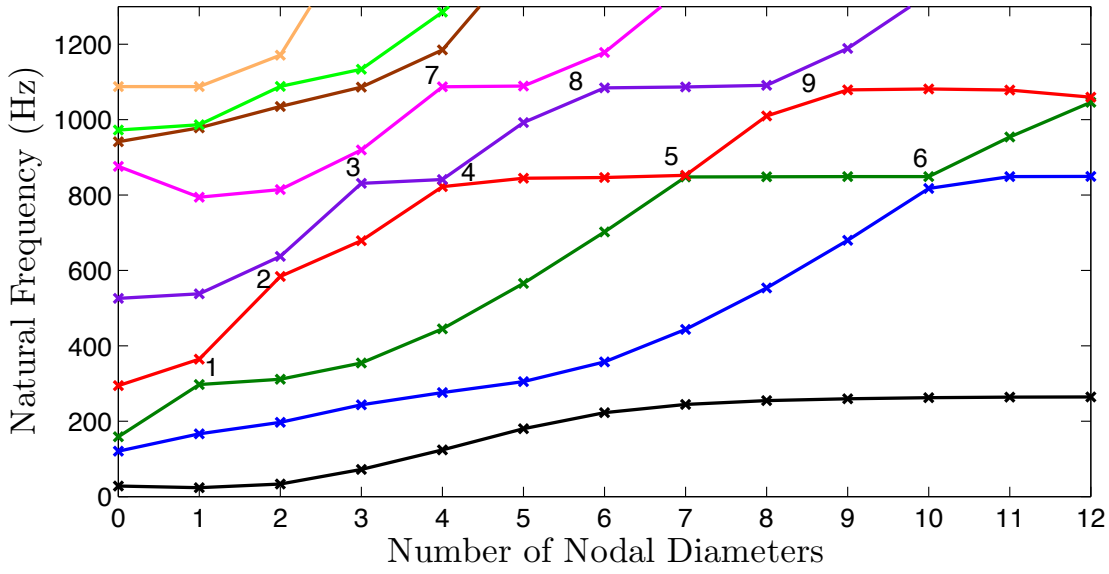

Figure 3.5: Discrete eigenvalue (natural frequency) loci

localization.

3.2.1 Characteristics of Mode Shapes

Figure 3.7 illustrate the characteristics of each family by showing the contour plots of 1-nodal-diameter modes in each family. For example, D-out-0 family indicates that mode shapes of this family have primarily out-of-plane, disk vibration with zero nodal circle. In the top left plot of Fig. 3.7, the contour lines are mostly shown in disk part without any nodal circle. It also has no obvious deformation in x-y plane which imply the displacement is in the out-of-plane direction. For another example, the top right plot in Fig. 3.7 has no contour lines in disk part but blades and deformation of each blade is shown in the x-y plane. This shows that the displacement of this mode shape is dominated on blades and has in-plane motion which is corresponding to the family legend, B-in-0.

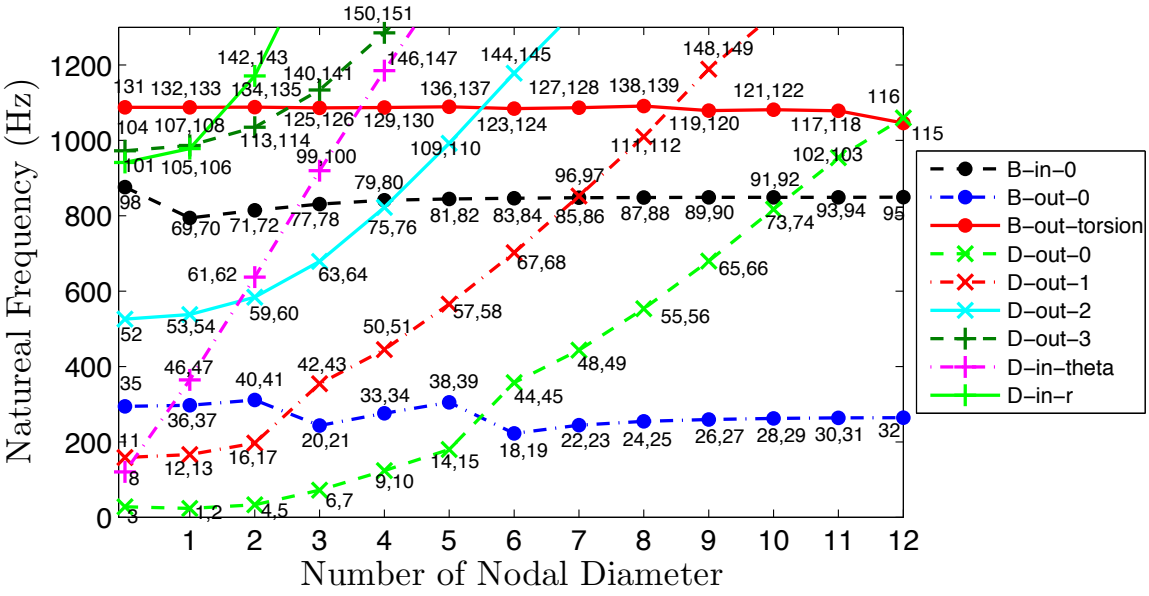

Figure 3.6: Family map of the cyclic symmetric system

As mentioned in Chapter 2, a mode shape of a tuned cyclic symmetric system not only contain the fundamental harmonic but also higher harmonics (cf. (2.16)). Figure 3.8 (a), (b), and (c) show the fast Fourier transform of the mode shape of the tuned mode 63 in $x-$, $y-$, and $z-$direction, respectively. Figure 3.8(d) shows Euler norm the nodal displacement of the tuned mode 63. Since the tuned mode 63 is an disk-dominant, so the magnitude of $\mathbf{A_k}(r,z)$ is obvious for $r \subset [200, 1200](mm)$ associated to the disk part. There are two lower sites of $\mathbf{A_k}(r,z), for r \subset [200, 1200]$ which is corresponding to the signature of 2-nodal-circle.

The tuned mode 63 is also an out-of-plan, 3-nodal-diameter mode, the highest $\mathbf{A_k}(r,z)$ is shown in the $z-$direction at $k = 3, 21, 27$. Since modes with phase indices n and $N - n$ are repeated modes and their mode shapes are complex conjugate in complex domain. When the mode shapes of this repeated modes convert to real domian, the mode shapes will be the real part and the imaginary part of complex form of the mode shapes and contain both phase indices. This is why the mode shape

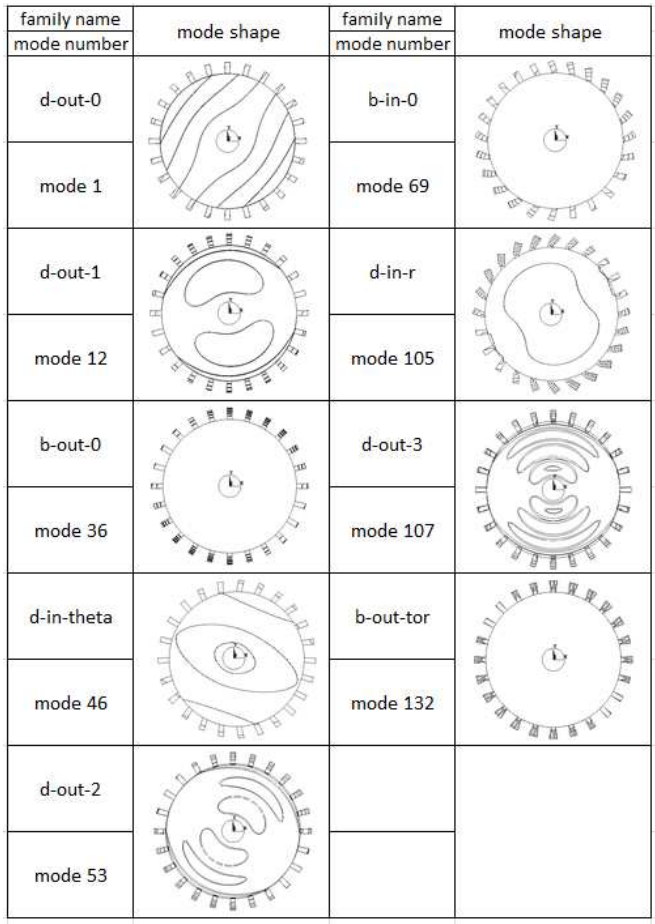

Figure 3.7: Contour plot of mode shapes with 1 nodal diameter

shown in Fig. 3.8 have $k = 3and21(24-3)$. The harmonic of $k = 27$ is the higher harmonic of $k = 3(3+24)$.

Figure 3.9 shows $\mathbf{A_k}(r,z)$ and the mode shape fo mode 127 in the same way as Fig. 3.8. Since mode 127 is an out-of-plane with 7 nodal diameters mode, the maximum of $\mathbf{A_k}(r,z)$ is shown in $z-$direction for $k = 7, 17(24-7), 31(24+7)$. Because mode 127 is a blade dominant mode, the magnitude of $\mathbf{A_k}(r,z)$ is very small for $r \subset [200, 1200]$.

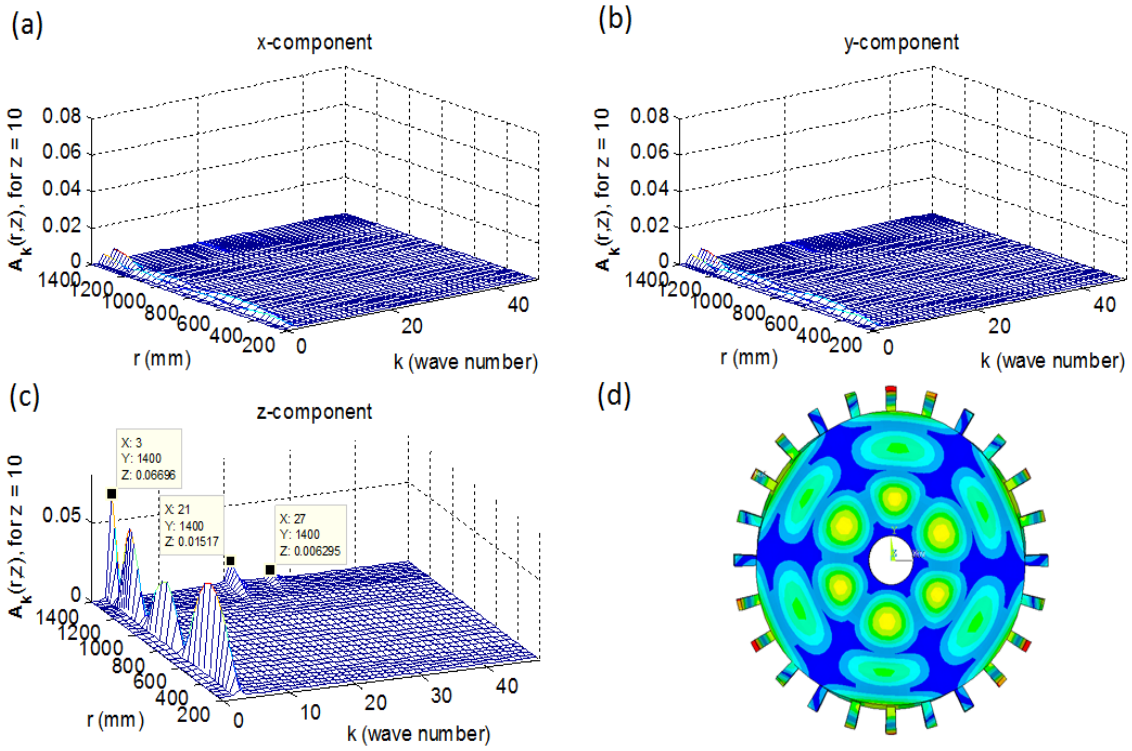

Figure 3.8: FFT of the tuned mode 63 in D-out-2 family

3.2.2 Eigenvalue Loci Veering

There are many sites in Fig. 3.5 that presents curve veering, and they are labeled in numbers. Moreover, vibration modes (denoted by their mode numbers) participating at each curve veering site are listed in Table 3.1 for future reference. For example, there are two points at veering site 1 in Fig. 3.5. According to Table 3.1, the lower point represents a pair of repeated modes 36 and 37. The higher point at veering site 1 corresponds to repeated modes 46 and 47. Modes 46 and 47 have higher natural frequency than modes 36 and 37 because the modes are labeled with ascending natural frequencies.

Table 3.1: Mode numbers at veering sites

Veering Site	Mode Numbers
1	36,37,46,47
2	59,60,61,62
3	77,78,99,100
4	75,76,79,80
5	85,86,96,97
6	73,74,91,92
7	129,130,146,147
8	123,124,144,145
9	111,112,138,139

Table 3.2: Frequency ranges around frequency veerings

	Centered Frequency(Hz)	Range (Hz)	Mode Numbers in the Range	Number of Modes	Number of Selected Modes
a	332.6	282.7 $\sim$ 382.5	35 $\sim$ 47	13	0
b	611.0	519.4 $\sim$ 702.7	52 $\sim$ 68	17	0
c	839.9	714.0 $\sim$ 966.0	69 $\sim$ 103	35	24
d	1083.8	921.2 $\sim$ 1246.4	101$\sim$149	49	24

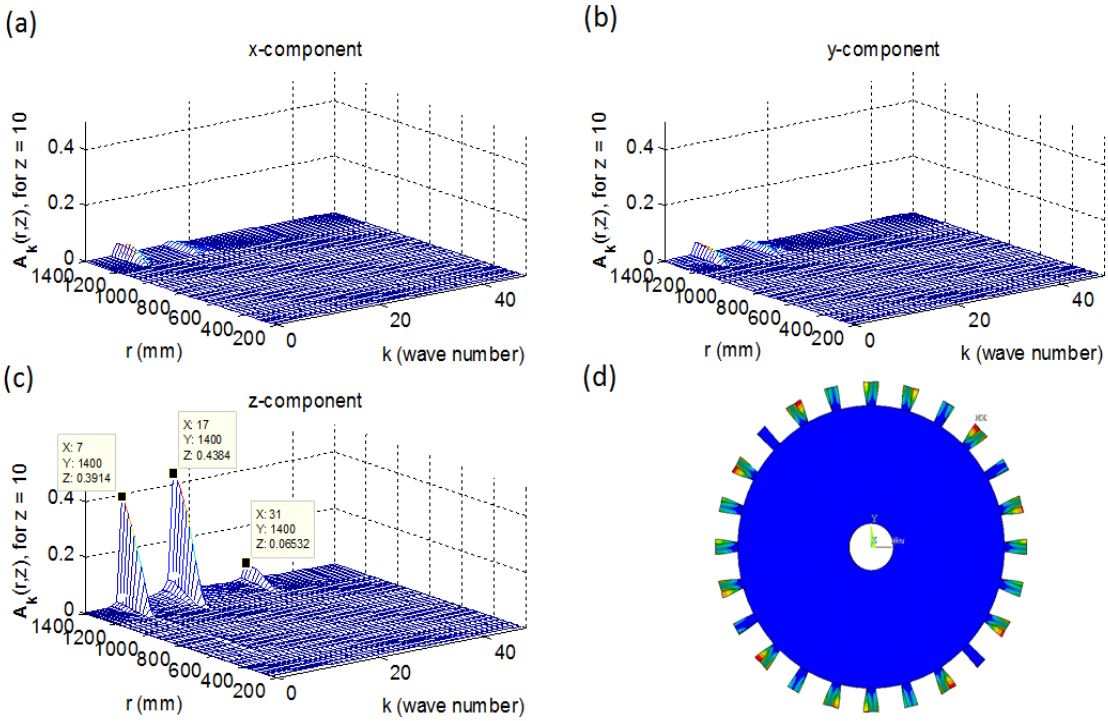

Figure 3.9: FFT of the tuned mode 127 in B-out-torsional family

Moreover, the nine curve veering sites locate roughly in four frequency bands. Table 3.2 lists the frequency region and the number of modes falling in these four bands in columns 2 and 3. The frequency regions are defined as ±15% centered at a curve veering frequency. Ranges (a) and (b) correspond to curve veering sites 1 and 2, respectively. In each of these two sites, the veering frequency is the average natural frequencies of the modes in Table 3.1. Range (c) includes veering sites 3, 4, 5 and 6. The veering frequency is chosen as the average frequency of B-in-0 family of modes. Range (d) includes veering sites 7, 8 and 9. The veering frequency is chosen as the average frequency of B-out-torsional family of modes.

Table 3.3: Mistuning for the numerical examples

Mistuning (%)	Set 1	Set 2	Set 3	Set 4
Source	Young's Modulus	Young's Modulus	Young's Modulus	Density
Blade Number	Pattern 1 SD 2.7%	Pattern 1 SD 5%	Pattern 2 SD 5%	Pattern 2 SD 5%
1	4.960	9.185	2.133	2.133
2	-0.875	-1.620	-3.607	-3.607
3	-5.306	-9.826	8.022	8.022
4	-0.011	-0.020	1.560	1.560
5	-3.685	-6.824	9.070	9.070
6	3.339	6.183	0.547	0.547
7	6.581	12.187	3.057	3.057
8	-0.190	-0.352	8.180	8.180
9	1.455	2.695	-0.163	-0.163
10	-1.140	-2.122	7.517	7.517
11	-0.050	-0.092	-3.759	-3.759
12	-0.029	-0.053	1.987	1.987
13	0.743	1.376	-5.220	-5.220
14	1.377	2.551	2.728	2.728
15	-2.861	-5.298	4.062	4.062
16	-0.762	-1.412	-1.634	-1.634
17	-1.652	-3.059	7.351	7.351
18	-1.399	-2.590	2.009	2.009
19	-1.188	-2.199	-5.800	-5.800
20	-0.408	-0.756	-3.435	-3.435
21	-2.500	-4.630	-10.730	-10.730
22	-1.416	-2.622	2.970	2.970
23	0.854	1.581	3.010	3.010
24	-4.441	-8.224	-1.301	-1.301

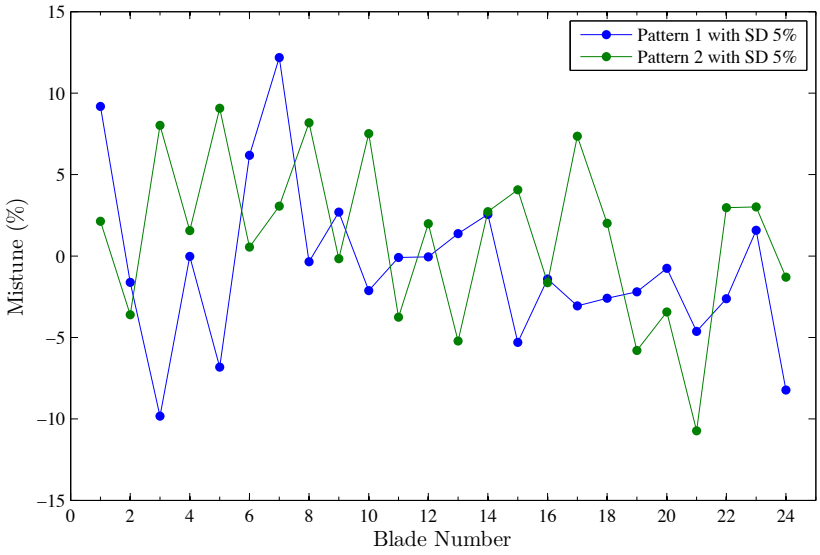

Figure 3.10: Mistuning patterns with standard deviation 5%

3.3 Mistuned Systems

3.3.1 Mistuning Configurations

In the following subsections, I will verify our hypothesis and theoretical analysis by using four sets of mistunes configurations listed in Table 3.3. The four configurations are combination of mistuning source, mistuning pattern, and amount of mistune. The mistuning source includes mistuning in Young's modulus and density to each blade. There are two mistuning patterns as shown in Fig. 3.10 with the corresponding blade numbers labeled in Fig. 3.1. The mistuning patterns are generated from random numbers. The amount of mistuning is either 2.7% or 5% standard deviation of the mistuning patterns.

3.3.2 Mistuning Set 1

Set 1 of numerical analysis consists of mistuning pattern 1, 2.7% standard deviation, and variation in Young's modulus to each blade. The finite element model is refreshed to generate the mistuning component $\Delta\mathbf{K}$. [3] In addition, natural frequencies λ and mode shapes $\mathbf{v}$ are calculated for the refreshed finite element model to look for mode localization. In the meantime, tuned mode shapes $\mathbf{u}_k$ in each frequency region of Table 3.2 are assembled to form the modal matrix $\mathbf{U}$. [4] Then the mistuning component $\Delta\hat{\mathbf{K}}$ can be calculated for the four regions in Table 3.2. Similarly, the deviatoric component $\hat{\mathbf{D}}$ is also calculated by equating $\bar{\omega}$ to the central frequency listed in Table 3.2. Finally, the matrix $\hat{\mathbf{L}}$ can be calculated via (2.37).

Figure 3.11(a) shows matrix $\hat{\mathbf{L}}$ for region (a). The abscissa and ordinate are the mode numbers involved in the region. Therefore, each abscissa and ordinate pair represents an element in the matrix $\hat{\mathbf{L}}$. Moreover, magnitude of each element of $\hat{\mathbf{L}}$ is represented via the color denoted in the color bar. Black and red indicate large magnitude, while light yellow and white indicate small magnitude. By doing so, the contents of matrix $\hat{\mathbf{L}}$ are presented visually in terms of colors. For the rest of the thesis, this presentation will be called "the visual method." [5]

For Fig. 3.11(a), major colors (i.e., black and red) show up in the diagonal elements and almost no color show up in the off-diagonal elements. This implies that the diagonal components from $\hat{\mathbf{D}}$ are significantly larger than the off-diagonal components from $\hat{\mathbf{K}}$. Based on the theoretical analyses above, region (a) will not present any mode localization, because it does not have enough number of modes to cover a wide range of phase indices and nor does it have the right order between the coupling (i.e., the

---

[3] Please refer to Appendix C for converting stiffness matrix from ANSYS output to MATLAB matrix

[4] Please refer to Appendix B for obtaining full mode shapes from ANSYS and refer to Appendix D for converting ANSYS output to modal matrix

[5] Please refer to Appendix E for plotting visual method

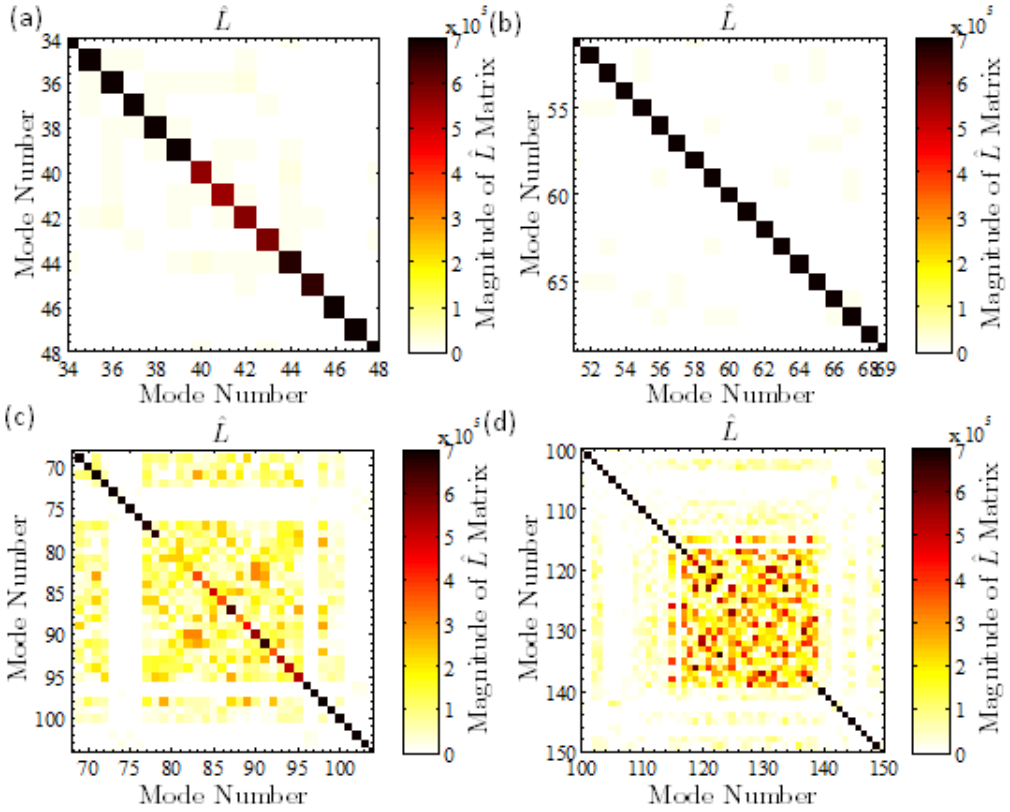

Figure 3.11: Visual method for frequency regions (a), (b), (c), and (d), respectively

diagonal terms) and the mistuning (i.e., the off-diagonal terms) to allow mode shape for linear combinations. The finite element simulation also confirms that there is no mode localization at curve veering site 1.

Figure 3.11(b) shows matrix $\hat{\mathbf{L}}$ for region (b). The situation is similar to that of region (a). All diagonal components are much bigger than the off-diagonal components except for two modes having the same number of nodal diameter. The low number of modes involved and the incorrect order prevent occurrence of localized modes. The finite element simulation also confirms that there is no mode localization at curve

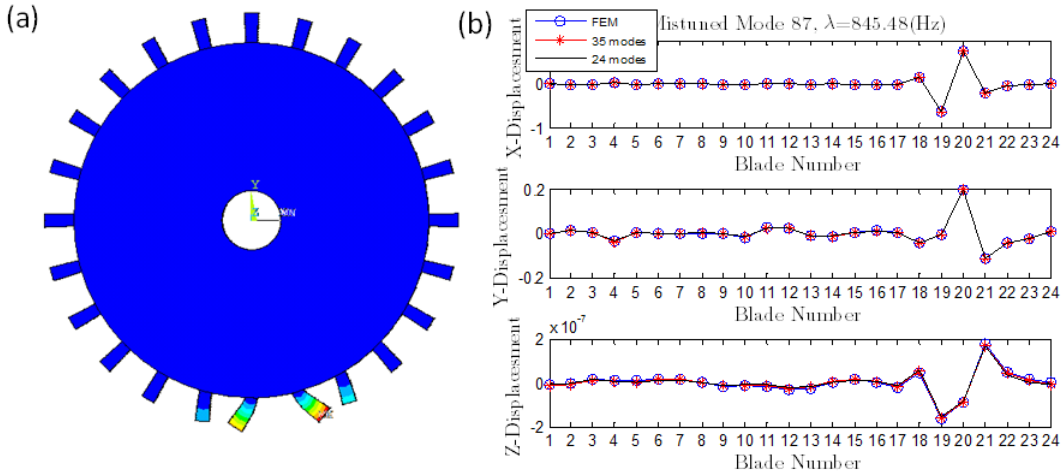

Figure 3.12: Mode shape of mistuned mode 87 in numerical analysis set 1

veering site 2.

Figure 3.11(c) shows matrix $\hat{\mathbf{L}}$ for region (c). The matrix shows that many diagonal and off-diagonal elements are of the same order. Also, some rows and columns contain small values with almost white color. These modes will not have significant contribution and can be eliminated from the mode localization calculations. In the end, the selected modes are modes 69∼72, 77∼95, and 98. The total number of these modes is 24 and it is listed in column 4 of Table 3.2.

From the discussion above, there is enough number of modes in frequency region (c) to incur mode localization. Moreover, the order of coupling and mistuning matches. Therefore, I expect to see mode localization in this frequency region.

The finite element analysis confirms the presence of mode localization in region (c). For example, Fig. 3.12(a) shows a localized B-in-0 mode shape for frequency region (c) as calculated from the finite element model with mistune. Figure 3.12(b) shows circumferential distribution of the same mode shape in the three orthogonal directions. Each plot actually contains three different curves. One is from the finite

element simulations with mistuning (denoted by "FEM"). One is from the Rayleigh-Ritz calculation (cf. (2.36)) with every mode in the frequency region retained (denoted by "35 modes"). The last is from the Rayleigh-Ritz calculation with reduced number of modes guided by matrix $\hat{\mathbf{L}}$ (denoted by "24 modes"). These three curves virtually coincide with one another indicating that the Rayleigh-Ritz approximation with reduced number of modes is very accurate.

The results are very interesting in several aspects. First, about one-fourth of the modes are eliminated. Only 24 modes are needed to predict localization, and the number 24 is exactly the number of substructures and the range of the phase index. Furthermore, the selected modes all come from the B-in-0 family in Fig. 3.6. Therefore, the selected modes have similar $\mathbf{A}_k(r, z)$, and contains the full range of the phase index. With Fig. 3.5 alone, it is very difficult to select proper modes to predict mode localization. In contrast, the matrix $\hat{\mathbf{L}}$ and the visual method offer an effective and efficient tool pinpointing the correct modes to predict mode localization. Second, modes 75, 76 at curve veering site 4, modes 96, 97 at curve veering site 5, and modes 73, 74 at curve veering site 6 are not needed to predict mode localization. As demonstrated in regions (a), (b), and (c), curve veering is not a critical factor contributing to mode localization for nearly cyclic symmetric rotors.

Figure 3.13(a), (b), (c) shows the fast Fourier transform for mistuned mode 87 in $x-$, $y-$, $z-$direction, respectively. Figure 3.13(d) shows the dominant displacement component in x-z plane to show containing wave numbers clearly. Since mistuned mode 87 is an blade dominant, in-plane mode, the major displacement is in x-direction and negligible magnitude of $\mathbf{A}_k(r, z)$ is shown for $r < 1200$. In Fig. 3.13(d), obvious magnitude of $\mathbf{A}_k(r, z)$ between $k = 5$ and $k = 20$ illustrates that a localized mode shape contains a wide range of phase indices.

Finally, Fig. 3.11(d) shows matrix $\hat{\mathbf{L}}$ for region (d). In a similar way, the selected modes in Fig. 3.11(d) are 115 and 117$\sim$139. Only 24 modes are needed to predict the mode localization. These 24 modes are all from the B-out-torsional family. Again,

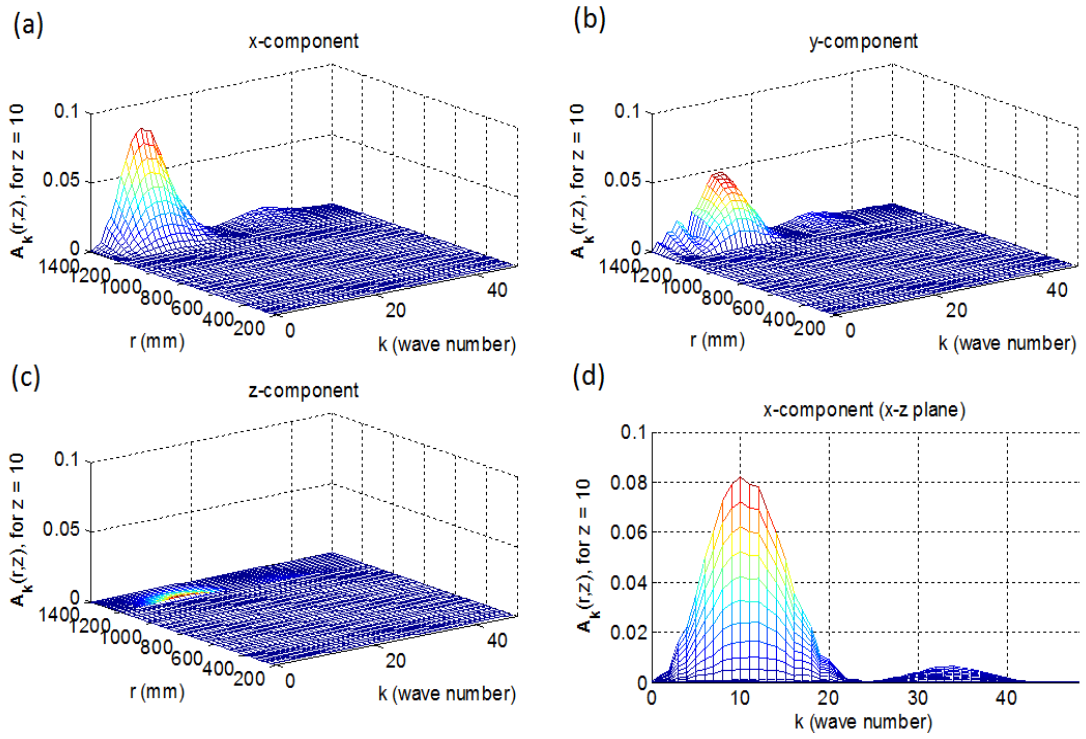

Figure 3.13: FFT of mistuned mode 87

I expect to see mode localization in frequency region (d). Also, not every mode involving in curve veering will participate in mode localization. For example, modes 111 and 112 at curve veering site 9 do not participate in mode localization, but modes 138 and 139 do.

The finite element analysis also confirms the theoretical predictions. Figure 3.14(a) shows a localized B-out-torsional mode shape for frequency region (d) as calculated from the finite element model with mistune. Figure 3.14(b) shows circumferential distribution of the same mode shape. Each plot also contains three curves as in Fig. 3.12(b). That is, "FEM" represents prediction by the finite element analysis, "49 modes" represents prediction by all modes in region (d), and "24 modes" represents

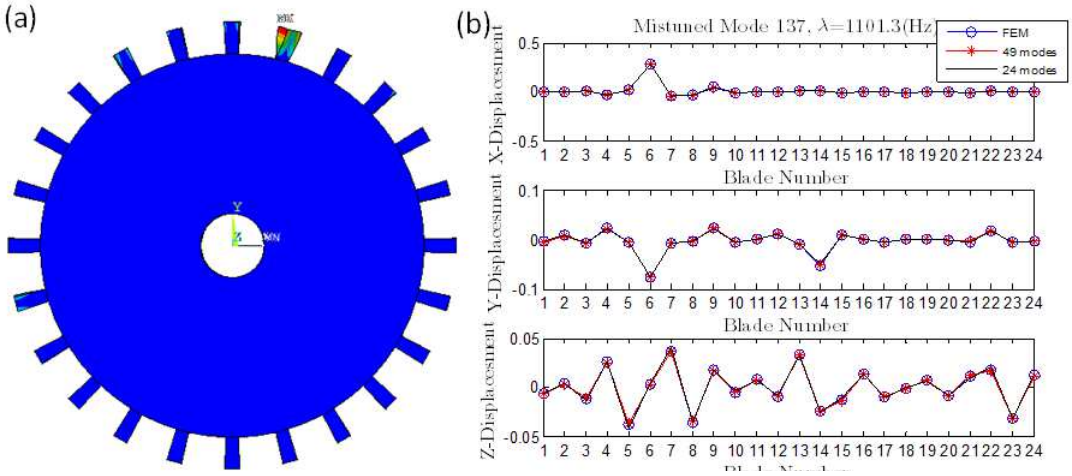

Figure 3.14: Mode shape of mistuned mode 137 in numerical analysis set 1

prediction by reduced number of modes. These three curves virtually coincide with one another indicating that the Rayleigh-Ritz approximation with reduced number of modes is very accurate. The calculations also confirm our hypothesis toward the mechanism causing mode localization in nearly cyclic symmetric rotors as well as the efficiency of our visual method to select modes for Rayleigh-Ritz approximations.

Figure 3.15 shows the fast Fourier transform of mistuned mode 137 in the same way as Fig. 3.13. Since mistuned mode 137 is an out-of-plane mode, the major displacement is in the $z-$direction. In Fig. 3.15(d), obvious magnitude of $\mathbf{A}_k(r, z)$ between $k = 5$ and $k = 30$.

3.3.3 Mistuning Set 2

Mistuning set 2 differs from set 1 only in the amount of mistune. The standard deviation of the mistuning is 5% instead of 2.7%. As shown in the theoretical analysis, mode localization can only occur when the coupling term, $\hat{\mathbf{D}}$, and the mistuning terms, $\Delta\hat{\mathbf{K}}$ and $\Delta\hat{\mathbf{M}}$, are of the same order. When the amount of mistuning is increased, $\hat{\mathbf{D}}$

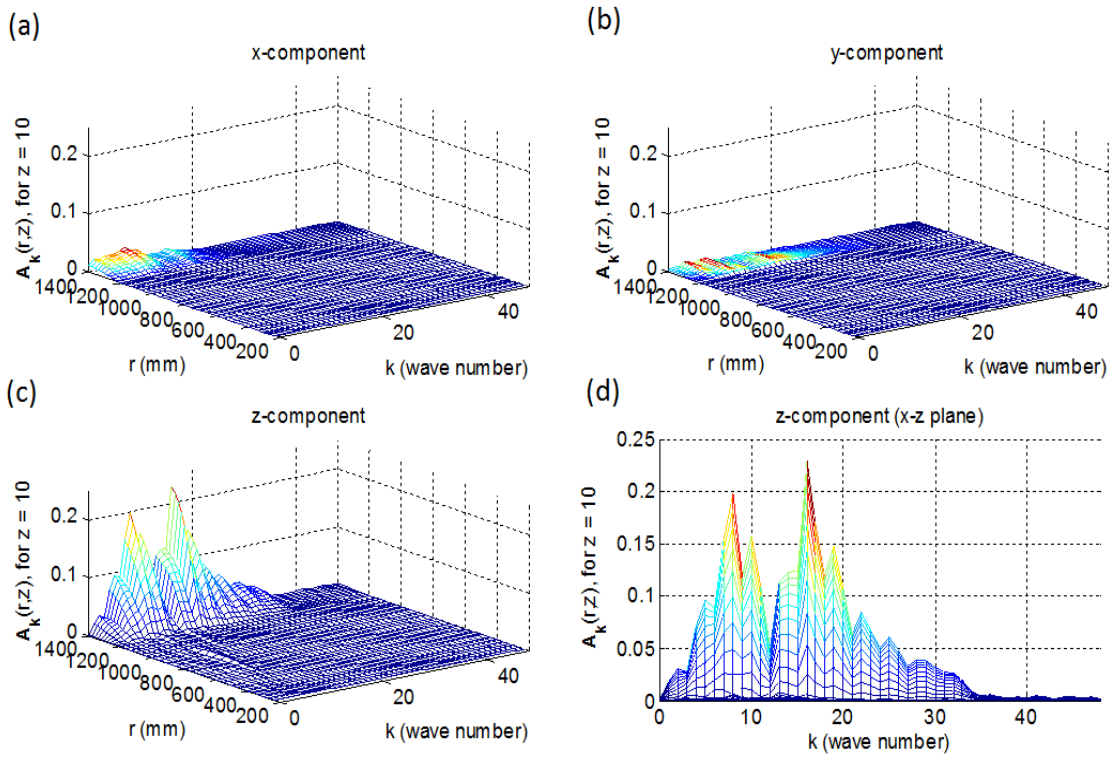

Figure 3.15: FFT of a localized, blade-torsional mode

remains the same. The mistuning term $\Delta\hat{\mathbf{K}}$ in (2.37) increases. (Note that $\Delta\hat{\mathbf{M}} = \mathbf{0}$ for this mistuning set 2 configuration.) As a result, additional modes may participate in the linear combinations to realize the mode localization occurring in frequency regions (c) and (d) as defined in Table 3.2.

Figure 3.16(a) shows $\hat{\mathbf{L}}$ for region (c) modes for mistuning set 2. Compared with Fig. 3.11(c) of mistuning set 1, the diagonal terms from $\hat{\mathbf{D}}$ and the off-diagonal terms from $\Delta\hat{\mathbf{K}}$ are now very close in magnitude (as judged from the contrast of their colors). The selected modes in Fig. 3.16(a) are the original 24 modes in B-in-0 family and modes 99, 100. The original 24 selected modes basically form the Group G modes that have nearly identical natural frequencies. The other 2 modes, 99, and

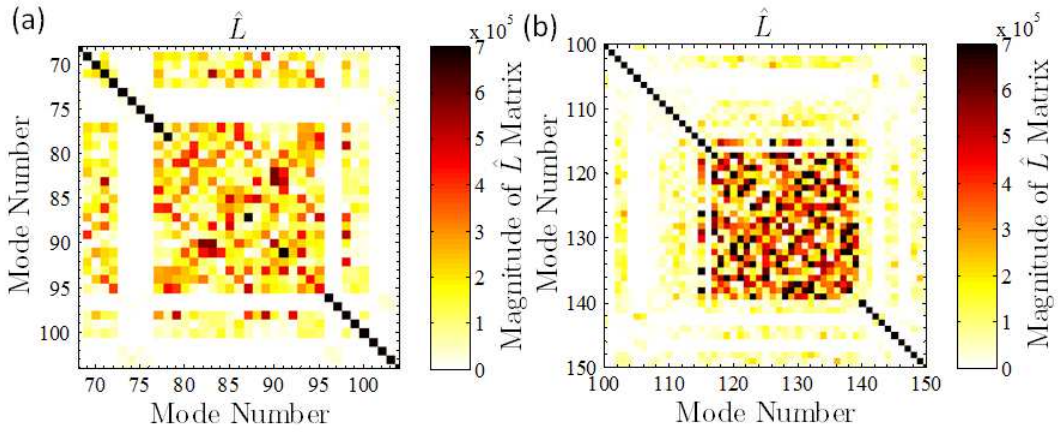

Figure 3.16: Visual Method for Numerical Analysis Set 2: $\hat{\mathbf{L}}$ in the region (c) and (d), respectively

100, are a pair of repeated modes. Although these two modes are dominated by the disk deformation, their blades have in-plane deformation which is similar as B-in-0 as shown in Fig. 3.17(b). When the mistuning is only 2.7% in the case of set 1, modes 99 and 100 have very small $\Delta\hat{\mathbf{K}}$ compared with the diagonal elements $\hat{\mathbf{D}}$; therefore, they did not participate in the linear combination to realize mode localization. When the mistuning is 5% in set 2, $\Delta\hat{\mathbf{K}}$ from these two modes is large enough and on the same order of $\hat{\mathbf{D}}$. Therefore, these two additional modes serve as the Group V modes, whose linear combinations will fine-tune the localized mode shapes.

On the contrary, modes 96 and 97 are at the veering site in Fig. 3.5 and are closer to B-in-0 family than modes 99, 100. Since their mode shapes have nothing in common with B-in-0 family, modes 96, 97 cannot serve as the Group V modes to fine-tune mistuned mode shapes in $r-$, $z-$directions. They are also in white or light yellow in the visual methods of both Mistuning Set 1, Fig. 3.11(c), and Mistuning Set 2, Fig. 2.33(a).

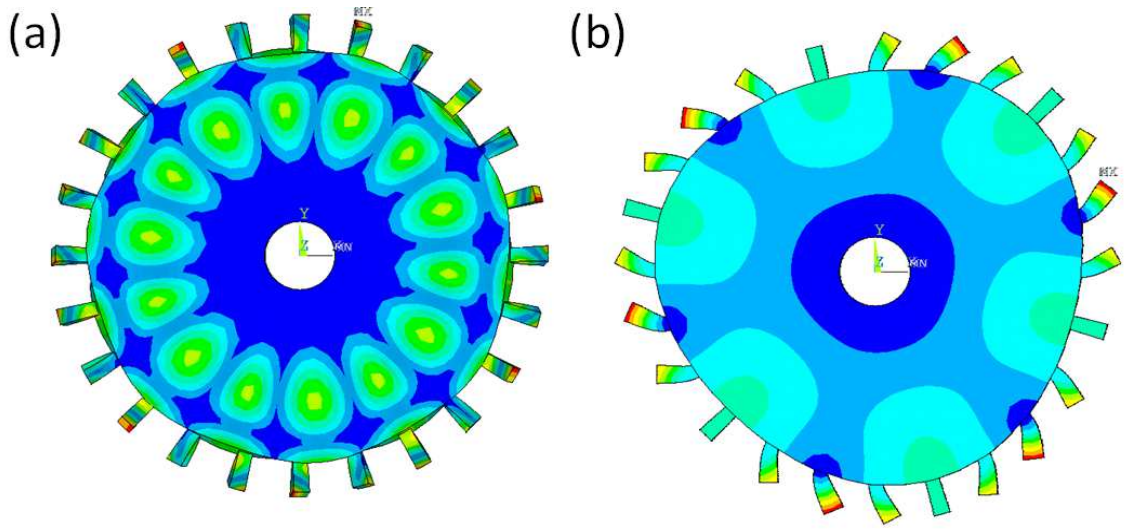

Figure 3.17: Mode shape of (a) tuned mode 96 (b) tuned mode 99

A finite element analysis is conducted to confirm the prediction of mode localization in regions (c) for the case of mistuning set 2. For example, Fig. 3.18 shows a localized mode in region (c). The right plot consists of three curves. The first curve, labeled as "FEM", is prediction from the finite element analysis. The second curve, labeled as "group G+V", is prediction from the Rayleigh-Ritz calculation (cf. (2.36)) with B-in-0 family (group G) and modes 99, 100 (group V) selected by the visual method. This red curve is right on top of the blue curve in all three directions indicating that the Rayleigh-Ritz approximation with reduced number of modes is very accurate. The last curve, labeled as "group G", is from the Rayleigh-Ritz calculation with only group G. This black curve coincides with the other curves in x-, y-directions, but is slightly different in the z-direction. This numerical result illustrates that retention of group G modes is sufficient to pinpoint localization and capture the localized blade but group V is needed to predict the localized mode shapes accurately.

Figure 3.16(b) show $\hat{\mathbf{L}}$ for region (d) modes for mistuning set 2. Compared with Fig. 3.11(d) of mistuning set 1, again, the diagonal terms from $\hat{\mathbf{D}}$ and the off-diagonal terms from $\Delta\hat{\mathbf{K}}$ are now very close in magnitude. Similar situation occurs in region (d), the selected modes in Fig. 3.16(b) are the original 24 modes in B-out-torsional family and modes 102, 103, 109∼112, 140, 141, 144, 145, 148 and 149. Again, they play as Group V to fine-tune the localized mode shapes.

Figure 3.19 shows a localized mode shape in region (d), and the three curves are the same as mentioned above in Fig. 3.18. The prediction with only group G can capture mode localization in the main direction (y-direction) but it cannot accurately predict the mode shape in the other two directions in which the mode shape is not localized. Group V, in this case, is needed to make the prediction converge to the FEM results in the other two directions. With more modes considered in group V, the predictions with and without group V show more significant difference in Fig. 3.19 than in Fig. 3.18. With larger mistuning, more additional modes are of the same order between diagonal components and off-diagonal components in $\hat{\mathbf{L}}$. Therefore, more modes are needed to predict mode localization accurately in all directions. These additional modes can be selected by the visual method effectively.

As a final remark, it should be clear now that the Rayleigh-Ritz approach is an extremely effective tool for predicting mode localization. It has very low order—roughly in the range of the number of substructure N. Also, it adapts automatically to different mistuning configuration. The flexibility and low order make it an ideal tool for Monte-Carlo simulations for example.

3.3.4 Mistuning Set 3

Mistuning set 3 differs from set 2 only in the pattern of mistune. Pattern 2 in Fig. 3.10 is used instead of pattern 1. Figures 3.20(a) and (b) show matrix $\hat{\mathbf{L}}$ for regions (c) and (d), respectively. In comparison with $\hat{\mathbf{L}}$ of mistuning set 2 (cf. Fig. 3.16, the change of mistuning pattern does not significantly change the fundamental structure

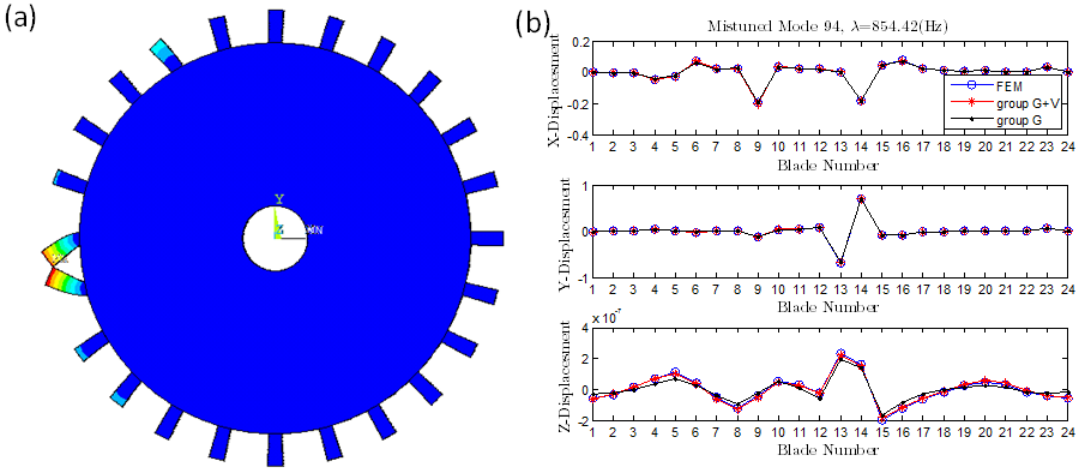

Figure 3.18: Mode shape of mistuned mode 94 in numerical analysis set 2

of $\hat{\mathbf{L}}$. The modes participating in the mode localization remain unchanged. Moreover, their diagonal and off-diagonal elements are about the same order. Therefore, mode localization will occur as in mistuning set 2.

To verify the prediction, I have conducted a Rayleigh-Ritz and a finite element analysis on the disk-blade system with mistuning set 3. I obtain similar results as from mistuning set 2. Since no new findings are found, the numerical results are not shown here to conserve space.

3.3.5 Mistuning Set 4

Mistuning set 4 differs from set 3 in the source of mistune. Set 4 has mass mistuning (i.e., $\Delta\mathbf{M}$), whereas set 3 has stiffness mistuning (i.e., $\Delta\mathbf{K}$).

The presence of mass mistuning brings in some subtle consequences. First of all, eigenvalues and eigenvectors of the mistuned system are now governed by a generalized eigenvalue problem (2.34). So the mathematical structure is more complicated, and so will its solutions.

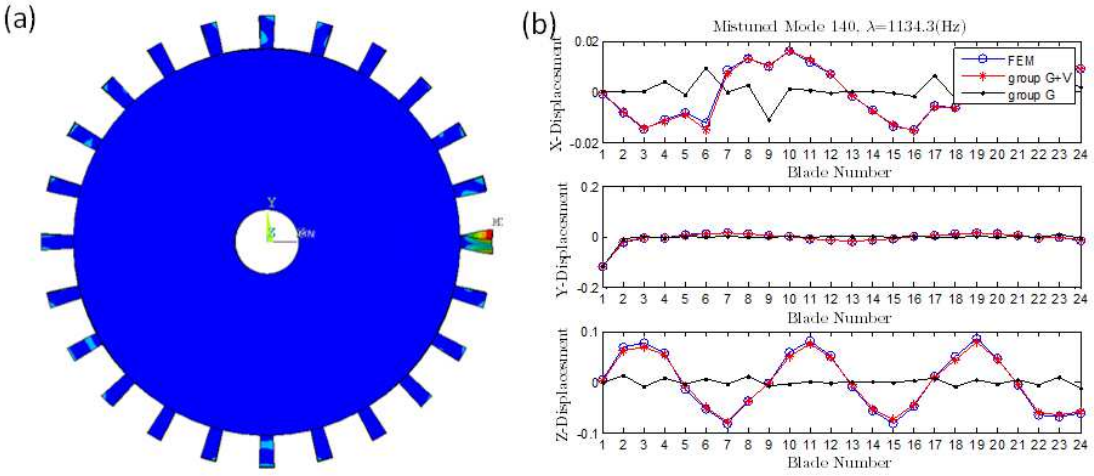

Figure 3.19: Mode shape of mistuned mode 140 in numerical analysis set 2

Second, the same amount of mass and stiffness mistuning (e.g., 5% standard deviation) could lead to slightly different effects. According to (2.37), $\Delta\hat{\mathbf{M}}$ is multiplied by $\left(\bar{\omega}^2\mathbf{I} + \hat{\mathbf{D}} + \Delta\hat{\mathbf{K}}\right)$, which amplifies the mass mistuning effect. This effect is demonstrated in the numerical results for mistuning set 4.

Figures 3.21(a) and (b) show the visual method to estimate $\hat{\mathbf{L}}$ for regions (c) and (d), respectively. The fundamental patterns remain similar as shown in Fig. 3.20, but the magnitudes of some off-diagonal components increase as expected. For example, there are more components in orange color within range of modes 69∼72 in Fig. 3.21(a) than in Fig. 3.20(a). However, there are no additional modes showing up with the same order of magnitude as diagonal terms. The selected modes remain the same to predict mode localization in this two regions.

Also, a finite element analysis is conducted to confirm the prediction of mode localization in regions (c) and (d) for mistuning set 4. For example, Fig. 3.22 and Fig. 3.23 show the localized modes in regions (c) and (d), respectively. The right plots in both

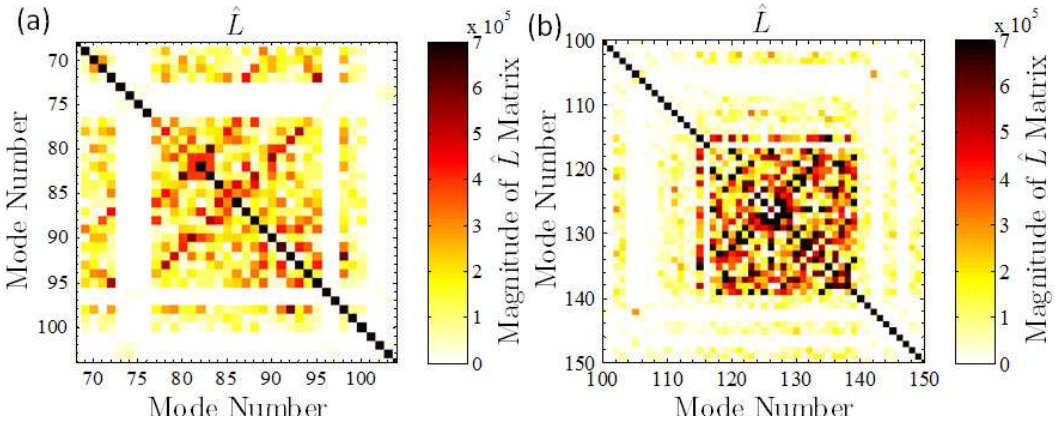

Figure 3.20: Visual method for numerical analysis set 3: $\hat{\mathbf{L}}$ in the region (c) and (d), respectively

figures consist of three curves. The first curve, labeled as "FEM", is prediction from the finite element analysis. The second curve, labeled with "Gen.", is prediction from the Rayleigh-Ritz method using the generalized eigenvalue problem (2.34). Moreover, the number of modes in the generalized eigenvalue problem is reduced through the use of the visual method (i.e., comparing diagonal and off-diagonal elements of the $\hat{\mathbf{L}}$ matrix). The third curve, labeled with "Appx.", is prediction from the Rayleigh-Ritz method using the approximation (2.36) and (2.37). The same tuned modes are considered in the approximate method as in the generalized eigenvalue problem. Since mass mistuning is considered in this set, "Gen." curves and "Appx." curves are slightly different in these two figures. With the approximation (2.36) and (2.37), the visual method is very effective in reducing the number of modes for mode localization. The numerical results show that the Rayleigh-Ritz method can predict the localized mode shape quantitatively with either stiffness mistuning or mass mistune.

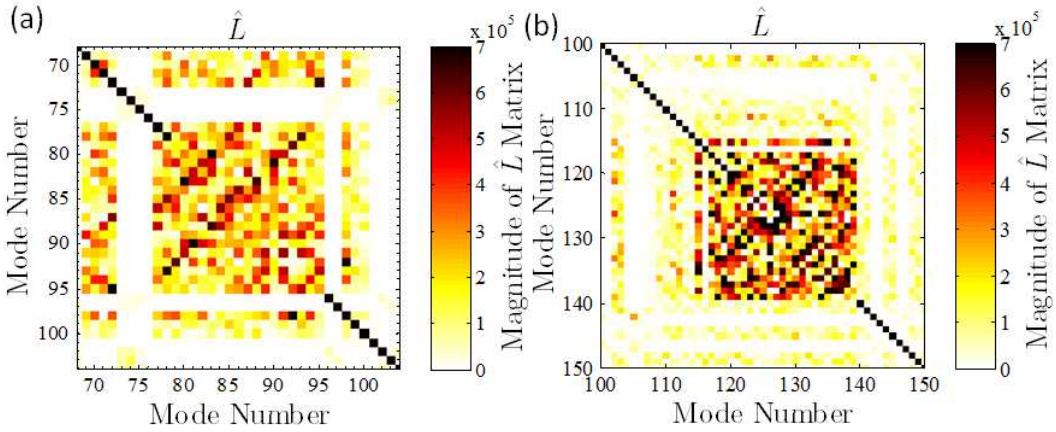

Figure 3.21: Visual method for numerical analysis set 4: $\hat{\mathbf{L}}$ in the region (c) and (d), respectively

3.4 The visual method affected by finite element mesh

The mesh of the finite element model not only affects how accurate the natural frequencies are solved but also may affect the visual method. In the section of convergence test, the natural frequencies of the interesting modes are compared among different meshes. In this section, I compare the visual methods that obtained from the rotor system with mesh (a) in Fig. 3.2 and the current model (cf. Fig. 3.1).

To save some space, only the visual method in region (d) is compared. Figure 3.24 shows the visual method obtained with mesh (a) and current mesh with the mistuning configuration the same as Mistuning Set 4. In Figure 3.24(b), the black entries are mainly located in the square which is corresponding to the B-out-torsional family modes. In Figure 3.5(a), however, the dark entries are not only shown up on the B-out-torsional family modes but other modes. This visual method indicates that wider frequency range and more modes are needed to solve the localized mode shapes when the mesh is not fine enough. The approximation amplification term for mass mis-

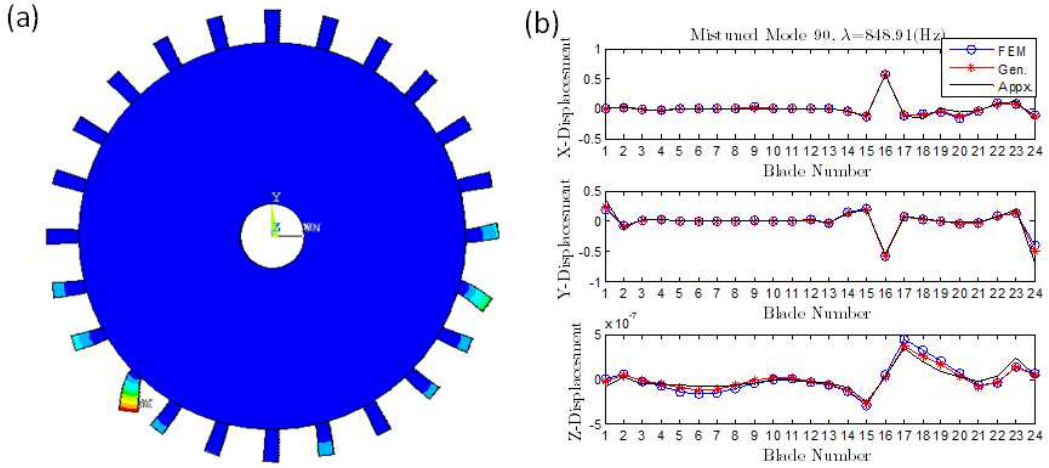

Figure 3.22: Mode shape of mistuned mode 90 in numerical analysis set 4

tuning ($\left(\bar{\omega}^2\mathbf{I} + \hat{\mathbf{D}} + \Delta\hat{\mathbf{K}}\right)$ in (2.37)) may the reason that amplified the error obtained from finite element model with coarse mesh.

Figure 3.25 shows the visual method for the Mistuning Set 3 which has the same mistuning standard deviation and pattern as Mistuning Set 4 but with different mistuning source. For only stiffness mistuning, the visual method is quite similar between the rotor system with coarse mesh Fig. 3.25(a) and current mesh Fig. 3.25(b). To be more specific, the distributions of the dark entries are mainly located in the square in both Fig. 3.25(a) and (b), since stiffness mistuning is not approximated in (2.37) and there is no other terms to amplify the effect of stiffness mistune.

3.5 Summary

Based on the theoretical analyses and numerical simulations, I reach the following conclusions for mode localization in a nearly cyclic symmetric rotor that contains mistune.

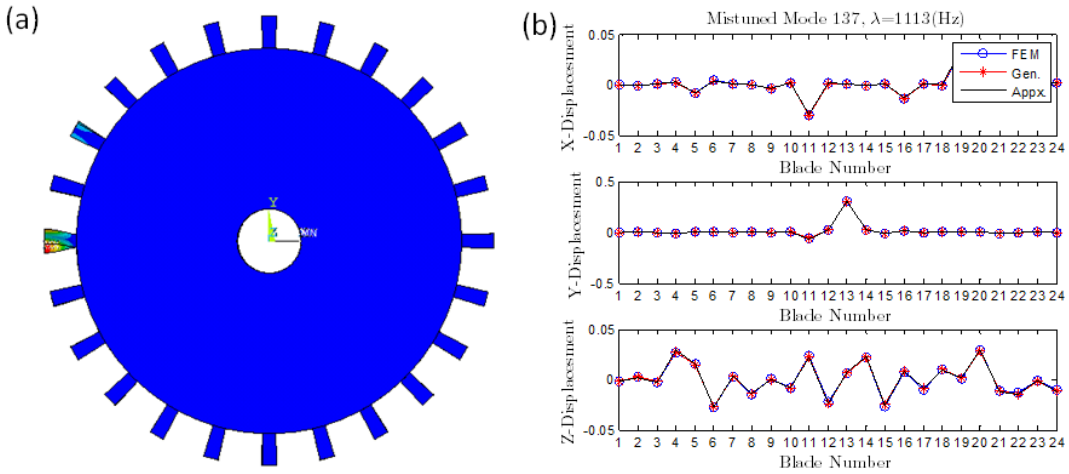

Figure 3.23: Mode shape of mistuned mode 137 in numerical analysis set 4

1. Mode localization may occur when the following two conditions are met: (a) there is a group of vibration modes of the tuned cyclic symmetric rotor whose natural frequencies are nearly identical and mode shapes have similar characteristics, and (b) the vibration modes in the group form a complete set in the circumferential direction. The completeness can be ensured when the group of modes includes all possible phase indices of the cyclic symmetric rotor. These conditions are valid not only for disk-blade systems but all nearly cyclic symmetric systems that contain slight mistune.

2. Whether or not a mode in the group will actively contribute to mode localization depends on the relative order of its coupling components and mistuning components. When these two components are roughly of the same order, the mode will actively contribute to mode localization.

3. One simple way to identify modes that actively contribute to mode localization

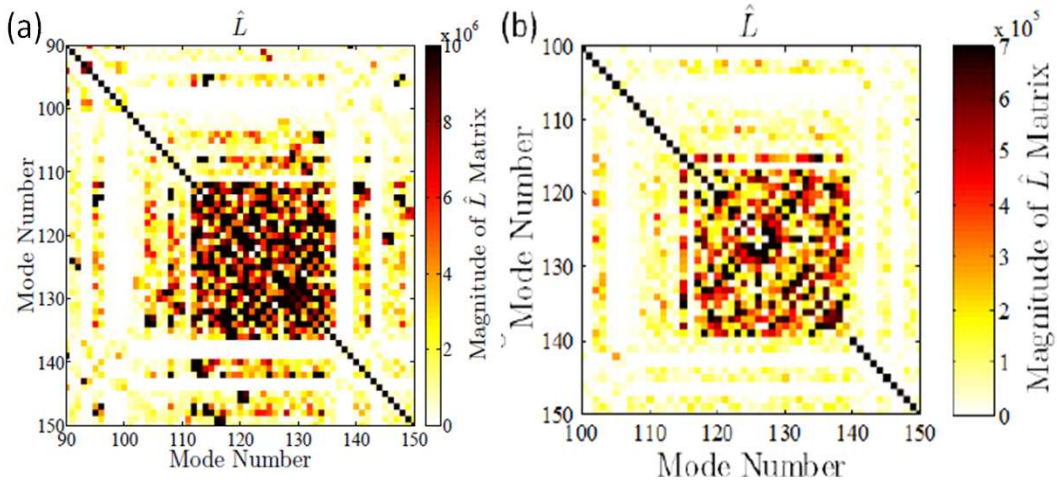

Figure 3.24: Visual method for mistuning set 4 in region (d) obtained with (a) mesh (a) in Fig. 3.2 (b) current mesh

is to evaluate the matrix $\hat{\mathbf{L}}$ using the visual method. If diagonal and off-diagonal elements of a mode are about the same order in $\hat{\mathbf{L}}$, the mode should be retained to estimate mode localization. This method is computationally efficient, because only matrix multiplications are involved. When a system presents large mass mistuning, the visual method may lose its accuracy because of the assumption made in (2.35).

4. Once those modes that may actively contribute to mode localization are identified, a Rayleigh-Ritz method can effectively predict natural frequencies and mode shapes of the localized modes. The Rayleigh-Ritz method will also be computationally efficient, because the size of the eigenvalue problem is about the same as the number of substructures of the cyclic symmetric rotor. Since the participating modes have been carefully screened, the predictions from the Rayleigh-Ritz method are very accurate.

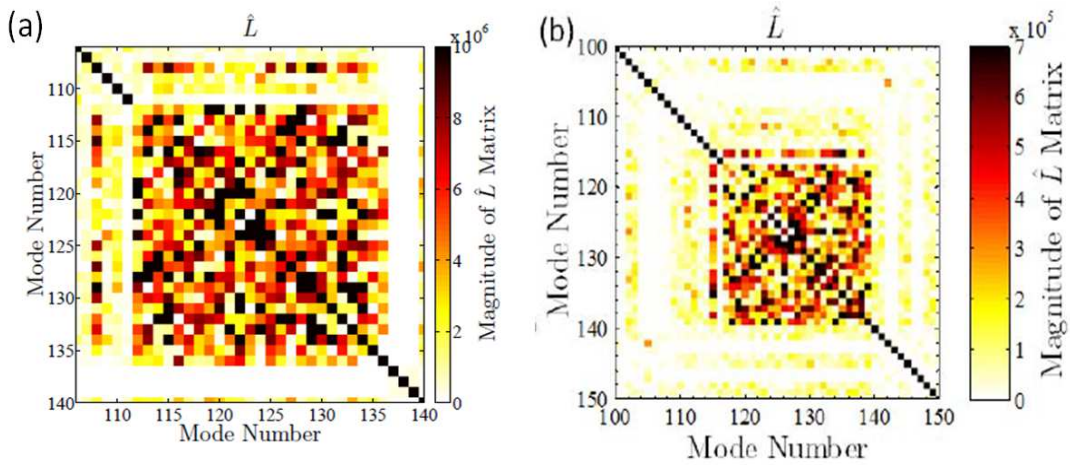

Figure 3.25: Visual method for mistuning set 3 in region (d) obtained with (a) mesh (a) (b) current mesh

5. Curve veering is not a key factor contributing to mode localization in the following ways. First, mode localization does not occur for every point where eigenvalue loci veer. Second, not every vibration mode involved in eigenvalue veering contributes significantly to occurrence of mode localization.

6. When standard deviation of mistuning increases, more modes may participate in mode localization. In order words, more modes from the tuned cyclic symmetric system are needed to enable linear combinations in realizing localized modes. The localized blade of a mistuned mode can be pinpointed by the prediction Rayleigh-Ritz method with group G modes. But in order to prediction a localized mode shape accurately in all directions, group V modes are necessary to be contained.

7. When a system presents mass mistuning, the underlying mathematical structure is more complicated as reflected in (2.34), (2.36), and (2.37). Given the

same mistuning (in terms of amount and pattern), the effect of mass mistuning is greater than that of stiffness mistune. For large mass mistuning, the visual method can identify tuned modes needed to realize mode localization. Nevertheless, the generalized eigenvalue problem should be used in the Rayleigh-Ritz approximation to obtain accurate results.

Chapter 4

EFFECTS OF BEARINGS AND HOUSING ON MODE LOCALIZATION

Although mode localization can be caused by both mass and stiffness mistuning (difference in geometry and/or natural frequency of each blade) [25, 29], the phenomenon of mode localization can be sufficiently demonstrated by only considering stiffness mistuning into the system. Since Chapter 4 aim to demonstrate the effects of bearings and housing, I only consider stiffness mistuning herein for the sake of computational efficiency.

To show the explicit effects of bearings and housing, the materials of blade and disk are changed from the bladed disk using in Chapter 3 as the reference system.

4.1 Reference System

The reference system consists of two versions: a tuned system and a mistuned system. Both systems are studied via FEA to establish a baseline. The reference system has the same geometry as the model used in Chapter 2 shown in Fig. 3.1. The reference system consists of a circular disk and 24 identical blades. The disk is annular with an inner rim and an outer rim. The circular disk has an outer diameter of 1200 mm, an inner diameter of 200 mm, and a thickness of 50 mm. A fixed boundary condition is imposed at the inner rim, while the 24 blades are evenly attached to the outer rim and are subjected to a free boundary condition. Blade numbers are labeled in Fig. 3.1 for further reference. The circular disk defines the xy plane and the out-of-plane direction is the z direction.

To show the explicit effects of bearings and housing, the materials of blade and

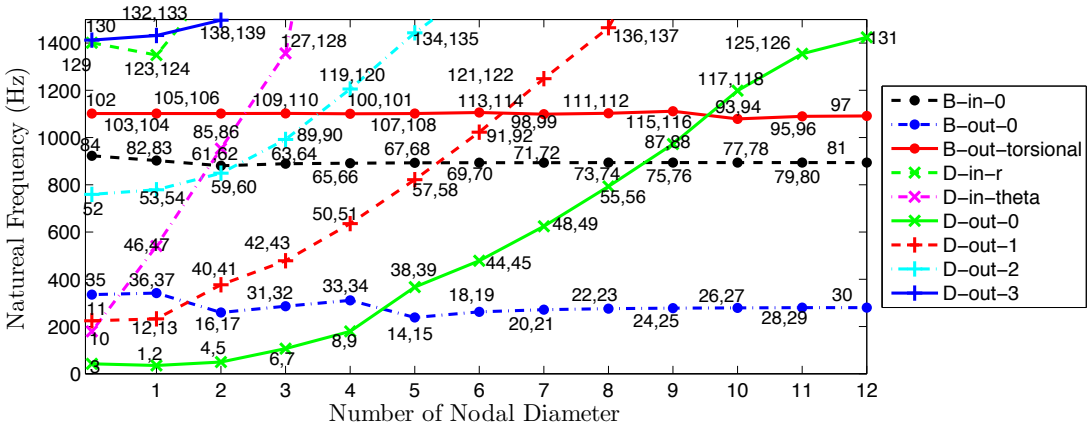

Figure 4.1: Natural frequencies of the tuned reference system; 24 identical blades and a disk with a fixed inner rim

disk are changed from the bladed disk using in Chapter 3. The material of the disk is Nickel-Chromium alloy with density of 855 kg/m^3 and Young's modulus of 189 GPa. The blades have a length of 200 mm, a width of 80 mm, and a thickness of 20 mm. The material of the tuned blades is Nickel-Titanium alloy with density of 855 kg/m^3 and Young's modulus of 85 GPa.

Figure 4.1 shows natural frequencies of the tuned reference system, plotted with respect to the number of nodal diameters. Based on their mode shapes, these natural frequencies are grouped into several families coded in three words as the same way mentioned in Chapter 3.2. The first word indicates the dominating part of the mode shapes. For example, D represents that the disk deformation dominates the mode shapes while B represents that blade deformation dominates the mode shapes. The second word indicates whether the mode shapes have out-of-plane displacement (out) or in-plane displacement (in) over the bladed disk. The third word shows the number of nodal circles or whether the modes have torsional vibration.

Figure 4.2 illustrate characteristics of each family by showing contour plots of 3-nodal-diameter modes in each family. As an example, mode shapes of the D-out-0

family name / mode number	mode shape	family name / mode number	mode shape
D-out-0 / mode 6	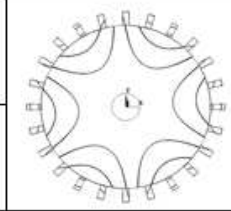	D-out-2 / mode 89	
B-out-0 / mode 31		B-out-torsional / mode 109	
D-out-1 / mode 42	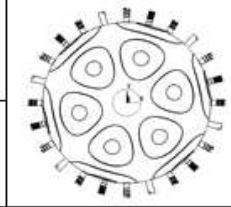	D-in-theta / mode 127	
B-in-0 / mode 63	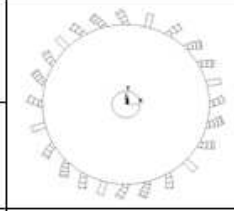		

Figure 4.2: Contour plot of mode shapes with 3 nodal diameters

Table 4.1: Mistuning for the Reference System

Blade	Mistune(%)	Blade	Mistune(%)	Blade	Mistune(%)
1	4.960	9	1.455	17	-1.652
2	-0.875	10	-1.140	18	-1.399
3	-5.306	11	-0.050	19	-1.188
4	-0.011	12	-0.029	20	-0.408
5	-3.685	13	0.743	21	-2.500
6	3.339	14	1.377	22	-1.416
7	6.581	15	-2.861	23	0.854
8	-0.190	16	-0.762	24	-4.441

family have primarily out-of-plane disk vibration with zero nodal circle. In Fig. 4.2, contour lines of the D-out-0 family (cf. the top left plot of Fig. 4.2) appear mostly in the disk without any nodal circle. It also has no obvious deformation in the xy plane implying that the displacement is in the out-of-plane direction. As another example, the bottom left plot in Fig. 4.2 corresponds to the B-in-0 family. It has no contour lines in the disk, but each blade deforms in the xy plane (i.e., in-plane deformation).

Natural frequencies are sorted in an ascending order, and corresponding mode numbers are also listed in Fig. 4.1 to index each natural frequency. Note that many natural frequencies have two mode numbers, because the natural frequencies are repeated. By constructing families of natural frequencies, I can easily identify the types of modes that contribute to a localized mode.

Based on the tuned reference system, mistuning of each blade is generated via random numbers with 2.7% standard deviation as shown in Table 4.1. The mistuning configuration is then modeled as a variation in Young's modulus of each blade in the tuned reference system Figure 3.1. Although mode localization can be caused by both

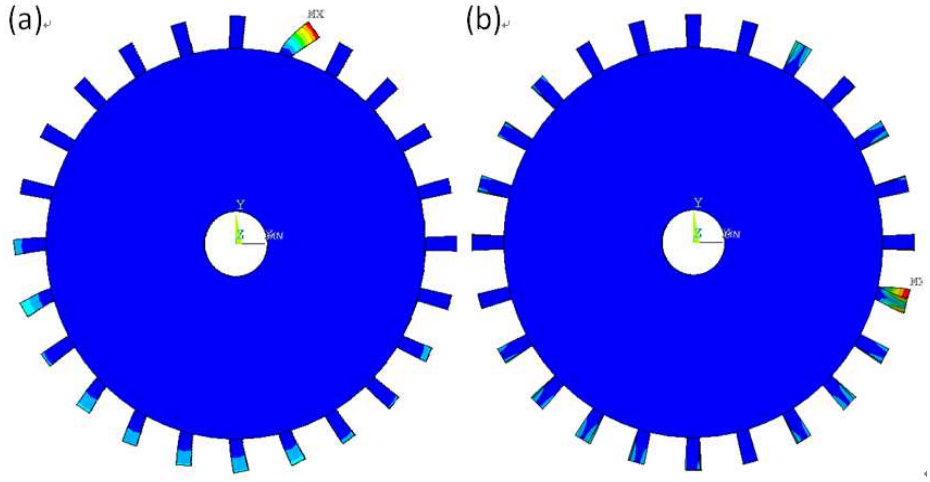

Figure 4.3: Localized mode shapes of the mistuned reference system: (a) mode 81 with blade in-plane vibration, and (b) mode 94 with blade torsional vibration

mass and stiffness mistune (difference in geometry and/or natural frequency of each blade) [25, 29], the phenomenon of mode localization can be sufficiently demonstrated by only considering stiffness mistune into the system. Since this chapter aims to demonstrate the effects of bearings and housing, I only consider stiffness mistune herein for the sake of computational efficiency.

FEA show that there are two sets of mode localization. The first set of mode localization occurs near 900 Hz, and the modes involved are from the B-in-0 family with blade in-plane vibration. There are 24 localized modes, and a typical mode shape is shown in Fig. 4.3(a). The second set of mode localization occurs near 1100 Hz, and the modes involved are primarily from the B-out-torsional family with blade torsional vibration. There are 24 localized modes, and a typical mode shape is shown in Fig. 4.3(b).

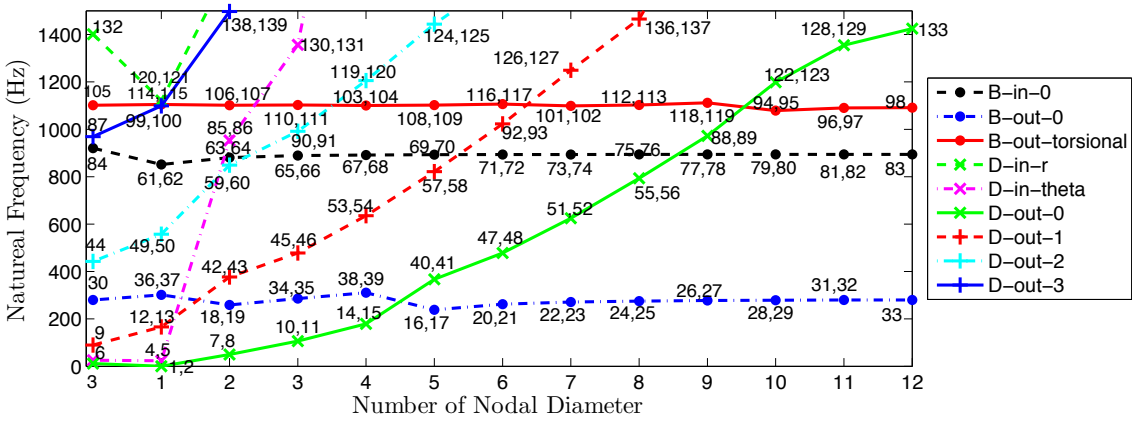

Figure 4.4: Natural frequencies of tuned rotor-bearing system

4.2 *Effects of Flexible Bearings*

To study effects of flexible bearings on mode localization, I modify the reference system with an elastic boundary condition at the inner rim. Specifically, two sets of contact elements are used to constrain upper and lower surfaces of the inner rim evenly. The movements of each set of contact elements are represented by a pilot point that is connected to a fixed point with a linear spring to simulate a flexible bearing. [1] The two pilot points are located at $z = 10$ mm and $z = -10$ mm, respectively. The linear springs have linear stiffness of 2.16×10^7 N/m in the in-plane directions (i.e., x- and y-directions), linear stiffness of 5.76×10^6 N/m in the out-of-plane direction (i.e., z-direction), and rotational stiffness of 58.5 N $\cdot$ m/rad for pitch and roll (i.e., about x- and y-axes, respectively). This formulation is referred to as the "rotor-bearing system" in the sequel. The rotor-bearing system also consists of two versions: a tuned system and a mistuned system.

Figure 4.4 shows natural frequencies of the tuned, bladed disk with the elastic

[1] Please refer to Appendix F for building bearings with contact elements and pilot points in ANSYS.

Table 4.2: Number of localized modes in the frequency range of B-in-0 and B-out-torsional families

	B-in-0	B-out-torsional
reference system	24 modes	24 modes
rotor-bearing system	24 modes	26 modes
rotor-bearing-housing system	26 modes	26 modes

bearings. By comparing Figure 4.4 with Figure 4.1, I confirm that only vibration modes with 0 or 1 nodal diameter have changed their natural frequencies when the elastic bearings are introduced. This observation is consistent with that predicted in [26]. Moreover, modes from the D-out-2 family significantly change their natural frequencies, while modes from the B-out-torsional family do not. In other words, disk-dominant modes change their natural frequencies more than blade-dominant modes. This result is not surprising. For blade-dominant modes, there is almost no deformation at the inner rim. Therefore, the boundary condition change at the inner rim minimally affects the natural frequencies of the blade-dominant modes.

The mistuning configuration in Table 4.1 is now added to the tuned rotor-bearing system. FEA show that mode localization occurs again in the frequency range of B-in-0 and B-out-torsional families. Moreover, the number of localized modes obtained from the FEA is listed in Table 4.2 for comparison. For the B-in-0 family, the number of localized modes remains 24 after the bearings are introduced. In contrast, the number of localized modes in the frequency range of the B-out-torsional family is now increased to 26 from 24. The two additional modes, due to the presence of the elastic bearings, are mode 111 (at 1102.6 Hz) and mode 112 (at 1104 Hz). Their mode shapes are shown in Figure 4.5 where the pink circle in the middle of each plot represents flexible bearings.

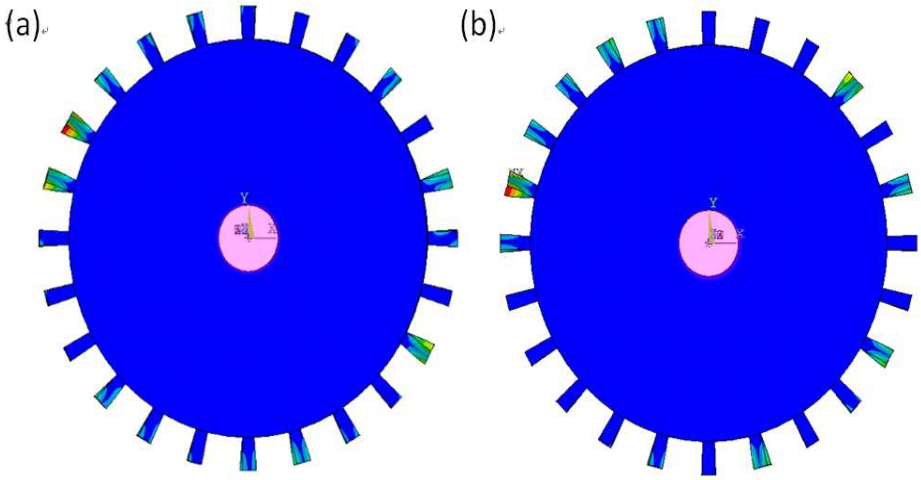

Figure 4.5: Two additional localized modes for the mistuned rotor-bearing system:(a) mode 111 at 1102.6 Hz (b) mode 112 at 1104 Hz

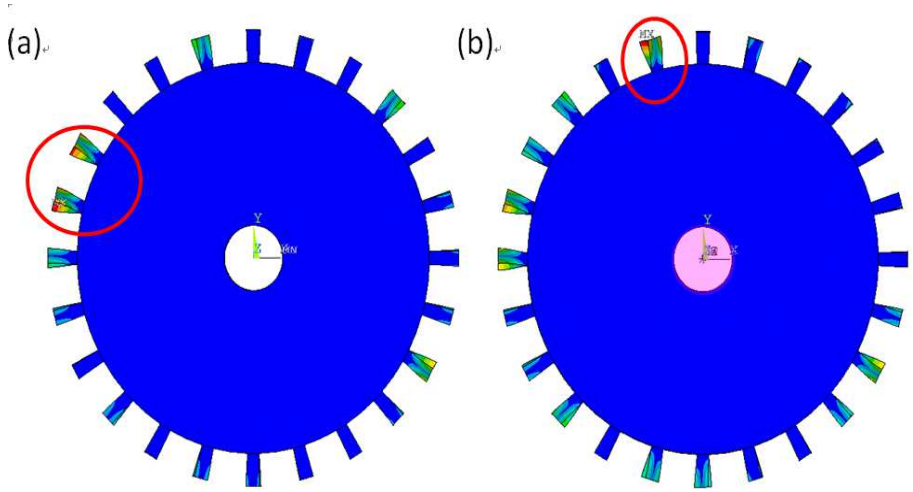

Figure 4.6: (a) Mistuned mode 108 with fixed inner rim (1102 Hz), (b) Mistuned mode 109 with bearings at inner rim (1101 Hz)

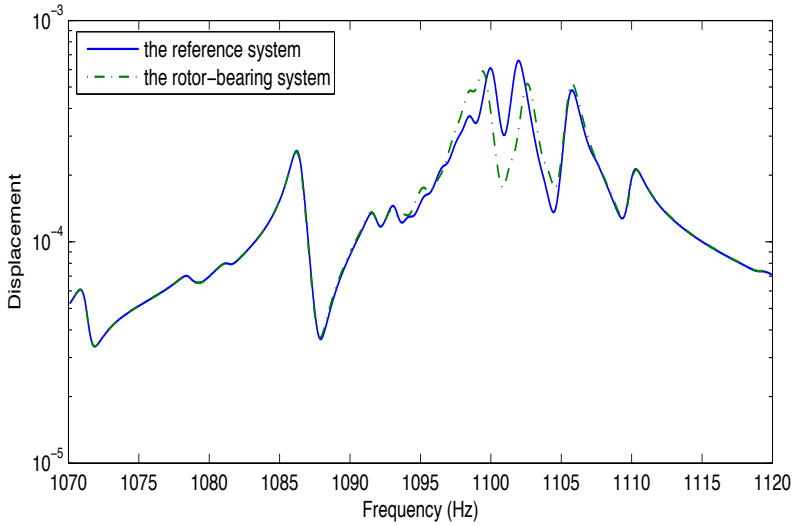

Figure 4.7: Frequency response function of displacement for blade 11

For the rest 24 modes that remain localized, the presence of the bearings can change their mode shapes too. For instance, Figure 4.6 shows the 16-th localized mode with blade torsional vibration before and after the bearings are introduced. This particular mode corresponds to mode 108 and 109 in the mistuning reference system and the mistuning rotor-bearing system, respectively. The natural frequency shifts only slightly from 1102 Hz to 1101 Hz. The mode shape, however, changes dramatically. The vibration was localized at two adjacent blades when the inner rim is fixed. Now the vibration is localized at a single and different blade when the bearing is present. From the FEA above, I reach the first conclusion—the presence of bearings may affect mode localization via the number and shape of localized modes.

That the presence of the bearing support may affect mode localization has two direct consequences. The first consequence is modification of forced response. For example, Figure 4.7 shows a frequency response function (FRF) of blade 11, labeled

in Fig. 3.1, from 1070 Hz to 1120 Hz covering the B-out-torsion family. [2] In obtaining Figure 4.7, a sinusoidal force is applied to the out-of-plane direction at the left tip of blade 11 while the displacement at the same location is calculated. The damping ratio is assumed to be 0.05%. As shown in Figure 4.7, the FRF changes significantly near 1100 Hz when the flexible bearing is introduced. The resonance peaks have shifted their frequencies because of the two additional localized modes in the B-out-torsion family (cf. Table 4.2). Moreover, the peak magnitude of the FRF is reduced implying that the bearing has alleviated the effects of mode localization.

Since the localized modes of the B-out-torsion family present only tiny displacements at the inner rim, the FRF in Figure 4.7 results primarily from the blade torsion instead of bearing deformation. This can be confirmed by plotting FRF of von Mises strain on blade 11 as shown in Fig. 4.8. To choose von Mises strain is because Von Mises strain is the most accurate predictor for isotropic and ductile metal yielding of the date, so it can help to determine whether a blade is in danger. If the displacement of the blade does not source from the deformation of the blade, von Mises strain of that blade will be small and the blade will not fatigue precipitately. The peaks of the von Mises strain in Fig. 4.8 is consistent as the peaks of the displacement in Fig. 4.7.

The second consequence is modification of bearing forces. Figures 4.9 shows Euclidean norm of modal bearing force of the tuned and mistuned rotor-bearing system. The modal bearing force is calculated by the multiplication of the bearings displacement of a mistuned mode shape and the stiffness of the bearings. The stiffness of bearings is determined in the beginning of this section. To obtian the displacement of the bearing, correpsonding degrees of freedom have to be found. By obtaining the mass and stiffness matrices of the reference system and the rotor-bearing system from ANSYS, the mapping files of the nodel numbers and the degrees of freedom can be got. By comparing the mapping file of the reference system and the rotor-bearing

[2]Please refer to Appendix F for solving frequency response function in ANSYS.

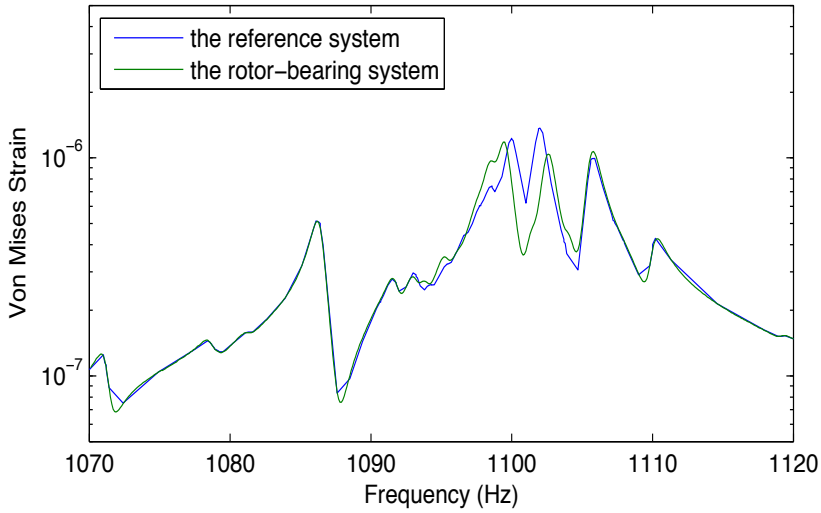

Figure 4.8: Frequency response function of von Mises strain for blade 11

system (with Beyond compare or other similar software), the additional degrees of freedom for the rotor-bearing system will be shown and the degrees of freedom corresponding to the bearings will be found. After obtaining all the mode shapes from ANSYS, the modal bearing forces can be calculated in MATLAB.

In Figure 4.9, the plus markers represent bearing forces from the tuned rotor. In contrast, the circle markers represent bearing forces from the mistuning rotor, with the larger circle markers representing contribution from modes that are extremely localized. The upper plot shows the bearing force from each mode with respect to the frequency, while the two bottom plots show the bearing forces from the B-in-0 family and the B-out-torsion family in the order of ascending frequencies. It is obvious from Figure 4.9 that most vibration modes except two have small bearing forces when the rotor is tuned. When the mistuning is introduced, all vibration modes have significant bearing forces.

Another perspective can be found in Figure 4.9 is that whether a mistuned mode is extremely localized or not, bearing forces of mistuned modes are about the same

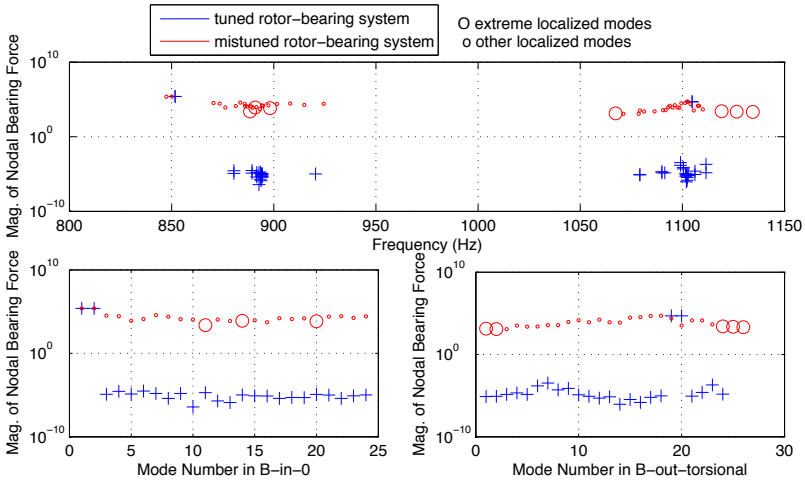

Figure 4.9: Bearing force comparison for tuned and mistuned rotor-bearing systems

order. For instant, the 9th and 11th mistuned modes in B-in-torsional family have about the same bearing force (cf. the bottom left plot in Fig. 4.9), but the 11th mistuned mode has extremely localized mode shape as shown in Fig. 4.10(b) but the 9th mistuned mode shown in Fig. 4.10(a) does not. A extremely localized mode does not necessary have high bearing force to expedite the wear or damage of the bearings.

4.3 Theoretical Investigation

The FEA above shows that presence of bearings may bring significant changes to the phenomenon of mode localization. It may change the number of localized modes, forced response, and also bearing forces. These changes can be explained and justified via theoretical analyses that are available in Chapter 2 and the literature [25, 26].

Number of Localized Modes. According to Chapter 2, mode localization occurs when the following two conditions are met for a tuned cyclic symmetric system. First, there must be a group of modes that have very close natural frequencies. Second, this group of modes contains a wide range of phase indices. When mistuning is

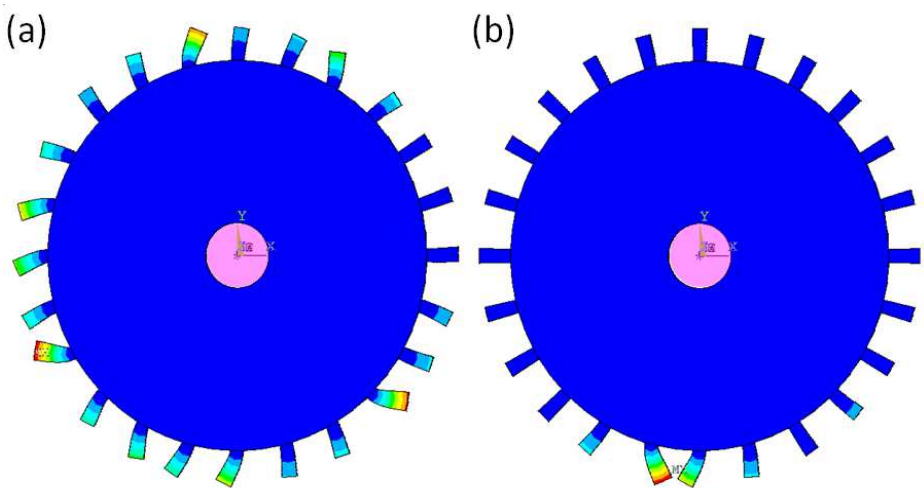

Figure 4.10: (a) mistuned mode 68 (the 9th mistuned mode in B-in-0) (b) mistuned mode 71 (the 11th mistuned mode in B-in-0)

present, vibration modes in the group can be linearly combined to form localized modes whose vibration is confined only at one or two blades. Moreover, vibration modes participating in the linear combination must have similar features in their mode shapes.

For the tuned reference system, there are two groups of modes that have very close natural frequencies; see Figure 4.1. One is around 1100 Hz, and the other around 900 Hz. Let us focus on the first group of modes around 1100 Hz. When the tuned system has no bearing, this group consists of 24 modes (i.e., modes 93 to 116 in Figure 4.1) with very close natural frequencies. These modes encompass 0 to 12 nodal diameters thus containing a wide range of wave numbers. These modes all come from the B-out-torsional family with a common feature of blade torsional vibration. Therefore, all the conditions for mode localization are met, and these 24 modes are linearly combined to form 24 localized modes shown in Table 4.2.

When the bearing is introduced, the group with a natural frequency around 1100

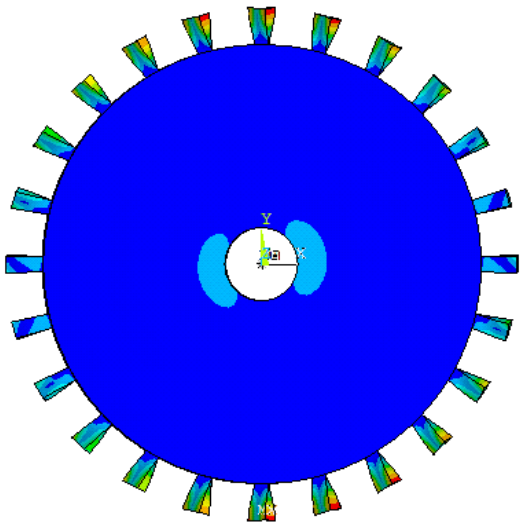

Figure 4.11: Shape of mode 114 of tuned bladed disk with bearing

Hz grows to 26 modes (i.e., modes 94 to 119 in Figure 4.4) when the mistuning is introduced. In addition to the original 24 modes from the B-out-torsion family, there are two modes (114 and 115) from the D-out-3 family. Although modes 114 and 115 are from the D-out-3 family, they have a significant blade torsion as in the B-out-torsion family; see the mode shape in Figure 4.11. In other words, all these 26 modes share the same feature of blade torsional vibration. Besides, these 26 modes encompass 0 to 12 nodal diameters thus containing a wide range of wave numbers. Again, all the conditions for mode localization are met and these 26 modes are linearly combined to form 26 localized modes in Table 4.2 when the mistuning is introduced.

The analysis above explains why the number of localized modes increases from 24 to 26 when the bearing is introduced. In essence, the presence of the bearings basically introduces additional degrees of freedom to the reference system, and thus provides additional modes that could form a group for mode localization. If the bearing coefficients are properly chosen so that the conditions for mode localization

are met, these additional modes would participate in the linear combination to form additional localized modes.

The same analysis above can also explain why the group around 900 Hz does not change its number of localized modes when the bearing is introduced. When the bearing is not present, there are roughly 26 modes in this group (i.e., modes 59 to 84 in Figure 4.1). Specifically, 24 of them are from the B-in-0 family with a common feature of blade in-plane vibration. Moreover, they encompass 0 to 12 nodal diameters thus containing a wide range of phase indices. The remaining two of the 26 modes (i.e., modes 59 and 60) are from the D-out-2 family without any blade in-plane vibration. Therefore, the 24 modes from the B-in-0 family meet the conditions of mode localization and are linearly combined to form the 24 localized modes. When the bearings are introduced, there are no additional vibration modes appearing in this frequency range. Moreover, all the vibration modes in this group around 900 Hz are almost unchanged. As a result, the mode localization form by the B-in-0 family remains the same.

Bearing Forces. First of all, major results from [26] are summarized below to facilitate the analysis of bearing forces. Consider a tuned cyclic symmetric system consisting of N identical substructures with a fixed boundary (e.g., a bladed disk with a fixed inner rim). Every mode shape of the cyclic symmetric system is then characterized via a phase index n that defines a phase difference between two neighboring substructures (cf. (2.16)). When bearings are introduced into the tuned cyclic symmetric system, some modes will be coupled to the bearings changing their natural frequencies. These modes are called *unbalanced modes*. Other modes will not be affected and are called *balanced modes*. Only the modes with phase indices $n = 1, N-1, N$ may be the unbalanced modes. For $n = N$, the vibration mode will be a balanced mode if its leading Fourier coefficient $\mathbf{A}_0(r, z) = \mathbf{0}$.

The physics behind the balanced and unbalanced modes is quite straightforward. When the tuned system vibrates in a balanced mode, the inertial force (and its mo-

ments) arising from the vibration turns out to be zero. No net forces or moments are transmitted to the fixed boundary; therefore, introduction of the bearings will not affect the state of the vibration. On the contrary, when an unbalanced mode vibrates, the inertial force results in a net force or moment acting on the fixed boundary. When the bearings are present, the net force or moment deforms the bearings leading to a coupled bearing-rotor vibration affecting the natural frequency of the unbalanced modes.

For the tuned, bladed disk shown in the reference system, the phase index is related to the number of nodal diameters. The 0-nodal-diameter modes correspond to phase index $n = N$, while the 1-nodal-diameter modes correspond to phase indices $n = 1$ and $n = N - 1$. Therefore, 0- and 1-nodal-diameter modes may be affected when the bearings are introduced. The most prominent changes appear in the D-out-3 family in Fig. 4.1 and Fig. 4.4.

The presence of unbalanced modes can also be seen in the modal bearing forces plotted in Fig. 4.9. For the tuned system, the unbalanced modes have significantly larger bearing forces than the balanced modes. As shown in Fig. 4.9, the blue plus markers represent the modal bearing forces from the tuned system. Note that only two blue plus markers in the B-in-0 family (bottom left plot) and in the B-out-torsional (bottom right plot) have large bearing forces. They correspond to the 1-nodal-diameter modes, which are unbalanced. The 0-nodal-diameter modes in the B-in-0 family and B-out-torsional family happen to have zero net inertia force and moment.

When mistuning is present, all localized modes can be expressed in terms of linear combinations of a group of modes from the tuned system. Since the group of modes must encompass a wide range of wave numbers, it will naturally include both balanced modes and unbalanced modes. Therefore, all localized modes will have contribution of unbalanced modes implying that all localized modes will incur a large bearing force as shown in the red circle markers in Fig. 4.9.

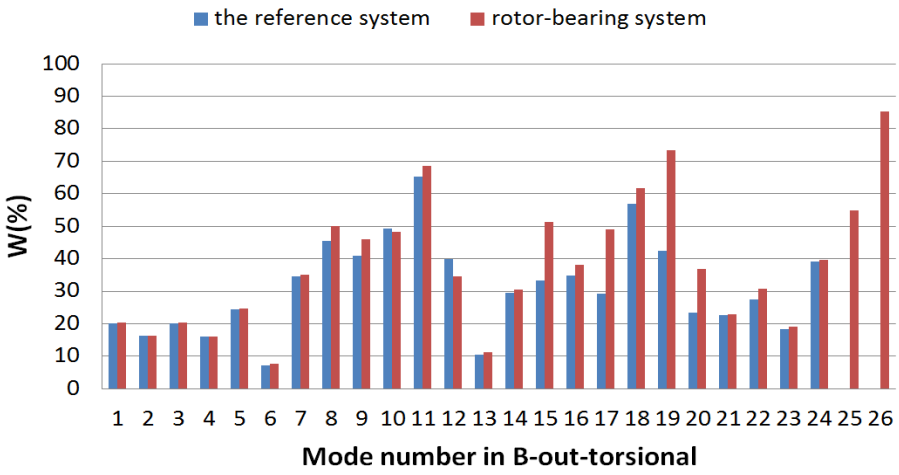

Figure 4.12: Weight of unbalanced modes

Since a localized mistuned mode shape $\mathbf{u}_n^*$ can be represented by a linear combination of a group of tuned modes, the weight of how much unbalanced modes is formed the localized mode can be calculated. Let us call this group of tuned modes as group T and denote their mode shapes as $\mathbf{u}_k$. Then

$$\mathbf{u}_n^* = \gamma_{nk}\mathbf{u}_k \tag{4.1}$$

, with $k = 1, 2, \ldots, n_T$. Note that the group T modes may potentially include balanced modes and unbalanced modes. The weight of each $\mathbf{u}_k$ is denoted as γ_{nk}^b if $\mathbf{u}_k$ is a balanced mode and is denoted as γ_{nk}^u if $\mathbf{u}_k$ is an unbalanced mode. The weight of unbalanced modes for the n-th localized mode is defined as below.

$$W_n(\%) = \frac{\sqrt{\sum_p {\gamma_{np}^u}^2}}{\sqrt{\sum_p {\gamma_{np}^u}^2 + \sum_q {\gamma_{nq}^b}^2}} \tag{4.2}$$

Figure 4.12 shows the weight of localized mode in B-out-torsional family for the reference system and the rotor-bearing system. When bearings are present, the two

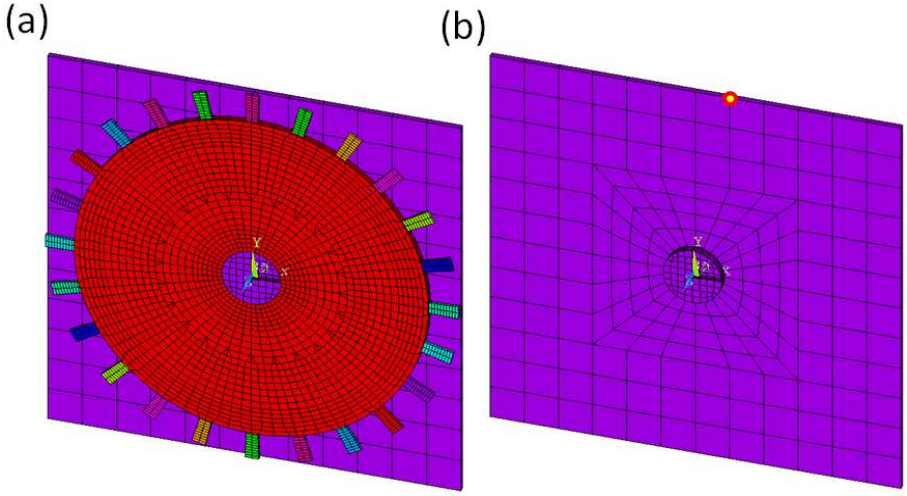

Figure 4.13: Rotor-bearing-housing system:(a) whole system (b) housing

additional modes participating in the linear combination to form localized modes are unbalanced modes. Therefore, the weight of unbalanced modes increases on some localized mode after bearings are introduced, such as the 15th to the 20th localized modes. Also, the additional localized modes (the 25th and 26th point of the rotor-bearing system) show high weight of unbalanced modes. This is because the two additional localized modes are mainly contributed by the two additional unbalanced modes. The change of the weight of unbalanced modes also implies how localized modes may change with the consideration of bearings.

4.4 Effects of Housing

To study effects of housing on mode localization, I use the finite element model shown in Figure 4.13(a). The model consists of a tuned, bladed disk (cf. Figure 3.1), a housing (see Figure 4.13(b)), and flexible bearings. The housing is a square plate with a central stud, on which the bladed disk can be supported. The housing is fixed

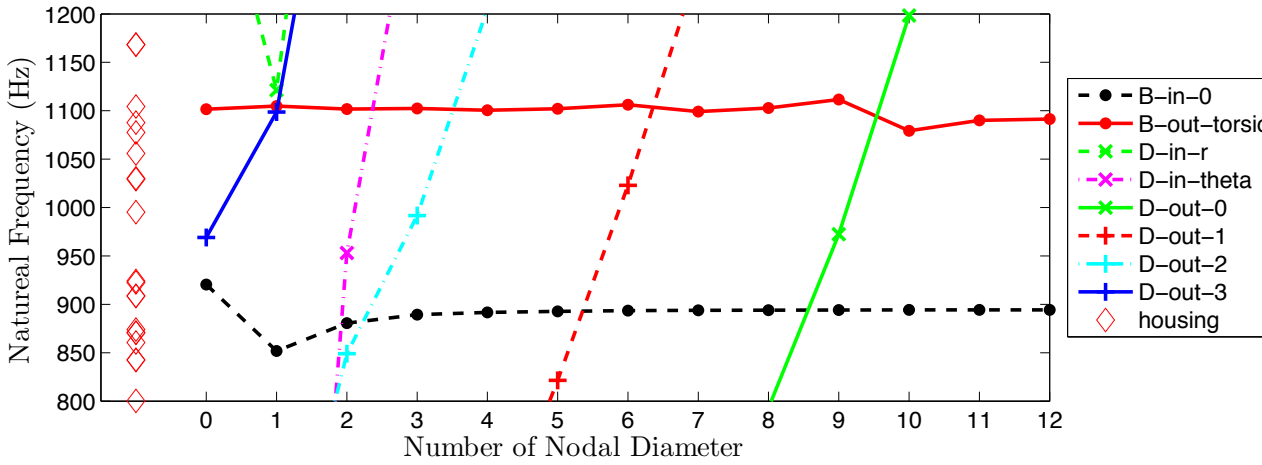

Figure 4.14: Natural frequencies of tuned rotor-bearing-housing system

at the four corners, and the material of the housing is Nickel alloy with density of 855 kg/m^3 and Young's modulus of 90 GPa. Contact elements are used to constrain the inner surface of the bladed disk and the outer surface of the stud (cf. Figure 4.13(b)), and their movements are represented via pilot points. A linear spring is then used to connect the two pilot points to model the flexible bearings. The bearing stiffness remains the same as that used in the rotor-bearing system in Chapter 4. This system with the bladed disk, housing, and bearings will be referred as the "rotor-bearing-housing system" henceforth. [3]

Figure 4.14 shows natural frequencies of the tuned rotor-bearing-housing system. In particular, Figure 4.14 is zoomed in to focus only on the frequency ranges of B-out-torsional and B-in-0 families, for which mode localization will occur. With the addition of the housing, the number of degrees of freedom increases drastically and so does the number of modes. Many of these newly added modes present vibration patterns that are heavily dominated by housing deformation. Natural frequencies

[3]Please refer to Appendix H for building the rotor-bearing-housing system in ANSYS.

of these housing-dominant modes are marked as red diamonds in Fig. 4.14 without reference to the number of nodal diameters. According to the theoretical analysis in Chapter 4, more localized modes may appear when mistuning is present.

The mistuning in Table 4.1 is then introduced into the tuned rotor-bearing-housing system shown in Fig. 4.13. FEA results show that there are 26 localized modes in the frequency range of B-in-0 family and 26 localized modes in the B-out-torsional family; see Table 4.2. Compared with the mistuned reference bladed disk with bearings, major changes occur in the frequency range of the B-in-0 family.

Regarding the two new localized modes, the most critical feature is presence of localized modes with significant housing deformation. Figure 4.15 shows the two newly added localized modes, with the bladed disk on the left and the housing on the right. One is mode 104 with frequency of 870.56 Hz and the other is mode 107 with frequency 873.97 Hz. In both modes, the housing undergoes considerable out-of-plane vibration. FEA results in Figure 4.15 clearly indicate that housing can affect mode localization via bearings.

The interaction between vibration of the housing and mode localization of the rotor is also observed in the forced response. For example, Figure 4.16 shows FRF of blade 3 as labeled in Fig. 3.1 from 850 Hz to 1120 Hz covering B-in-0 and B-out-torsional families. A sinusoidal force is applied in the out-of-plane direction at a point on the housing marked by the yellow dot in Fig. 4.13(b). The damping ratio is assumed to be 0.05%. Two reactions are calculated: (1) Euler norm of displacement at the left tip of blade 3 and (2) von Mises strain at the left root of blade 3. In Fig. 4.16, the highest peaks of the displacement are at 860.6 Hz, 870.56 Hz, 874.0 Hz, and 924.1 Hz. The three modes at 860.6 Hz, 874.0 Hz, and 924.1 Hz are out-of-plane housing dominated modes. Since these three modes do not have rotor deformation, their von Mises strain is small (cf. Fig. 4.16). On the contrary, the mode at 870.56 Hz is one of the newly added localized modes that has rotor vibration localized on blade 3 with significant housing deformation. As a result, the von Mises strain at 870.56

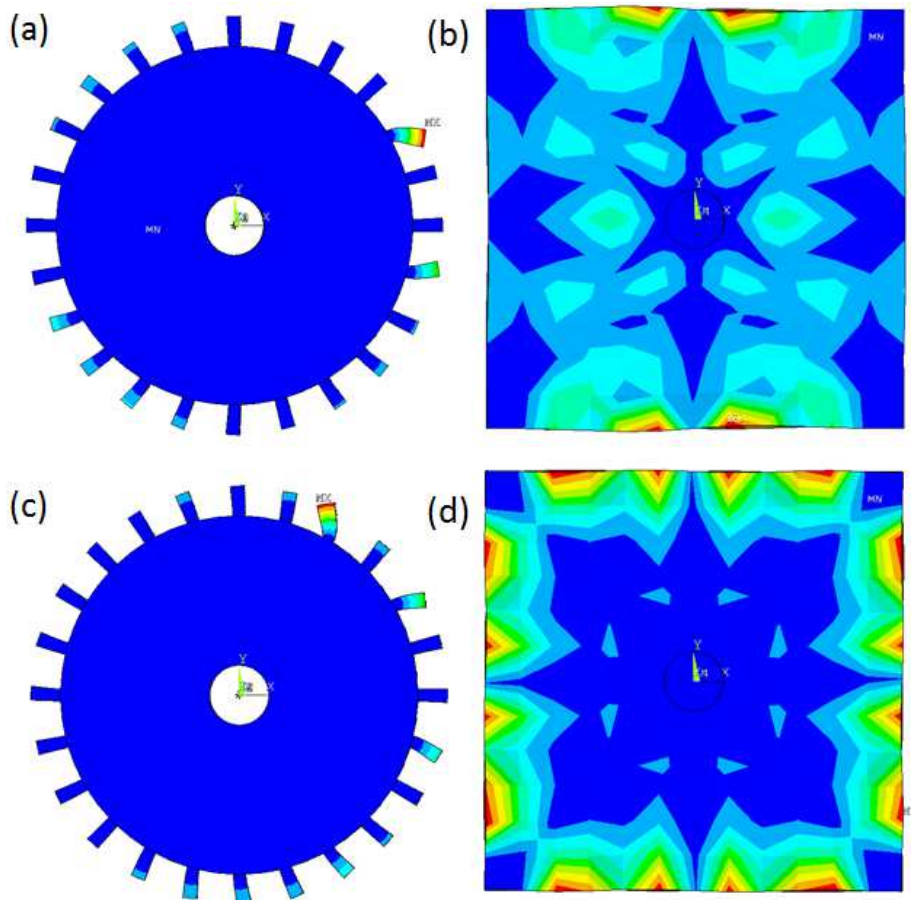

Figure 4.15: Additional localized mode shapes with significant deformation on the housing unique to the bladed disk with bearing and housing: (a) mode shape on the rotor of mode 104 (b) mode shape on the housing of mode 104 (c) mode shape on the rotor of mode 107 (b) mode shape on the housing of mode 107

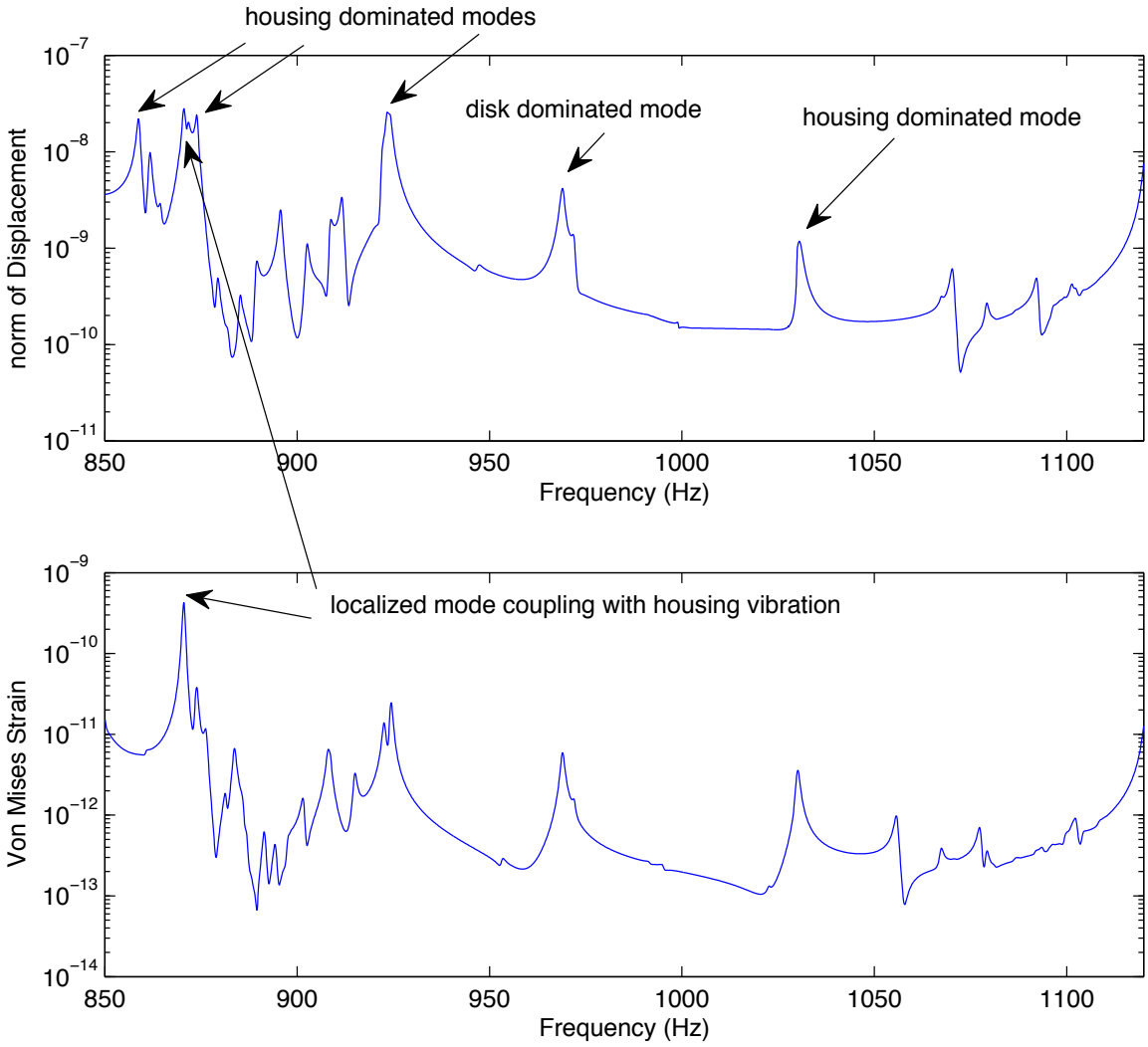

Figure 4.16: Frequency response function of for blade 3

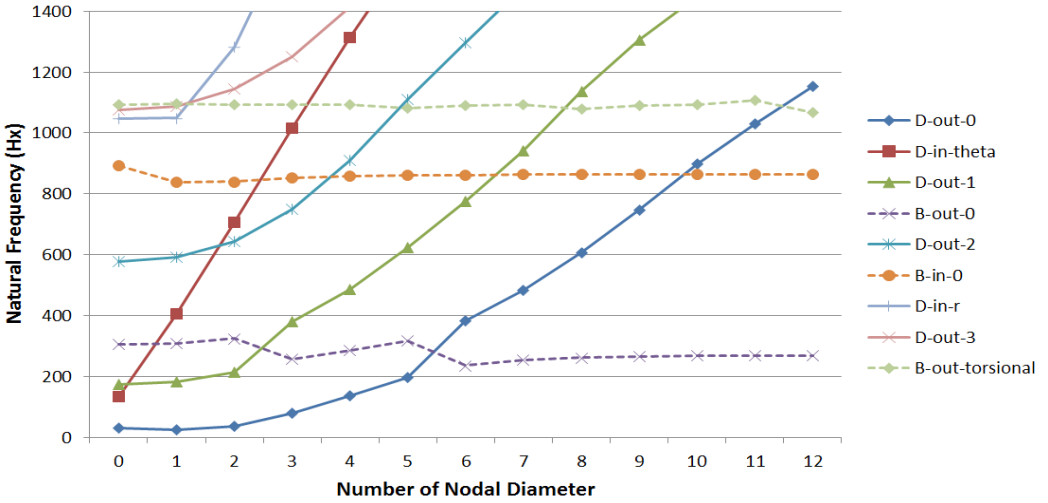

Figure 4.17: Natural frequencies of the tuned reference system (Drop-out case)

Hz has the highest peak between 850 Hz and 1120 Hz. This example demonstrates that forces exerted on the housing may also excite a localized mode on the rotor via bearings.

4.5 Effects of bearing - drop out case

In the previous sections, the examples show that the effects of boundary conditions may bring additional modes participate in the linear combination and ,in turn, form additional localized modes. This section will show an example that the change of boundary conditions may also reduce the number of localized modes.

To demonstrate that, some material parameters of the reference system and rotor-bearing system are modified. For the rotor component, the material of the disk is now considered with density of 855 kg/m^3 and Young's modulus of 105 GPa in this section. The material of the tuned blades remains the same as Nickel-Titanium alloy with density of 855 kg/m^3 and Young's modulus of 85 GPa. Figure 4.17 shows the

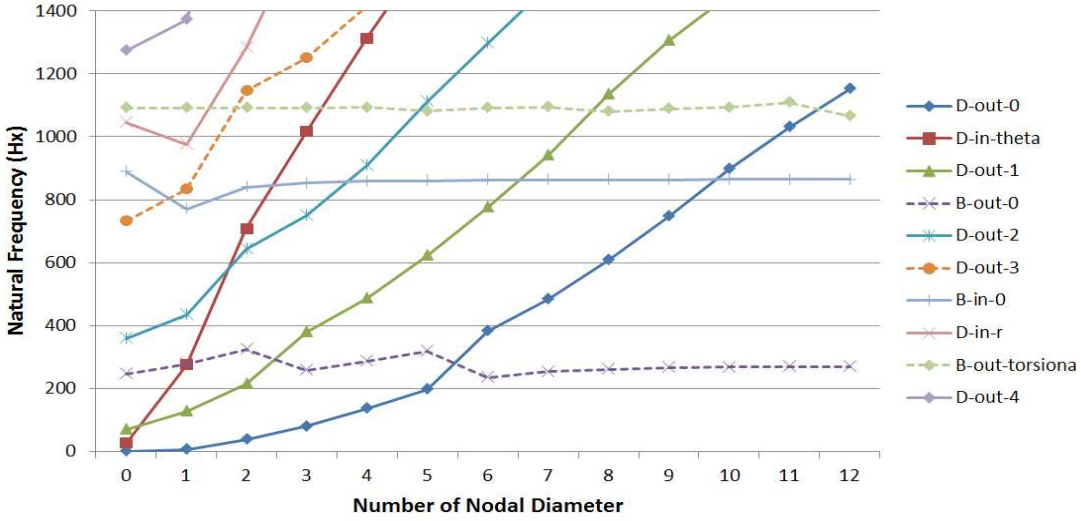

Figure 4.18: Natural frequencies of the tuned rotor-bearing system (Drop-out case)

family map of the modified, tuned reference system.

For the bearing components, the linear springs are modified to have linear stiffness of 5×10^9 N/m in the in-plane directions (i.e., x- and y-directions), linear stiffness of 5.76×10^6 N/m in the out-of-plane direction (i.e., z-direction), and rotational stiffness of 58.5 N $\cdot$ m/rad for pitch and roll (i.e., about x- and y-axes, respectively). Figure 4.18 shows the family map of the modified, tuned rotor-bearing system.

By comparing Fig. 4.17 and Fig. 4.18, two differences are found consistent as the observations mentioned in the section of Effects of Flexible bearing. First, only natural frequencies of the unbalanced modes change when the bearings are introduced. Second, the natural frequencies of disk-dominant modes are effectively affected by the boundary condition while the natural frequencies of blade-dominant modes only have subtle difference. The interesting difference here is the distance between unbalanced modes of D-out-3 family and B-out-torsional family. With the fixed boundary condition at the inner rim, the unbalanced modes (mode shapes with 0 and 1 nodal

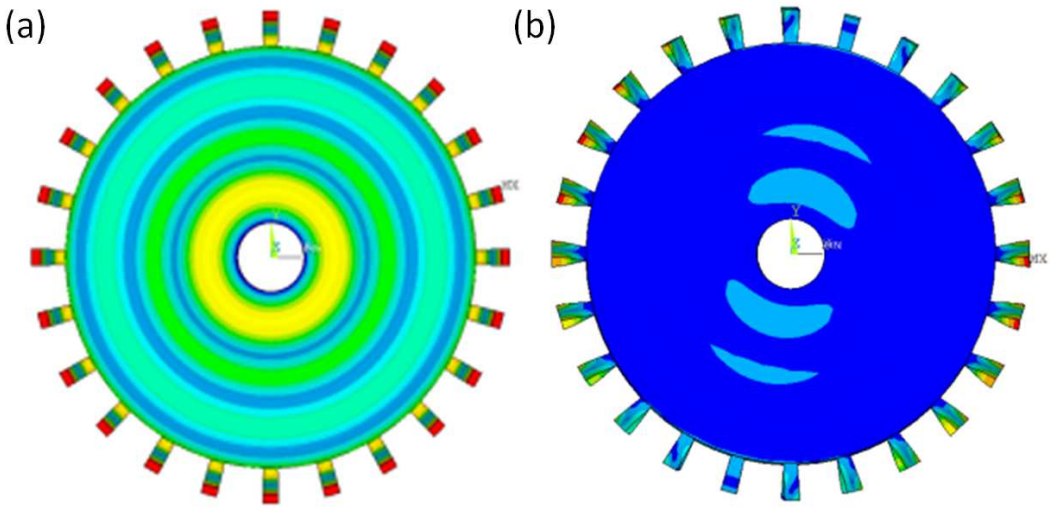

Figure 4.19: Mode shapes of D-out-3 family of the reference system with (a) 0-nodal diameter (b) 1-nodal-diameter

diameter) of D-out-3 family are very close to B-out-torsional family. The mode shape of the 1-nodal-diameter mode as shown in Fig. 4.19(b) shares the same characteristics (blade torsion) as B-out-torsional family. According to the hypothesis, when a group of modes is close to the group G modes and also has similar characteristics of mode shapes as group G. This group of modes can be group V modes to participate the linear combination to form mode localization. Therefore, the 1-nodal-diameter modes of D-out-3 family can be the group V modes to form mode localization with B-out-torsional family when the mistuning is present.

However, when bearings are introduced, the natural frequencies of D-out-3, 0- and 1-nodal-diameter modes drop out of the frequency band of the B-out-torsional family. Also their mode shapes (shown in Fig. 4.20) do not share similar characteristics as B-out-torsional modes. Hence, these modes will not participate into the linear combination for localized B-out-torsional modes when mistuning is present.

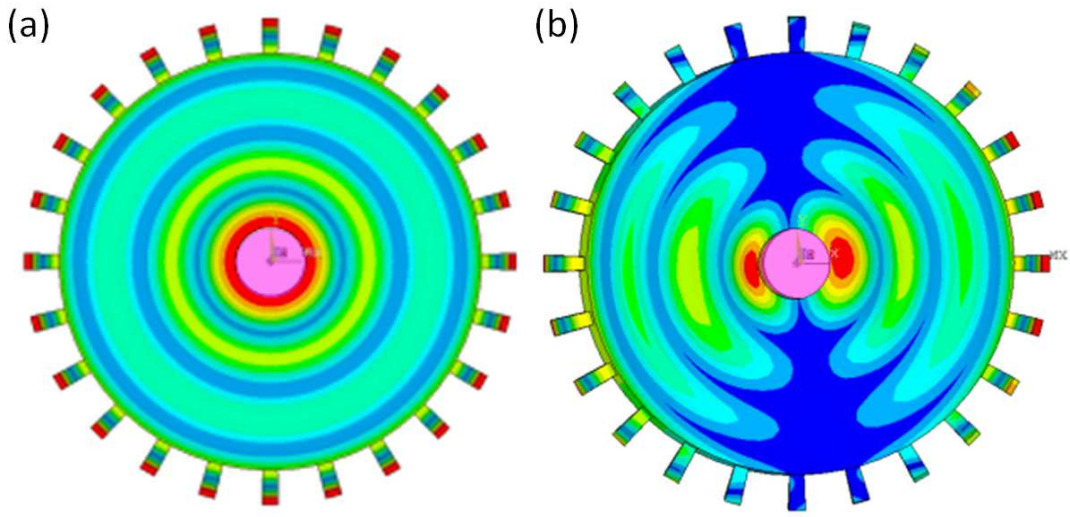

Figure 4.20: Tuned mode shapes of D-out-3 family of the rotor-bearing system with (a) 0-nodal diameter (b) 1-nodal-diameter

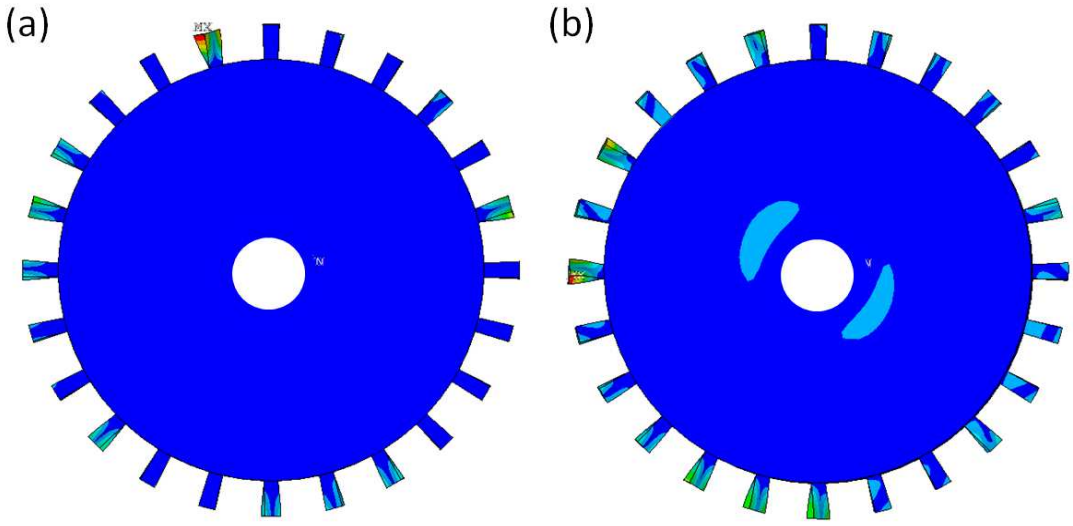

Figure 4.21: Virtual mistuned mode shapes of the reference system

The mistuning configuration is considered the same as shown in Table 4.1 and applied on the blades as a variation in Young's modulus. Finite element analysis of the mistuned reference system shows that there are 31 localized modes with blade torsional vibration. When bearings are introduced, only 29 localized, blade torsional modes are found due to the reduction of the two D-out-3 modes participating into the linear combination. The two additional modes for the reference system are shown as Fig. 4.21.

4.6 Summary

Through finite element simulations and deductive reasoning from existing theoretical analyses, I reach the following conclusions.

1. Boundary conditions are critical to the mode localization phenomenon of a nearly cyclic symmetric system with mistune.

2. Presence of bearings and housing may not only change the number of localized modes (either increase or decrease), but may also dramatically change the shape of existing localized modes without the bearings and housing. As a result, frequency response functions may change significantly should additional localized modes occur. Whether or not presence of bearings and housing may affect mode localization depends on the stiffness of the bearings and housing.

3. Presence of mistuning causes all localized modes to become unbalanced, thus resulting in a net force or moment transmitted to the bearings for every localized mode.

4. If the tuned system doesn't have any rotor-housing-coupling mode, the mistuned system will not have it either.

5. The conclusions above are well justified in the context of theoretical analyses developed in [25, 26].

Chapter 5

CONCLUSIONS AND FUTURE WORK

5.1 Conclusions

The conclusions and findings of this research are summarized here. The key factors for the occurrence of mode localization in a nearly cyclic symmetric system is clarified. When mistuning is present, mode localization can only occur when the following two conditions are met: (a) there is a group of tuned modes with nearly identical natural frequencies, and (b) this group of modes contains many wave numbers. Sufficiency of the wave numbers can be ensured when the group of modes includes all possible phase indices of the cyclic symmetric rotor. These two conditions are supported theoretically and mathematically.

In the theoretical analysis, the study of perturbation theory shows that mistuned mode shapes may change dramatically from tuned mode shapes only when a group of modes has identical natural frequencies. When mistuning is present, the zeroth order perturbation of the mistuned mode shapes will be formed as linear combinations of the group of tuned mode shapes. Since mode localization has changed dramatically from the tuned mode shapes, the change is happened at the zeroth order of perturbation. Therefore, there must be a group of modes has very close natural frequencies. For the second condition, Fourier analysis shows that the Dirac delta function in the circumferential direction is the linear combination of infinite wave numbers. Hence, an extremely localized mode shape has to be formed by the linear combination of a group of modes containing many wave numbers.

In the mathematical derivation, mistuned mode shapes can be predicted by linear combinations of the group of tuned mode shapes. The linear combinations are solved

as a eigenvalue problem by the Rayleigh-Ritz method. Whether or not a mode in the group will actively contribute to mode localization depends on the relative order of its coupling components and mistuning components. When these two components are roughly of the same order, the mode will actively contribute to mode localization. Since the coupling components are corresponding to the diagonal terms in $\hat{\mathbf{L}}$ and the mistuning terms are corresponding to the off-diagonal terms in $\hat{\mathbf{L}}$, a visual method is developed to pinpoint active modes by plotting the magnitude of each entry in $\hat{\mathbf{L}}$. With the visual method, the dimension of eigenvalue problem can be reduced significantly without guessing the width of frequency range.

Numerical examples validate the criteria for the occurrence of mode localization and the methodology to predict mode localization. A bladed disk with 24 blades evenly located at outer rim is used as the numerical model. All the frequency ranges satisfying the two conditions are found mode localization after mistuning is present. On the contrary, not all the frequency ranges containing eigenvalue loci veering are found mode localization. Moreover, even in a frequency range found mode localization, not all the modes at the eigenvalue loci veering site are actively participating into the linear combinations to form mode localization. Therefore, curve veering is not a key factor for mode localization.

In the first stiffness mistuning case, the visual method helps to select 24 modes from 35 modes in one range and select 24 modes from 49 modes in the other ranges to predict mode localization accurately. In the following mistuning cases, mode localization is compared among different mistuning amounts, mistuning patterns, and mistuning sources. With increment of the standard deviation of mistuning, more modes show compatible magnitudes between diagonal and off-diagonal entries in $\hat{\mathbf{L}}$ and are selected by the visual method. In order words, more modes from the tuned cyclic symmetric system are needed to enable linear combinations in realizing localized modes. When a system presents mass mistune, the underlying mathematical structure is more complicated as reflected in (2.34) and (2.37). Given the same mis-

tune (in terms of amount and pattern), the effect of mass mistune is greater than that of stiffness mistune. For large mass mistune, the visual method can identify tuned modes needed to realize mode localization. Nevertheless, the generalized eigenvalue problem should be used in the Rayleigh-Ritz approximation to obtain accurate results.

With the understanding about how mode localization occurs in an independent rotor with fixed boundary condition at inner rim, the effects of bearings and housing on mode localization are studied extendedly. Presence of bearings and housing may not only change the number of localized modes (either increase or decrease), but also dramatically change the shape of existing localized modes without the bearings and housing. Consequently, frequency response functions may change significantly should additional localized modes occur. Whether or not presence of bearings and housing may affect mode localization depends on the stiffness of the bearings and housing.

The mechanism of how mode localization is affected by the boundary conditions is investigated. When bearings are introduced into the tuned cyclic symmetric system, some modes will be coupled to the bearings changing their natural frequencies. These modes are called unbalanced modes. When an unbalanced mode shifts into or out of a frequency range where mode localization occurs, the number of selected modes participating into linear combinations may change and, thus, affect the results of mode localization in terms of the number of localized modes and the existing mode shapes. Similar mechanism is underlying the effect of housing. When the housing is introduced into the system, housing modes may show in the frequency range of mode localization. With additional degrees of freedom for the linear combinations, additional localized modes may found and some localized mode shapes may even have significant vibration on the housing. Frequency response function also shows that the vibration of housing may excite a localized mode on the rotor. Furthermore, presence of mistune causes all localized modes to become unbalanced, thus resulting in a net force or moment transmitted to the bearings for every localized mode.

5.2 Future Work

Based on the research progress achieved in this paper, current work has established well understanding about how mode localization occurs when a rotor is static and can be extended to the forced response while the rotor is spinning. Researchers believe that mode localization will be amplified while spinning. Due to the complication of how air dynamics interacts with a cyclic symmetric system, many studies focus on predicting the forced response numerically [30, 31, 32]. Some are tried to observe the amplification on a simplified modal experimentally [33, 34]. But seldom literatures investigate the physical reasons or the underlying mechanism.

To gain the physical insights for forced response while a rotor spinning, the gyroscopic and Coriolis effects have to be studied. Ewins et al. [35] studied the mutual interaction of gyroscopic effects and blade mistuning with a lumped-parameter modal. The result shows that effects of gyroscopic force produce higher maximum forced response than the non-gyroscopic model. Also, steady state response of an individual blade were found to be different with and without the considering of gyroscopic force. However, the modal was simplified and only two kinds of mode shapes are considered. The findings may not be general enough for any cyclic symmetric system.

One of gyroscopic effect is that when a system is vibrating with respect to a rotating frame of reference, repeated natural frequencies will be split and become individual. According to this research, one of the necessary conditions for mode localization is when there is a group of modes with almost identical natural frequencies. With considering the gyroscopic effects, the natural frequencies may not be close enough to considered as nearly identical. When there is no enough modes to linearly combine with each other after mistuning is introduced, mode localization may not even occur. At least, the number of active modes will change and so does the number of localized modes. Therefore, the amplification effect of gyroscopic force on mode localization still remains debatable.

The following steps are proposed to help the investigation on the effects of gyroscopic force. First, study the gyroscopic effect on a tuned cyclic symmetric system. By evaluating how significant the split of natural frequencies is caused by gyroscopic force, the revised family map may help to identify whether any group of modes satisfies the two conditions for mode localization to occur. If any group of modes is found, a mistuned system with and without introducing gyroscopic force should be analyzed. By comparing the numerical results, it may be able to tell whether gyroscopic force play an important role to amplify mode localization or not.

BIBLIOGRAPHY

[1] A. V. Srinivansan, "Flutter and Resonant Vibration Characteristics of Engine Blades," *Journal of Engineering for Gas Turbines and Power*, vol. 119, pp. 742–775, June 1997.

[2] D. S. Whitehead, "Effect of Mistuning on the Vibration of Turbomachine Blades Induced by Wakes," *Journal of Mechanical Engineering Science*, vol. 8, pp. 15–21, March 1966.

[3] D. E. Thomson and J. T. Griffin, "The national turbine engine high cycle fatigue program," *Global Gas Turbine News*, 1999.

[4] A. Sinha, "Mistuning analyses of a bladed disk: Pole-zero and modal approaches," in *ASME Turbo Expo 2008: Power for Land, Sea, and Air*, pp. 277–287, American Society of Mechanical Engineers, 2008.

[5] A. F. Vakais and C. Cetinkaya, "Mode localization in a class of multidegree-of-freedom nonlinear systems with cyclic symmetry," *SIAM Journal on Applied Mathematics*, vol. 53, no. 1, pp. 265–282, 1993.

[6] R. C. F. Dye and T. A. Henry, "Vibration Amplitudes of Compressor Blades Resulting From Scatter in Blade Natural Frequencies," *Journal of Engineering for Gas Turbines and Power*, vol. 91, pp. 182–187, July 1969.

[7] D. Ewins, "The Effects of Detuning Upon the Forced Vibrations of Bladed Disks," *Journal of Sound and Vibration*, vol. 9, no. 1, pp. 65–79, 1969.

[8] J. H. Griffin and T. M. Hoosac, "Model Development and Statistical Investigation of Turbine Blade Mistuning," *Journal of Vibration and Acoustics*, vol. 106, pp. 204–210, April 1984.

[9] G. Ottarsson, M. P. Castanier, and C. Pierre, "A Reduced Order Modeling Technique for Mistuned Bladed Disks," *Journal of Vibration and Acoustics*, vol. 119, pp. 439–447, July 1997.

[10] R. Bladh, M. P. Castanier, and C. Pierre, "Component-Mode-Based Reduced Order Modeling Techniques for Mistuned Bladed Disks Part I: Theoretical Models," *Journal of Engineering for Gas Turbines and Power*, vol. 123, pp. 89–99, January 2001.

[11] J. Griffin and M.-T. Yang, "A Reduced-Order Model of Mistuning Using a Subset of Nominal System Modes," *Journal of Engineering for Gas Turbines and Power*, vol. 119, pp. 161–167, October 2001.

[12] D. M. Feiner and J. H. Griffin, "A Fundamental Model of Mistuning for a Single Family of Modes," *Journal of Turbomachinery*, vol. 124, pp. 597–605, October 2002.

[13] D. M. Feiner and J. H. Griffin, "Mistuning Identification of Bladed Disks Using a Fundamental Mistuning ModelPart I: Theory," *Journal of Turbomachinery*, vol. 126, pp. 150–158, March 2004.

[14] A. Sinha, "Reduced-Order Model of a Bladed Rotor With Geometric Mistuning," *Journal of Turbomachinery*, vol. 131, p. 031007, July 2009.

[15] A. Sinha, "Computation of Eigenvalues and Eigenvectors of a Mistuned Bladed Disk Via Unidirectional Taylor Series Expansions," *Journal of Turbomachinery*, vol. 132, p. 044501, October 2010.

[16] S. H. Lim, R. Bladh, M. P. Castanier, and C. Pierre, "Compact, Generalized Component Mode Mistuning Representation for, Modeling Bladed Disk Vibration," *AIAA Journal*, vol. 45, pp. 2285–2298, September 2007.

[17] C. Pierre, "Mode Localization and Eigenvalue Loci Veering Phenomena in Disordered Structures," *Journal of Sound and Vibration*, vol. 126, no. 3, pp. 485–502, 1988.

[18] H. C. Chan and J. K. Liu, "Mode Localization and Frequency Loci Veering in Disordered Engineering Structures," *Chaos, Solitons and Fractals*, vol. 11, pp. 1493–1504, August 2000.

[19] C. H. Hodges, "Confinement of Vibration by Structural Irregularity," *Journal of Sound and Vibration*, vol. 82, no. 3, pp. 411–424, 1982.

[20] S.-T. Wei and C. Pierre, "Localization Phenomena in Mistuned Assemblies with Cyclic Symmetry Part I: Free Vibrations," *Journal of Vibration, Acoustics, Stress, and Reliability in Design*, vol. 110, pp. 429–438, October 1988.

[21] A. Sinha, "Reduced-order model of a mistuned multi-stage bladed rotor," *Journal of Turbo and Jet Engines*, 2008.

[22] D. Laxalde, J.-P. Lombard, and F. Thouverez, "Dynamics of multi-stage bladed disks systems," *Journal of Engineering for Gas Turbines and Power*, 2007.

[23] R. Bladh, M. P. Castanier, and C. Pierre., "Effects of multistage coupling and disk flexibility on mistuned bladed disk dynamics," *Journal of Engineering for Gas Turbines and Power*, 2003.

[24] K. D'Souza, C. Jung, and B. I. Epureanu, "Analyzing mistuned multi-stage turbomachinery rotors with aerodynamic effects," *Journal of Fluids and Structures*, 2013.

[25] Y. F. Chen and I. Y. Shen, "Mathematical insights of mode localization in nearly cyclic symmetric rotors with mistune," in *Proc. ASME 2013 International Design Engineering Technical Conferences and Computers and Information in Engineering Conference, Portland, OR.*

[26] H. Kim, N. T. K. Colonnese, and I. Y. Shen, "Mode Evolution of Cyclic Symmetric Rotors Assembled to Flexible Bearings and Housing," *Journal of Vibration and Acoustics*, vol. 131, p. 051008, October 2009.

[27] H. Kim and I. Y. Shen, "Ground-Based Vibration Response of a Spinning, Cyclic, Symmetric Rotor With Gyroscopic and Centrifugal Softening Effects," *Journal of Vibration and Acoustics*, vol. 131, p. 021007, April 2009.

[28] J. A. Kenyon, J. H. Griffin, and N. E. Kim, "Frequency Veering Effects on Mistuned Bladed Disk Forced Response," *Journal Of Propulsion And Power*, vol. 20, pp. 863–870, September-October 2004.

[29] A. Sinha, "Reduced-order model of a bladed rotor with geometric mistuning," *Journal of Turbomachinery*, vol. 131, no. 3, p. 031007, 2009.

[30] D. J. EWins, "The effects of detuning upon the forced vibrations of bladed disks," *Journal of Sound and Vibration*, vol. 9, no. 1, pp. 65–79, 1969.

[31] J. A. Kenyon, J. H. Griffin, and D. M. Feiner, "Maximum bladed disk forced response from distortion of a structural mode," in *ASME Turbo Expo 2002: Power for Land, Sea, and Air*, pp. 965–980, American Society of Mechanical Engineers, 2002.

[32] C. Martel and R. Corral, "Asymptotic description of maximum mistuning amplification of bladed disk forced response," *Journal of engineering for gas turbines and power*, vol. 131, no. 2, p. 022506, 2009.

[33] E. Petrov, L. Di Mare, H. Hennings, and R. Elliott, "Forced response of mistuned bladed disks in gas flow: A comparative study of predictions and full-scale experimental results," *Journal of Engineering for Gas Turbines and Power*, vol. 132, no. 5, p. 052504, 2010.

[34] D. Hemberger, D. Filsinger, and H.-J. Bauer, "Investigations on maximum amplitude amplification factor of real mistuned bladed structures," in *ASME Turbo Expo 2012: Turbine Technical Conference and Exposition*, pp. 1041–1052, American Society of Mechanical Engineers, 2012.

[35] M. Nikolic, E. P. Petrov, and D. J. Ewins, "Coriolis forces in forced response analysis of mistuned bladed disks," *Journal of Turbomachinery*, 2006.

Appendix A

BUILD FEA MODEL OF A BLADED DISK IN ANSYS

```
/prep7
! select element
et,1,plane42
et,2,solid95
! Define material constants
!Disk
mp,dens,1,8.55e-6 !density
mp,ex,1,8.5e7    !young's modulus
mp,prxy,1,0.33   !poisson ratio
! constant
Bdens=8.55e-6
Bex=8.5e7
Bprxy=0.33
! Housing
mp,dens,2,Bdens
mp,ex,2,Bex
mp,prxy,2,Bprxy
! blade 1
mp,dens,3,Bdens
mp,ex,3,Bex
mp,prxy,3,Bprxy
.
```

```
..
...
! blade 24
mp,dens,26,Bdens
mp,ex,26,Bex
mp,prxy,26,Bprxy
! build key points
csys,0 ! coordinate system 0
k,1,0,0,0
csys,1
k,2,200,-360/48,0
k,3,200,360/48,0
k,4,400,-360/48,0
k,5,400,360/48,0
k,6,600,-360/48,0
k,7,600,360/48,0
k,8,800,-360/48,0
k,9,800,360/48,0
k,10,1000,-360/48,0
k,11,1000,360/48,0
k,12,1200,-360/48,0
k,13,1200,360/48,0
csys,0
k,14,1200,-40,0
k,15,1200,40,0
k,16,1400,-40,0
k,17,1400,40,0
! create lines
```

```
!! create arcline by GUI> by end KPs and Rad >
!!! pick 2 KPs on arc->ok > pick center->ok >
!!! type radius > apply
!! create area > arbitrary>by lines
allsel
aglue,all
lsel,s,p
!! pre mash, pick the line you want to have 1 mesh
lesize,all,,,1
lsel,s,p
!! pre mash, pick the line you want to have 3 meshes
lesize,all,,,3
!! use meshtool > area > quad free > mesh > pick all areas
!! after mesh save as backbone
csys,0
type,2
! after you extrude body element, it'll clean selected area elements
extopt,aclear,1
asel,all
esize,,1
vext,all,,,0,0,20
! extrude disk top and bottom separately
csys,0
type,2
extopt,aclear,1
asel,s,p
!!selet the area u want
esize,,1
```

```
vext,all,,,0,0,-15
! if there is any plane element left, use following code to delete
esel,s,type,,1
eplot
asel,s,p
aclear,all
allsel
eplot
elist
!cyclic symmetric the model
csys,1
allsel
vgen,24,all,,,0,360/24,0,,0,0
! glue repeated elements together
nummrg,all
csys,0
!move model to be symmetric to coordinates
VGEN,, all,,,0,0,-10,,, 1 !modeling>move>volumn>circle  z:-10
!assign materials
esel,s,p !choose blades
emodif,all,mat,2
!boundary conditions
csys,1
nsel,s,loc,x,200
d,all,all
csys,0
!harmonic solution, be careful about frequency range and mode number
/solu
```

```
allsel
csys,0
type,2
antype,2
modopt,lanb,250,0,10000000,,off
lumpm,0
pstres,0
eqslv,spar
MXPAND, 250,,,1
solve
! obtain mass and stiffness metrices
/aux2
file,<dbfilename>,full
hbmat,<stiffnessFileName>,,,ascii,stiff,no,yes
hbmat,<massFileName>,,,ascii,mass,no,yes
```

Appendix B

OBTAIN BLADE DISPLACEMENT FROM FEA

1. save the code below into a text file in the ANSYS project folder.

2. in the ANSYS commend window type: `/INPUT, <Fname>, txt`

```
/prep7
endm=250 !rotor mode number
*dim,fnumr,array,endm
*do,iiii,1,endm
fnumr(iiii)=iiii
*enddo
/post1
file,'<dbFilename>','rst'
/output
csys,1
nsel,s,loc,x,1400
nsel,r,loc,z,10
!! for full modeshape uncomment below
! allsel
! nsel,u,loc,x, !unselect constrained nodes
!! for full modeshape uncomment above
*get,tnode,node,,count

*dim,freq2,array,tnode,endm
```

```
*dim,dix2,array,tnode,endm
*dim,diy2,array,tnode,endm
*dim,diz2,array,tnode,endm
*dim,ncount,array,tnode

*do,tt,1,tnode
*get,ncount(tt),node,,num,min
nsel,u,node,,ncount(tt)
*enddo

csys,1
nsel,s,loc,x,1400
nsel,r,loc,z,10
!! for full modeshape uncomment below
! allsel
! nsel,u,loc,x,200
!! for full modeshape uncomment above
csys,0
rsys,0

*do,ik,1,endm
jj=fnumr(ik)
set,order,jj
*do,jk,1,tnode
*get,freq2(jk,ik),active,,set,freq
*get,dix2(jk,ik),node,ncount(jk),u,x
*get,diy2(jk,ik),node,ncount(jk),u,y
*get,diz2(jk,ik),node,ncount(jk),u,z
```

```
*enddo
*enddo
rsys,0
/output,Ni2R_Tn_BCart_1to250,txt
*do,j,1,endm
!*do,10520,1,endm
*vwrite,dix2(1,j),diy2(1,j),diz2(1,j),freq2(1,j)
(7e15.5)
*enddo
/output
fnumr(1)= $
freq2(1,1)= $  freq2(1,1)=
dix2(1,1)= $  diy2(1,1)= $  diz2(1,1)=
:end
```

Appendix C

COVERT MASS AND STIFFNESS MATRICES FROM ANSYS OUTPUT TO MAT FILE

```
% this script will use functions in "hb to msm" matlab package
clear all; clc; close all;


for i=4:5
    switch i
        case 1
            modelN = 'Tn_Dex85e6';
        case 2
            modelN = 'Kmis';
        case 3
            modelN = 'Kmis5Pv1';
        case 4
            modelN = 'Kmis5Pv2';
        case 5
            modelN = 'Mmis5Pv2';
    end


tic
modenum=101;
secnum=24; %substructure number
M =importdata(strrep(...
```

```
'<folder>\6_Ni\NiFx_Kmis\NiFx_Kmis_allCart_1to250.txt',...
'Kmis',modelN), ' ', 2);

E=M.data;
[N M]=size(E);
a=(modenum-1)*(N/250)+1;
e=E(a:a+(N/250)-1,1:3);
ushp=reshape(e',1,[]);
ushp=ushp';
freq=E(a,4)

mainfold = strrep('<folder>\6_Ni\NiFx_Kmis','Kmis',modelN);
hbK = hb_to_msm ( fullfile(mainfold,...
strrep('NiFx_Kmis_KstiffCart.matrix','Kmis',modelN)) );

hbK=hbK+hbK'-diag(diag(hbK));
fid = fopen(fullfile(mainfold,...
strrep('NiFx_Kmis_KstiffCartMap.txt','Kmis',modelN)));

C = textscan(fid, '%f %f %s');%, 'delimiter', ',', 'EmptyValue', -Inf);
fclose(fid);
k_ix=C{2};
bb=[];
for k=1:length(k_ix)/3
    bb=[bb,0.1 0.2 0.3];
end
k_ix=k_ix+bb';
[B, KIX] = sort(k_ix, 1);
```

```
nKstiff=[];
for k=1:length(k_ix)
    j=KIX(k);
    nKstiff=[nKstiff; hbK(j,:)];
end
nnKstiff=[];
for k=1:length(k_ix)
    j=KIX(k);
    nnKstiff=[nnKstiff, nKstiff(:,j)];
end
toc
assert(isequal( round((ushp'*nnKstiff*ushp)^0.5/2/pi),round(freq)),...
'natural freq is not the same as Ansys')
% [Ki,Kj,Kval] = find(nnKstiff);
% nnKstiff_dump = [Ki,Kj,Kval];
% save('fAlBfx_Kmis_CartK_dump.txt','nnKstiff_dump','-ascii', '-double' )
eval(strrep( 'save NiFx_Kmis_CartK.mat nnKstiff','Kmis',modelN))
disp('K matrix is saved')

tic
hbM = hb_to_msm ( fullfile(mainfold,...
strrep('NiFx_Kmis_MassCart.matrix','Kmis',modelN)) );

hbM=hbM+hbM'-diag(diag(hbM));
fid = fopen(fullfile(mainfold,...
strrep('NiFx_Kmis_MassCartMap.txt','Kmis',modelN)));
```

```
C = textscan(fid, '%f %f %s');%, 'delimiter', ',', 'EmptyValue', -Inf);
fclose(fid);
M_ix=C{2};
bb=[];
for k=1:length(M_ix)/3
    bb=[bb,0.1 0.2 0.3];
end
M_ix=M_ix+bb';
[B, MIX] = sort(M_ix, 1);
nMass=[];
for k=1:length(M_ix)
    j=MIX(k);
    nMass=[nMass; hbM(j,:)];
end
nnMass=[];
for k=1:length(M_ix)
    j=MIX(k);
    nnMass=[nnMass, nMass(:,j)];
end
assert(round(ushp'*nnMass*ushp)==1,...
'mode shape is not normailized to mass matrix ')
toc
% [Mi Mj Mval] = find(nnMass);
% nnMmass_dump = [Mi,Mj,Mval];
% save('fAlBfx_Kmis_CartM_dump.txt','nnMmass_dump','-ascii', '-double' )
eval( strrep('save NiFx_Kmis_CartM.mat nnMass','Kmis',modelN))
disp('M matrix is saved')
end
```

Appendix D

COVERT MODE SHAPES FROM ANSYS OUTPUT TO MAT FILE

```
function [Ueigvec,nafreq] = saveAllCartTxt2mat(folder,systype)
cd(folder)
switch systype
    case 'R'
        txtU = dir('*allCart_1to250*.txt');
        totalmod = 250;
    case 'RB_all'
        txtU = dir('*allCart_1to250*.txt');
        totalmod = 250;
    case 'RB_br'
        txtU = dir('*brCart_1to250*.txt');
        totalmod = 250;
    case 'RBH'
        txtU = dir('*brCart_1to350*.txt');
        totalmod = 350;
end
if numel(txtU)~=1
    txtU.name = input('input the .txt mode shape file: ','s');
end

Mtn = importdata(txtU.name, ' ',2);
```

```
Etn = Mtn.data;
[Ntn Mtn] = size(Etn);
nafreq = nan(1,totalmod);
Ueigvec =[];
for i_mod = 1:totalmod
    ind_1st = (i_mod-1)*(Ntn/totalmod)+1;
    ind_end = (i_mod)*(Ntn/totalmod);
    e = Etn(ind_1st:ind_end,:);
    nafreq(i_mod) = e(1,end);
    switch systype
        case 'R'
            e=e(:,1:3);
            ushp = reshape(e',1,[]);
        case 'RB_all'
            shp1 = reshape(e(1:7638,1:3)',1,[]);
            shp2 = e(7639,3); % node num 12207
            shp3 = reshape(e(7640:7889,1:3)',1,[]);
            shp4 = e(7890,2); %node num 12588
            shp5 = reshape(e(7891:14930,1:3)',1,[]);
            % node num 24385~24388
            shp6 = reshape(e(14931:14934,1:6)',1,[]);
            % node num 24390
            shp7 = e(14935,1:4);
            % node num 24392~24397,24400,24401
            shp8 = reshape(e(14936:14943,1:6)',1,[]);
            ushp = [shp1 shp2 shp3 shp4 shp5 shp6 shp7 shp8];
        case {'RBH','RB_br'}
            e=e(:,1:6);
```

```
            ushp = reshape(e',1,[]);
    end
    ushp = ushp';
    Ueigvec = [Ueigvec,ushp];
end
slashloc = strfind(folder,filesep);
tempname = folder(slashloc(end)+1:end);
cd(folder)
switch systype
    case {'RBH','RB_br'}
        eval(['save ' tempname '_CartUbr.mat Ueigvec'])
        eval(['save ' tempname '_nafreq.mat nafreq'])
    otherwise
        eval(['save ' tempname '_CartU.mat Ueigvec'])
        eval(['save ' tempname '_nafreq.mat nafreq'])
end
end
```

Appendix E

PLOT VISUAL METHOD

```
clear all; clc; %close all;
tunemod = 1:250; %all
totalmod = 250;
secnum = 24; %substructure number

foldTn = uigetdir(pwd,'nominal system');
cd(foldTn)
fileM = dir('*CartM*.mat');
load(fileM.name)
tunedM = nnMass;
fileK = dir('*CartK*.mat');
load(fileK.name)
tunedK = nnKstiff;
fileBin = dir('*binfam*.txt');
fileBtor = dir('*btorfam*.txt');
binfam = load(fileBin.name); %get binfam
btorfam = load(fileBtor.name); %get btorfam
try
    fileU = dir('*CartU*.mat');
    load(fileU.name) %get binfam
    Utn = Ueigvec;
catch error
```

```
    txtU = dir('*allCart_1to250*.txt');
    if numel(txtU)~=1
        txtU.name = input('input the .txt mode shape file: ','s');
    end
    Mtn = importdata(txtU.name, ' ',2);
    Etn = Mtn.data;
    [Ntn Mtn] = size(Etn);
    Ueigvec =[];
    for modenum = tunemod
        a = (modenum-1)*(Ntn/totalmod)+1;
        e = Etn(a:a+(Ntn/totalmod)-1,1:3);
        ushp = reshape(e',1,[]);
        ushp = ushp';
        Ueigvec = [Ueigvec,ushp];
    end
    slashloc = strfind(foldTn,filesep);
    tempname = foldTn(slashloc(end)+1:end);
    cd(foldTn)
    eval(['save ' tempname '_CartU.mat Ueigvec'])
    Utn = Ueigvec;
    op
end

foldMis = uigetdir(pwd,'mistuned system');
cd(foldMis)
fileM = dir('*CartM*.mat');
load(fileM.name)
mistunedM = nnMass;
```

```
fileK = dir('*CartK*.mat');
load(fileK.name)
mistunedK = nnKstiff;

deltaK = mistunedK - tunedK;
deltaM = mistunedM - tunedM;
delKhat = Utn'*deltaK*Utn;
delMhat = Utn'*deltaM * Utn;
omgs = Utn'*tunedK*Utn;
omgvec = diag(omgs);

modeRange = [34 48;51 69;68 104;100 150];%38 45;55 62; 69 100; 111 149
numRange = size(modeRange,1);
cenFreqHz = [332.6 611 839.9 1083.8];
for i_range = 1:numRange
curRange = modeRange(i_range,:);
cenFreqRad2 = (cenFreqHz(i_range)*2*pi)^2;
Dhat = omgs - cenFreqRad2*eye(length(tunemod));
if isequal(max(max(abs(delMhat))),0)
    L=Dhat+delKhat;
    logL=log10(L);
    nn=3;
else
    nn=4;
    L=(Dhat+delKhat-delMhat*...
    (cenFreqRad2*eye(length(tunemod))+Dhat+delKhat));
    logL=log10(L);
end
```

```
for i=1:nn
    if i==1
        matrix=L; s='$\hat{L}$';
    elseif i==2
        matrix=delKhat; s='$\Delta \hat{K}$';
    elseif i==3
        matrix=Dhat; s='$\hat{D}$';
    elseif i==4
        matrix = delMhat*(cenFreqRad2*eye(length(tunemod))+Dhat+delKhat);
        s='$\Delta \hat{M}$ associated term';
    end

    figure
    set(gcf,'visible','off')
    mat =(abs(matrix));

    imagesc(mat);          % Create a colored plot of the matrix values
    colormap(flipud(hot));
    colorbar
    set(gca,'CLim',[0 7e5])
    axis equal
    axis([curRange(1) curRange(2) curRange(1) curRange(2)])

    FS=14;
    xlabel('Mode Number','interpreter','latex','FontSize',FS)
    ylabel('Mode Number','interpreter','latex','FontSize',FS)
    title(s,'interpreter','latex','FontSize',FS)
    %set(gca,'YTick',1:1:length(Rrange)) %edit tick
```

```
    h = colorbar;ylabel(h, 'Magnitude of $\hat{L}$ Matrix',...
    'interpreter','latex','fontsize',FS);
    set(gca,'FontSize',FS-4,'FontName','Times New Roman')
end
end

allhands= get(0,'children'); allhands = sort(allhands);
for i_fig=1:numel(allhands)
plottools(allhands(i_fig)); set(allhands(i_fig),'visible','on');
end
```

Appendix F

MODELING AND OBTAIN MODE SHAPES FOR ROTOR-BEARING SYSTEM

1. Use the same model (.db) with fixed BC so the node number would be the same
2. Before build model with bearing, delete fixed BC first
3. Modeling bearing use the script below
4. Remember to give mass21 element property
5. Get MK matrices
6. Open mapping file to check degree of freedoms (use "beyond compare" to compare the mapping files between fixed and bearing system)
7. Try to obtain one mode shape and confirm it's normalized to mass matrix
8. Obtain mode shapes for all solved modes

```
/prep7
csys,1
n,4465,0,0,10
n,4466,0,0,10
n,4467,0,0,-10
n,4468,0,0,-10
n,4469,0,0,0
```

```
n,4470,0,0,0
csys,0
! step 1: Define a pilot node at the joint node
et,6,170
keyopt,6,2,1
real,6
tshap,pilot
type,6
e,4470
! step 2: select the nodes of the corresponding surfaces
csys,1
nsel,s,loc,x,200
! step 3: create the contact elements on the surface
et,7,174
keyopt,7,2,2
keyopt,7,4,2
keyopt,7,12,5
type,7
real,6
esurf
nsel,all

real,1
!rigid beam
et,3,mpc184
keyopt,3,1,1 !1:rigid beam
keyopt,3,2,1 !lagrange multiplier
mat,1
```

```
type,3
e,4465,4470
e,4467,4470
e,4466,4469
e,4468,4469

!bearing
csys,0
et,4,mpc184
keyopt,4,1,16 !general link
keyopt,4,4,0 !1:only dis DOF are activated,
 !0:dis&rot DOFs are activated
sectype,4,joint,gene !general joint
local,12,0,0,0,10
local,13,0,0,0,10
secjoint,,12,13
sectype,5,joint,gene !general joint

/prep7
kyyy=2.16e7 !!changed
kxxx=2.16e7 !!changed
kzzz=5.76e6  !!changed
krotx=58.5  !!changed
kroty=58.5  !!changed
krotz=2e13  !!changed
tb,join,2,,,stif  !2 is material number
tbdata,1,kxxx
tbdata,7,kyyy
```

```
tbdata,12,kzzz
tbdata,16,krotx
tbdata,19,kroty
tbdata,21,krotz

csys,0
mat,2
secnum,4
type,4
e,4465,4466
secnum,5
type,4
e,4467,4468


!point mass
et,5,mass21
keyopt,5,1,0
keyopt,5,3,2
!!remember to add real constant as mass before create element
!!real no.=1 , mass=1

mat,1
type,5
e,4469

! boundary condition
nsel,s,,,4469
```

```
d,all,all

/solu
allsel
csys,0
!type,2
antype,2
modopt,lanb,250,0,10000000,,off
lumpm,0
pstres,0
eqslv,spar
mxpand,250,,,1
solve
```

Appendix G

SOLVE FREQUENCY RESPONSE FUNCTION

```
! solve modal analysis
/solu
allsel
csys,0
type,2
antype,2
modopt,lanb,250,0,10000000,,off
lumpm,0
pstres,0
eqslv,spar
mxpand,250,,,1
solve
/post1
set,list
Finish

/config,nres,5000  ! increase the result sets for hamornic solutions

!  Obtain the Mode Superposition Harmonic Solution
!  check model solution first
/SOLU  ! Enter SOLUTION
ANTYPE,HARMIC  ! Harmonic analysis
```

```
HROPT,MSUP  ! Mode superposition method; number of modes to use
HROUT,OFF,ON,OFF  ! Harmonic analysis output options; cluster option
csys,0
selNode = 10881 !! blade11
nsel,s,,,selNode
F,ALL,FZ,50
NSEL,ALL
HARFRQ,1070,1120  ! Forcing frequency range
DMPRAT,0.0005  ! Damping ratio
NSUBST,50*10  ! Number of harmonic solutions
KBC,1  ! Ramped or stepped loads
Allsel,all
SOLVE  ! Initiate solution
FINISH
/POST26
FILE,,RFRQ
! Postprocessing file is Jobname.RFRQ,
! check whether the folder contains it,
! this line cannot ignore for superposition solver for ANSYS 11 &14.5!
NSOL,2,selNode,U,Z,UZ_bladeTip_11
NSOL,3,selNode+1,U,Z,UZ_bladeRoot_11

STORE,MERGE
PRVAR,2,3,4,5   ! Print data
PLVAR,2,3   ! Plot data
/GROPT,LOGY,ON
/REPLOT
PLVAR,4,5
```

```
/REPLOT

!  Expand the Solution (for Stress Results)
/SOLU ! Re-enter SOLUTION
EXPASS,ON ! Expansion pass
NUMEXP, all, 1070, 1120, yes !expand to all solu in the freq range
HREXP,all ! Phase angle for expanded solution
SOLVE
FINISH

! Review the Results of the Expanded Solution
/POST26
ESOL,4,2652,selNode,EPEL,1,strain1_bladeTip_11
ESOL,5,2643,selNode+1,EPEL,1,strain1_bladeRoot_11
STORE,MERGE
PRVAR,2,3,4,5   ! Print data
PLVAR,4,5
/REPLOT
```

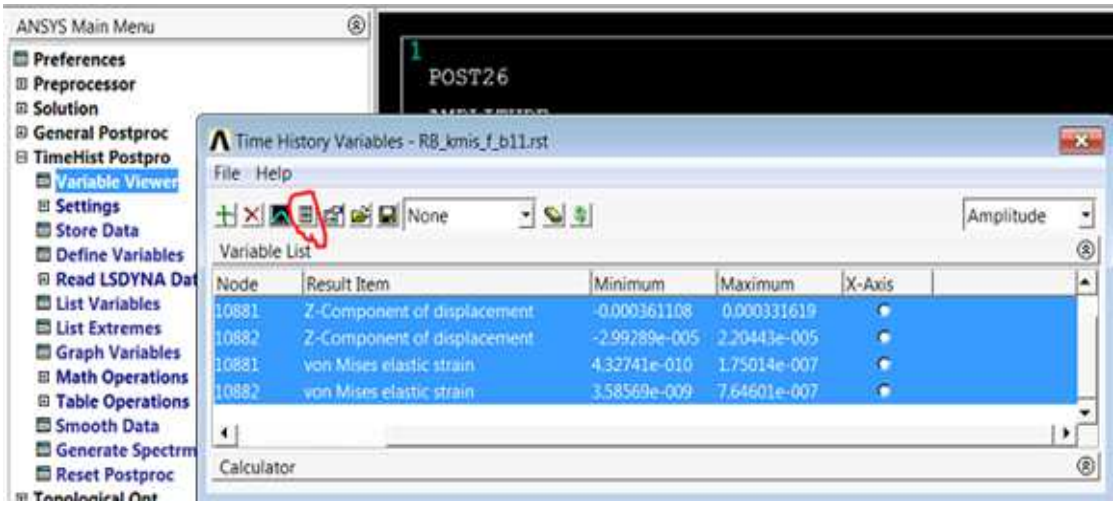

Figure G.1: To list FRF with amplitude and phase

Appendix H

MODELING FOR ROTOR-BEARING-HOUSING SYSTEM

Create finite element model for housing

```
/prep7
et,1,plane42
et,2,solid95
!! create a rectangle and a solid quarter circle
allsel
aovlap,all
!! Create a 45 degree line: create>keypoints>on line>pick, csys,0
k,8,700,0,0
k,9,0,700,0
k,10,1400,700,0
k,11,700,1400,0
k,12,700,700,0
!!create>lines>straight line>pick two pts
!! create two arcs: create>lines>arcs>by end KPs & Rad>
!!! >pick end pts>ok>pick center>ok>enter rads
!! create>areas>arbitrary>by line> make 2 almost triangles
allsel
aovlap,all
!! Glue all areas:operate>booleans>glue>areas>pick all

lsel,s,p
```

```
lesize,all,,,3
lsel,s,p
lesize,all,,,4
!! use meshtool > area > quad free > mesh > pick areas
!!! (mesh with mesh tool. smart size unselect,
!!! size control>area>set>pick the area>
!!! 60, meshtool,quad,mapped,mesh)

!! save as db file
!! arsym twice: Modeling>Reflect>Areas>pick all areas>
!!! ok, modeling>reflect>areas>x-z plane
allsel
nummrg,all

! extend plate
type,2
asel,all
esize,,1
vext,all,,,0,0,-40

! extend shaft
! the extend length is corresponding to the rotor
type,2
asel,s,p
esize,,1
vext,all,,,0,0,10
! the following extend lengths is corresponding to the rotor
type,2
```

```
asel,s,p
esize,,1
vext,all,,,0,0,15
type,2
asel,s,p
esize,,1
vext,all,,,0,0,20
type,2
asel,s,p
esize,,1
vext,all,,,0,0,15

! if there are some plane element lest, use following code to delete
esel,s,type,,1
eplot
asel,all
aclear,all
allsel
eplot
elist
allsel
nummrg,all
esel,all
emodif,all,mat,2

!! modeling>move>volumn>circle  z:-35
!! list>keypoints>coordinate, check key point numbers
!! save as base db
```

```
! save it as cdb file by the following script
/prep7
CDWRITE,All, wholebase, cdb
!! copy wholebase.cdb and wholebase.iges to the target folder
```

Combine housing and rotor models

```
!! resume from rotor.db and delete all loads
!! GUI: solution>define Loads>Delete>All Load Data>All Loads & Opts

!! copy wholebase.cdb and wholebase.iges to the target folder
! inport housing part
/prep7
CDREAD, All, wholebase, cdb

/prep7
et,1,plane42
et,2,solid95
Bdens=8.55e-6
Bex=8.5e7
Bprxy=0.33
!Housing
mp,dens,2,Bdens
mp,ex,2,Bex
mp,prxy,2,Bprxy
!check the material numbers
mergeMat = 2
!Disk
mp,dens,mergeMat+1,8.55e-6
```

```
mp,ex,mergeMat+1,10.5e7
mp,prxy,mergeMat+1,0.33
!blade 1
mp,dens,mergeMat+3,Bdens
mp,ex,mergeMat+3,Bex
mp,prxy,mergeMat+3,Bprxy
.
..
...
!blade 24
mp,dens,mergeMat+26,Bdens
mp,ex,mergeMat+26,Bex
mp,prxy,mergeMat+26,Bprxy
/prep7
! boundary nodes
csys,0
nsel,s,loc,z,-75
nsel,r,loc,x,1166,1400
nsel,r,loc,y,1166,1400
cm,buttonru,node
nsel,s,loc,z,-75
nsel,r,loc,x,-1400,-1166
nsel,r,loc,y,1166,1400
cm,buttonlu,node
nsel,s,loc,z,-75
nsel,r,loc,x,-1400,-1166
nsel,r,loc,y,-1400,-1166
cm,buttonld,node
```

```
nsel,s,loc,z,-75
nsel,r,loc,x,1166,1400
nsel,r,loc,y,-1400,-1166
cm,buttonrd,node
cmsel,s,buttonru,node
cmsel,a,buttonlu,node
cmsel,a,buttonld,node
cmsel,a,buttonrd,node
cm,bcnode,node
! inner rim of rotor
allsel
esel,s,mat,,3 ! the rotor
nsle
csys,1
nsel,r,loc,x,200
cm,hubnode,node
! upper surface of the shaft
allsel
esel,s,mat,,2 ! the housing
nsle
csys,1
nsel,r,loc,x,200
nsel,r,loc,z,5,25
cm,shaftu,node
! lower surface of the shaft
allsel
esel,s,mat,,2 ! the housing
nsle
```

```
csys,1
nsel,r,loc,x,200
nsel,r,loc,z,-25,-5
cm,shaftl,node
csys,0
! for fixed bc and get matrix map
cmsel,s,bcnode,node
d,all,all

! list>node>coordinate, check node numbers
allsel
nlist

! pilot points
maxnodenum = 26210
csys,1
n,maxnodenum+1,0,0,0    ! pilot node for hub
n,maxnodenum+2,0,0,17   ! node for rotor to upper bearing
n,maxnodenum+3,0,0,-17  ! node for rotor to lower bearing
n,maxnodenum+4,0,0,17   ! pilot node for upper shaft
n,maxnodenum+5,0,0,-17  ! pilot node for lower shaft
csys,0

! rotor
! step 1: Define a pilot node for rotor
et,6,170
keyopt,6,2,1
real,6
```

```
tshap,pilot
type,6
e,maxnodenum+1
! step 2: select the nodes of the corresponding surfaces
cmsel,s,hubnode,node
! step 3: create the contact elements on the surface
et,7,174
keyopt,7,2,2
keyopt,7,4,2
keyopt,7,12,5
type,7
real,6
esurf

! rigid beam: connect pilot node of hub to upper and lower bearings
real,1
et,3,mpc184
keyopt,3,1,1 !1:rigid beam
keyopt,3,2,1 !lagrange multiplier
mat,1
type,3
e,maxnodenum+2,maxnodenum+1
e,maxnodenum+3,maxnodenum+1

! upper shaft
! step 1: Define a pilot node for upper shaft
et,6,170
keyopt,6,2,1
```

```
real,7
tshap,pilot
type,6
e,maxnodenum+4
! step 2: select the nodes of the corresponding surfaces
cmsel,s,shaftu,node
! step 3: create the contact elements on the surface
et,7,174
keyopt,7,2,2
keyopt,7,4,2
keyopt,7,12,5
type,7
real,7
esurf

! lower shaft
! step 1: Define a pilot node for lower shaft
et,6,170
keyopt,6,2,1
real,8
tshap,pilot
type,6
e,maxnodenum+5
! step 2: select the nodes of the corresponding surfaces
cmsel,s,shaftl,node
! step 3: create the contact elements on the surface
et,7,174
keyopt,7,2,2
```

```
keyopt,7,4,2
keyopt,7,12,5
type,7
real,8
esurf
nsel,all

! bearing
csys,0
et,5,mpc184 ! a1 = 5;
keyopt,5,1,16 !general link  ! a1 = 5;
keyopt,5,4,0
! 1:only dis DOF are activated, 0:dis&rot DOFs are activated
! a1 = 5;
sectype,4,joint,gene !general joint  ! b1 = 4;
local,12,0,0,0,17
local,13,0,0,0,17
secjoint,,12,13
sectype,5,joint,gene !general joint ! b2 = 5;
! here we use only 3 dof,
! so we don't need to constraint more dof by secjoint and
! don't need to name local coord as below
local,14,0,0,0,-17
local,15,0,0,0,-17
secjoint,,14,15
/prep7
kyyy=2.16e7 !!changed
kxxx=2.16e7 !!changed
```

```
kzzz=5.76e6  !!changed
krotx=58.5  !!changed
kroty=58.5  !!changed
krotz=2e13  !!changed
tb,join, mergeMat+27,,,stif  !27 is material number
tbdata,1,kxxx
tbdata,7,kyyy
tbdata,12,kzzz
tbdata,16,krotx
tbdata,19,kroty
tbdata,21,krotz
csys,0
mat, mergeMat+27
secnum,4 !b1=4
type,5 !a1=5
e,maxnodenum+2,maxnodenum+4
mat, mergeMat+27
secnum,5 !b2=5
type,5 !a1=5
e,maxnodenum+3,maxnodenum+5

!! check whether the component exists, List>components>by name
! boundary condition
cmsel,s,bcnode,node
d,all,all

/solu
allsel
```

```
csys,0
!type,2
antype,2
modopt,lanb,350,0,10000000,,off
lumpm,0
pstres,0
eqslv,spar
mxpand,350,,,0
solve
```